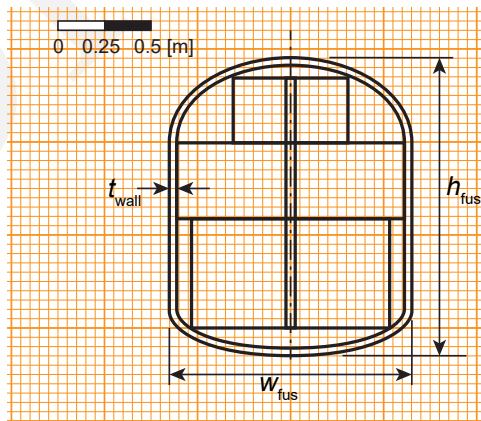


- Step 4* We draw the floor as a single line and decide to draw the floor structure once the frame thickness has been determined.
- Step 5* We skip this step because there is no allocation of cargo in the cross-section (see Example 6.1).
- Step 6* We draw the inner perimeter of the fuselage slightly outside of the dots. As this fuselage is not going to be pressurized, the inner perimeter is not perfectly circular. However, we do try to minimize the perimeter to minimize the wetted area of the fuselage as well as the structural mass.
- Step 7* Based on (6.1), we have a wall thickness of $t_{wall} = 40$ mm. We draw the outer perimeter with an offset of 40mm from the inner perimeter (see below). The resulting fuselage cross-section has the following dimensions: $w_{fus} = 131$ cm and $h_{fus} = 161$ cm.



- Step 8* We skip this step because there is no allocation of cargo in the cross-section (see Example 6.1).

Table 6.4: Recommended scales to be used for drawing airplane components.

Recommended scales				
1:2	1:4	1:5	1:10	
1:20	1:25	1:40	1:50	1:100
1:200	1:250	1:400	1:500	1:1000

In the previous example we inserted for w_{aisle} the desired width between the two passengers. Also, note that the dimensions that we set in Step 1 were derived from an experimental analysis where the body dimensions of a random person were used to define the various heights and widths of the cabin. In practice, you might have to do some research on the dimensions of the passengers that you wish to transport in your airplane. An anthropometric database such as DINED² could be employed to perform such research. Alternatively, you can research the dimensions of seats that are used in, for example, your reference airplanes. If dimensional data of these seats can be found, they can be used to determine the required dimensions in Step 1. In the following example, we show how this works.

An important aspect when making a drawing is to choose an appropriate scale. In the previous example, we chose a scale of 1:10. This ensured a simple conversion from the full-scale dimensions to the dimensions on the drawing while resulting in a drawing that (1) fitted on the paper and (2) was large enough to communicate the design. These two aspects should be taken into account when choosing an appropriate scale for your drawing. Table 6.4 gives an overview of recommended scales. However, you can deviate from these recommendations for functional reasons.

Example 6.4

In this example, we draw the cross-section of a passenger transport airplane. The following requirements have been derived. This airplane needs to seat 180 passengers in a single class. We have a seat width of 44 cm, an armrest width of 5 cm, and a stand-up height in the aisle of 200 cm. To store luggage and cargo, an LD3-45 container is to be used below the passenger floor. This container has a height of 114 cm (45 inches), a roof width of 242 cm, and a base width of 156 cm with 45° walls between the base and either side.³

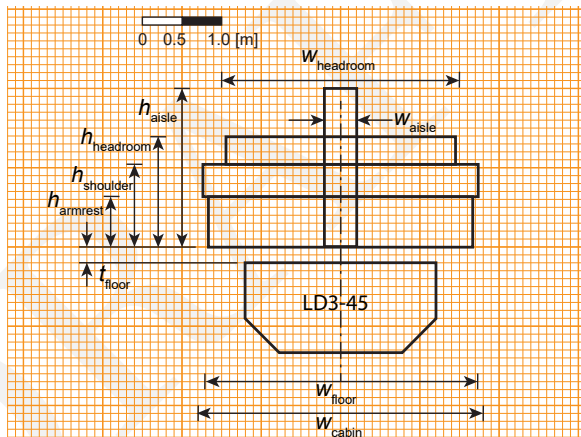
Step 1 Using (6.5), we decide to use a six-abreast cabin with a single aisle. The aisle width is determined with the help of Table 6.2. Above the armrests, the aisle measures 51 cm, while between the armrests, the aisle measures $51 - 2 \cdot 5 = 41$ cm, which is more than the minimum required of 38 cm. Now, we employ (6.6), (6.7), and (6.8), to find $w_{\text{cabin}} = 3.61$ m, $w_{\text{floor}} = 3.47$ m, and $w_{\text{headroom}} = 3.01$ m. We have no explicit requirements for the height of the armrest, shoulder, and headroom. Therefore, we decide to add 5cm to the height values of Example 6.3 such that the seat cushion is raised. The armrest height, shoulder height,

²For more information on anthropometric data, visit dined.io.tudelft.nl.

³Information on ULDs can be found at [wikipedia.org](https://en.wikipedia.org)

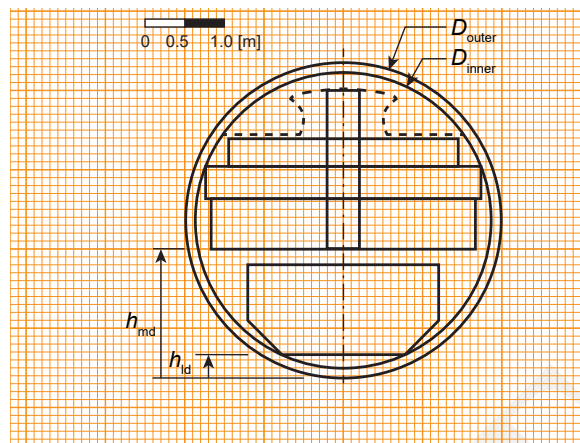
and headroom height have dimensions $h_{\text{armrest}} = 64 \text{ cm}$, $h_{\text{shoulder}} = 105 \text{ cm}$, and $h_{\text{headroom}} = 140 \text{ cm}$, respectively.

- Step 2** We assume that our drawing paper has a width of 18 cm. Based on the computed cabin width, we choose a drawing scale of 1:20.
- Step 3** Based on the dimensions of the previous step, we draw four rectangular blocks. Three blocks are positioned on top of each other. The block representing the aisle partially overlaps the three blocks that cover the seats (see below). A symmetry line is added to show where the symmetry plane of the cross-section is located.
- Step 4** For the passenger floor, we choose a floor depth of 20 cm. This is added below the passengers.
- Step 5** A cross-sectional geometry of the LD3-45 container is added below the passenger floor.



- Step 6** It is decided to use a circle to enclose the boxes above the floor and the container below the floor. By means of trial and error⁴, this circle is constructed (see below). We measure its diameter and find $d_{f, \text{inner}} = 375 \text{ cm}$. Note that the lower corner points of the container and the upper corner points of the shoulder block are the sizing points for this cross-section.
- Step 7** Using (6.3), we find an outer diameter, $d_{f, \text{outer}} = 400 \text{ cm}$. We have a wall thickness of 12.5 cm. We can also measure the height of the lower deck (ld) and main deck (md), measured from the lowest part of the cross-section: $h_{\text{ld}} = 29 \text{ cm}$, $h_{\text{md}} = 1.63 \text{ m}$.

⁴A process of finding the smallest circle is shown in this video



Step 8 Respecting the headroom height, the aisle width, and the aisle height, we draw a notional perimeter of the overhead bins using a dashed line.

As you can see from the examples, the design of the fuselage cross-section requires you to perform calculations as well as to draw. To draw accurately, we recommend using grid paper in combination with a ruler and a geometric compass. Finding the origin of the inner circle can be done using trial-and-error with your geometric compass. You choose one of the corner points and select a location for the origin of your circular arc. When you then draw the circular arc, you can evaluate whether all corner points fall within the arc and how much clearance is left between the arc and the other corner points. Once you have found the smallest circular arc that encloses all the corner points, you have finished.⁵

ASSIGNMENT 6.2

In this assignment, you will design the cross-section of your fuselage.

- Use the design sequence for the cabin cross-section to design the cabin cross-section of your airplane.
- List the values for w_{cabin} and, if applicable, $d_{\text{f, inner}}$ and $d_{\text{f, outer}}$.
- What is the resulting height (h_{fus}) and width (w_{fus}) of the fuselage cross-section that you have designed?
- What is the total perimeter length of your fuselage cross-section?

6.4. DESIGN OF THE FUSELAGE IN TOP VIEW

Now that we have a cross-section of the fuselage, the next step is to design the fuselage in the top view. The design of the fuselage in the top view is determined by various factors. First of all, there is the explicit requirement that the fuselage should have sufficient volume to store the payload. The level of comfort to the passengers can be driving the

⁵To further demonstrate this process, you can also watch this video.

length of the cabin through a required seat pitch. For large airplanes, we might also have two or three different classes, each with their individually defined seat pitch. In addition, we have the requirement that we need to accommodate the pilot(s) in a (separate) cockpit. Finally, we have the implicit requirement that a tail should be mounted to the fuselage and that the fuselage should be connected to the wing.

In addition, we need a design objective statement such that we can justify the choices we make when we design the top view of the fuselage. We propose to use the minimization of drag as a design objective. With a given cross-section, minimization of the (friction) drag implies we need to minimize the wetted area (S_{wet}). However, we also realize that an aerodynamically shaped nose and tail are needed to have low pressure drag. In addition, the size of the horizontal and vertical tails is dependent on their respective distances from the center of gravity of the airplane. In other words, a short fuselage might result in large tail surfaces, which themselves would have a large wetted area. So, we refine the design objective as follows: to minimize the drag of the fuselage while having an acceptable tail arm to the tail surfaces.

Before we present you with a possible design sequence to design the fuselage in the top view, let us first present some general design features of the fuselage that we can recognize in the top view of most tubular fuselage geometries. We have visualized the top view of a single-prop, small passenger airplane in Figure 6.13. You can see that the fuselage outer mold line consists of three components that are attached to each other: the nose cone, the cylindrical part, and the tail cone. The addition of these three components forms the complete fuselage length. Even though we use the word ‘cone’ in relation to the nose and tail geometry, the three-dimensional shapes are not necessarily conical. If we look at the inside of the fuselage, we see that the various internal components are distributed a bit differently. For example, within the nose cone, we have the nose and part of the cockpit. The perimeter of the nose is indicated with a dashed line because the nose consists of an engine cowling. The design of the engine cowling is not part of the fuselage design and is discussed in Chapter 8. However, it still contributes to the fuselage length. Since this is a small airplane, the cockpit is deemed part of the cabin. The cabin is located mostly in the cylindrical part of the fuselage but also extends into the nose cone and tail cone. In this example, we have chosen to give the tail cone the shape of a tadpole tail, where we have used a simplified trapezoid shape as a drawing guide (also shown in dashed lines in Figure 6.13). You can see that behind the cabin, there is still ample volume for storing luggage or cargo.

If we look at the definitions for a large passenger airplane (Figure 6.14), we can distinguish the same three components that make up the outer mold line of the fuselage: the nose cone, the cylindrical part, and the tail cone. Also, the nose, cabin, and tail are present. However, the cockpit is no longer part of the cabin but is a separate component inside the nose and the nose cone. The cabin starts behind the cockpit. For the large passenger airplane, we have given the tail cone a more conical shape. When drawing the tail, we smoothly transition from the cylindrical part to the tail cone to avoid local flow separation and provide ample cabin width at the start of the tail cone. The shape of the nose cone is constructed as an ellipse with a blunt nose, which is common in large passenger transports.

The length of the cabin is dominated by the size of the payload. When only pas-

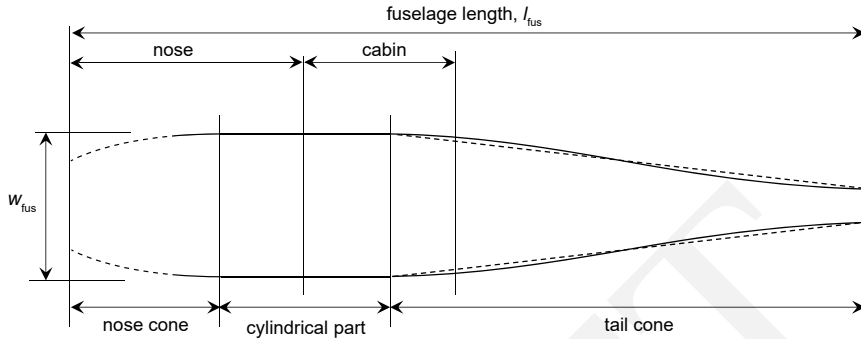


Figure 6.13: Top view of a fuselage design with distinct sections indicated. The dashed lines are for reference only.

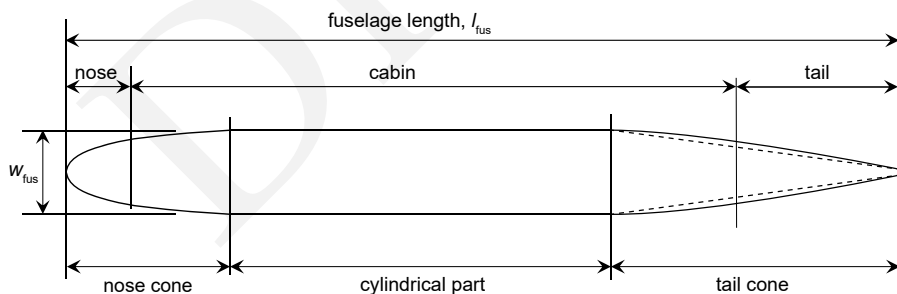


Figure 6.14: Top view of a fuselage for a large passenger airplane with definitions for the geometric parameters.

sengers occupy the cabin, you can use the seat pitch to estimate how much length is needed to accommodate all the passenger seats. Example values for seat pitch can be found in Table 6.3. For small airplanes, the seat pitch might be enough to accommodate the length of the cabin. For large passenger airplanes, cross-aisles (for evacuation), crew seats, galleys, and lavatories also need to be added. Each of these has standardized dimensions that can be easily found online. To determine the length of the cabin, you can position all required cabin items in the top view of the cabin and measure the resulting length. To perform this exercise, you need to decide on the number of galley carts you need, the number of lavatories to install, and how many cross-aisles are required. If you decide to also store cargo on the same deck as the passengers, the length of the passenger cabin might also increase. In other words, determining the length of the cabin requires the generation of a floor plan to accommodate the various items within the cabin. To perform this exercise can be quite labor intensive for large passenger airplanes.

In lieu of this laborious effort, we propose a statistical method to determine the length of the cabin for large passenger airplanes without making a floor plan. We use a statistical factor k_{cabin} , which represents the length in meters per available seat row in the cabin. The cabin length can then be computed as:

$$l_{\text{cabin}} = k_{\text{cabin}} \frac{n_{\text{pax}}}{n_{\text{SA}}} \quad (6.9)$$

with

$$k_{\text{cabin}} = \begin{cases} 1.08 & [\text{m}] \text{ for short/medium-range airplanes;} \\ 1.17 & [\text{m}] \text{ for long-range airplanes.} \end{cases}$$

The value of k_{cabin} is subject to statistical validation.

Now that we have determined the length of the cabin, we compute the length of the nose, nose cone, tail cone, and tail, respectively. To support this process, we have proposed values for various dimensions and fineness ratios, which are grouped in Table 6.5.

The length of the nose is a function of human dimensions, where we assume that there are two people sitting side-by-side in the cockpit. For propeller airplanes, the length of the nose should be chosen between 2.0 and 4.0 meters, whereas smaller airplanes typically have a shorter nose. For jet airplanes, which generally fly faster than propeller airplanes, the nose is typically a bit longer. However, the maximum length from the tip of the nose to the back of the cockpit should still be chosen between 3.0 and 4.5 meters. The nose cone can either be longer than the nose (e.g., for large airplanes) or shorter (e.g., for small airplanes). Typical values for the nose-cone fineness ratio ($l_{\text{nc}}/d_{\text{fus}}$) are listed in Table 6.5. Here we use the equivalent fuselage diameter, d_{fus} , which we define as:

$$d_{\text{fus}} = \frac{w_{\text{fus}} + h_{\text{fus}}}{2} \quad (6.10)$$

You can see that for jet airplanes, the nose cones have a higher suggested fineness-ratio range than for propeller airplanes. This is because jet airplanes typically have a high subsonic cruise Mach number, which can cause additional drag if the nose is too blunt.

The length of the tail cone can be computed by choosing an adequate tail cone fineness ratio ($l_{\text{tc}}/d_{\text{fus}}$), for which suggested ranges are given in Table 6.5. Even though small propeller airplanes might not require a tail cone with a high fineness ratio from a drag

Table 6.5: Proposed range of values for dimensional parameters of the nose and tail cones

	l_n (m)	l_{nc}/d_{fus}	l_{tc}/d_{fus}	l_t/d_{fus}
propeller	2.0-4.0	1.2-2.0	2.5-4.0	0.5-1.0
jet	3.0-4.5	1.5-2.5	2.0-5.0	0.5-1.0

point of view, a high fineness ratio results in a long tail arm, which reduces the necessary size of the horizontal and vertical tailplanes (see Chapter 9). Once you have chosen a value of the tail cone fineness ratio, you must decide how much of the cabin is still located inside the tail cone. This is reflected in the tail-to-tail-cone ratio, l_t/l_{tc} . For example, when $l_t/l_{tc} = 0.7$, it means that the first 30% of the tail cone is used as part of the cabin. We suggest to choose a tail-to-tail-cone ratio between 0.5 and 1.0. With a selected tail fineness ratio and tail-to-tail-cone ratio, you can compute the length of the tail cone and tail.

In summary, we propose the following design sequence for the fuselage perimeter in the top view:

- Step 1* Compute the cabin length
- Step 2* Select a nose length, a tail-cone fineness ratio, and a tail-to-tail-cone ratio. Subsequently, compute the fuselage length, l_{fus}
- Step 3* Based on the size of your paper and the fuselage length, determine the scale of your drawing.
- Step 4* Draw the fuselage length.
- Step 5* Draw fuselage width based on the design of the cross-section
- Step 6* Select a nose-cone fineness ratio and draw the dimensions of the nose cone and the tail cone.
- Step 7* Construct the fuselage perimeter in top view
- Step 8* Draw the aft cabin wall

Note that the determination of the scale of your drawing should ensure that the resulting airplane design fits on your paper. In Figure 6.15, you can see how the final three-view drawing is going to develop. We have a paper width that we denoted with a , and we have assumed a paper aspect ratio of 3:4. We have created three notional boxes where the three views of the airplane are located, respectively. The top view of the airplane occupies the largest box. To construct the three views, we use the American projection. To ensure your drawing fits on the paper, you choose an appropriate scale from Table 6.4. When the length of the fuselage is computed, it is advised to choose a scale that results in the largest drawing while satisfying $l_{fus} < 3a/4$.

In the following two examples, we demonstrate how this process works for the four-seat airplane and the 130-seat airplane.

Example 6.5

In this example, we design the fuselage of a 4-seat airplane in top view. We follow the design sequence that is shown above as well as data from Example 6.3.

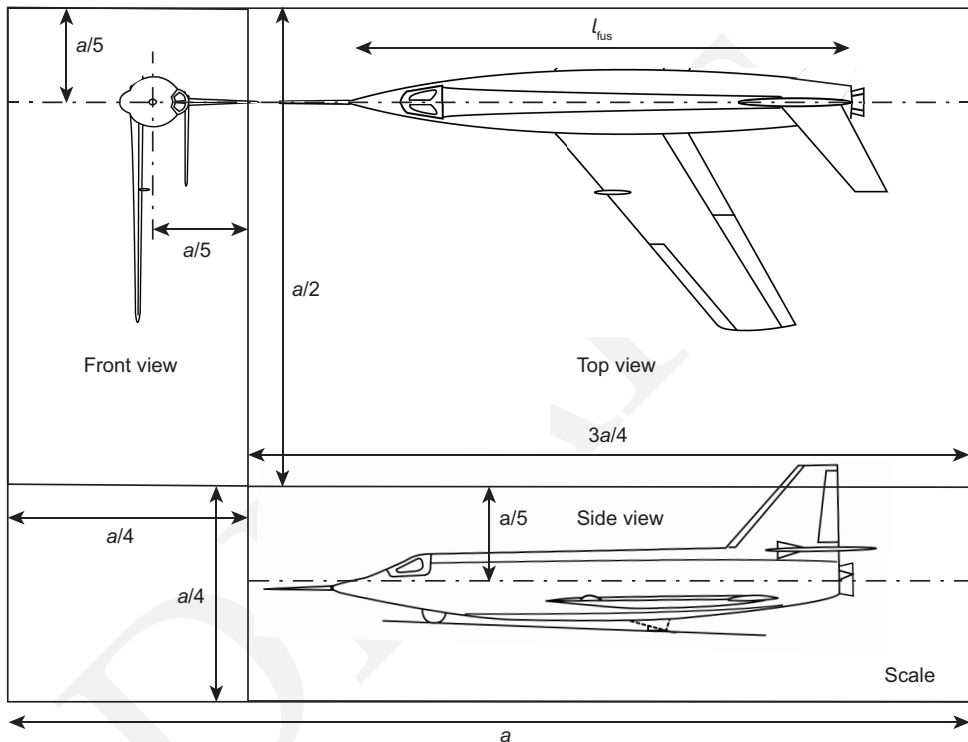
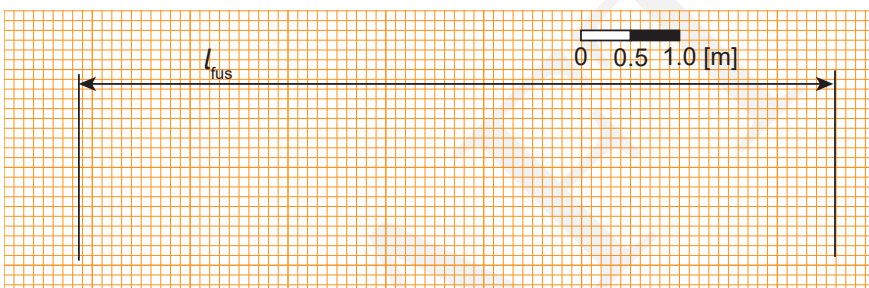


Figure 6.15: Example of three-view drawing of an airplane using American projection.

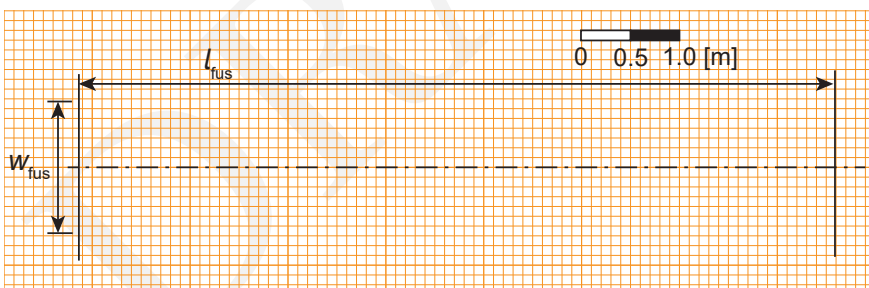
- Step 1** The length of the cabin is basically one seat row behind the cockpit. We do not allocate additional space for galleys, lavatories, or storage. We choose a seat pitch of 85 cm, which becomes the length of the cabin. Note that the cockpit is located in the nose and that we do not count the two front seats as part of the cabin.
- Step 2** We choose a nose length of 3.0 meters, based on Table 6.5. For the tail-cone fineness ratio, we select a value of 3.1, which results in a tail-cone length of 4.06 meters. Furthermore, we select a tail-to-tail-cone ratio of 0.8, which results in a tail length of 3.77 meters. The fuselage length then becomes $l_{\text{fus}} = 3.0 + 0.85 + 3.77 = 7.6$ m.

Step 3 We determine the scale of our drawing.

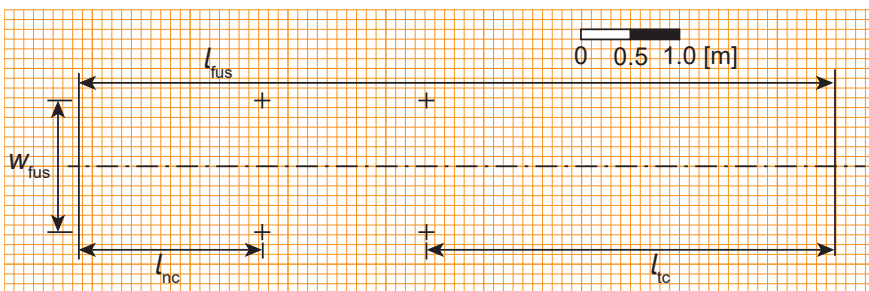
Step 4 We draw the length of the fuselage and mark the beginning and end by vertical lines.



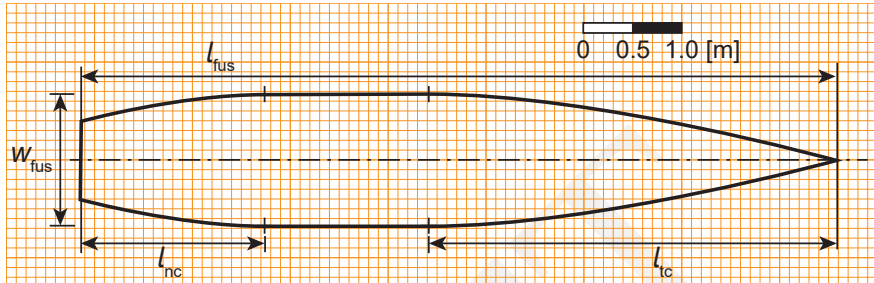
Step 5 The width of the fuselage measures 131 cm. We draw this dimension together with the symmetry line in the drawing below.



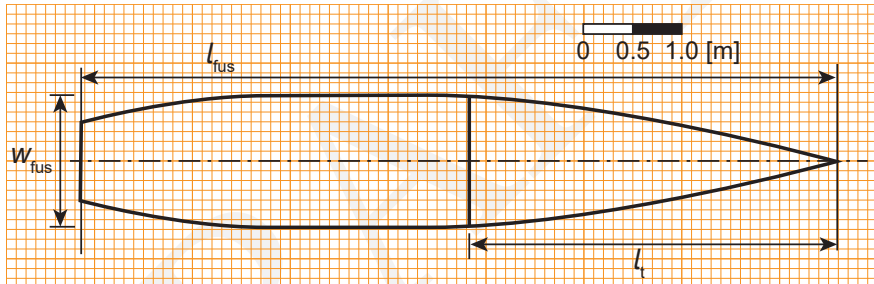
Step 6 We choose a nose fineness ratio of 1.4. This results in a nose length of 1.83 m. We add the dimensions of the nose cone and tail cone to the drawing.



Step 7 Because this four-seat airplane has the propeller attached to the nose, we decide to leave 80 cm of width at the nose to provide sufficient space for the engine. On the tail, we decide to let the fuselage end at a single point on the centerline. Finally, we decide that the nose cone curve and tail cone curve are connected tangent to the constant cross-section of the fuselage. With these decisions and the lines we constructed in the previous four steps, we now construct the perimeter of the fuselage in the top view (see below).



Step 8 We add the aft cabin wall to show where the cabin ends.



In the previous example, we have made a few choices that ask for some elaboration. First of all, we have allocated part of the cabin in the tail cone. If you do this, you should make sure that the narrower cross-section is still wide enough to accommodate the passengers in the cross-section. Secondly, we have not yet drawn the nose of the airplane. In Chapter 8, we will determine the physical dimensions of the electric motor. Then, we will also add a cowling around the engine and finish the nose of the airplane.

In the following example, we show how the fuselage of a large passenger airplane is designed in top view.

Example 6.6

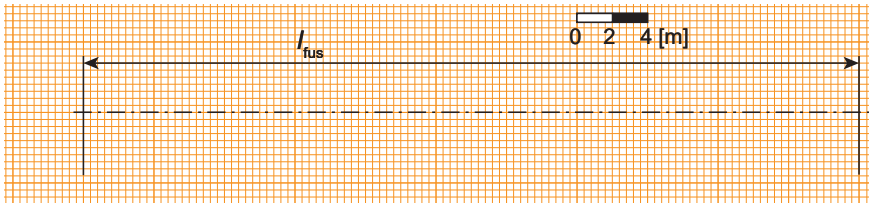
In this example, we design the fuselage of Example 6.4 in the top view. We follow the step-by-step procedure as in Example 6.5, but we make different choices.

Step 1 Using (6.9), we compute the cabin length to be 32.4 m.

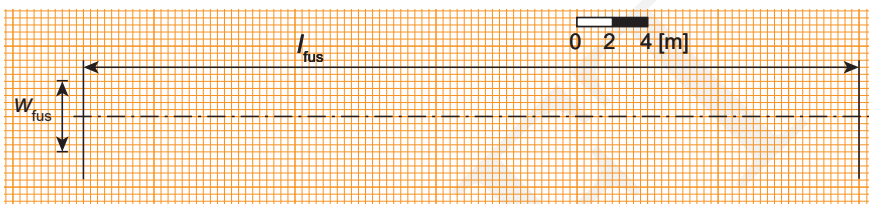
Step 2 We select a nose length of $l_n = 4.0$ m. We select a tail-cone fineness ratio of 3.2 and a tail-to-tail-cone ratio of 0.65. This gives a tail-cone length of $l_{tc} = 3.2 \cdot 4.00 = 12.8$ m and $l_t = 0.65 \cdot 10.6 = 8.3$ m. The fuselage length is $l_{fus} = 32.4 + 4.0 + 8.3 = 44.7$ m.

Step 3 We select an appropriate scale.

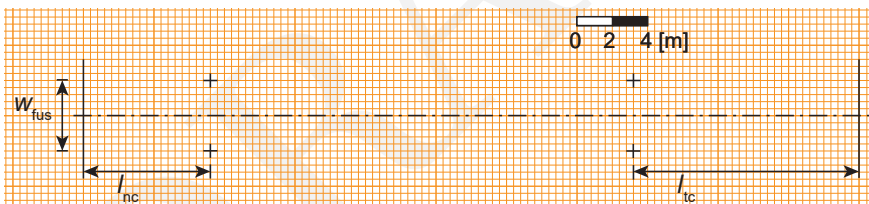
Step 4 We draw the fuselage length.



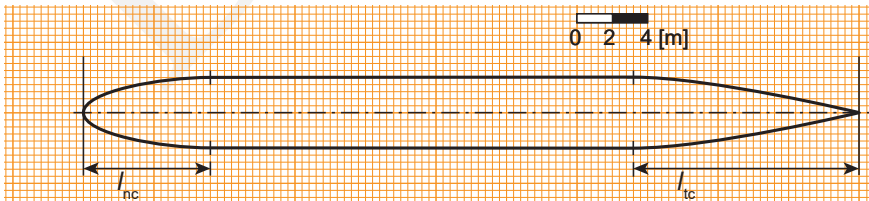
Step 5 The width of the cross-section is 4.0 m. We first draw a symmetry line, and then we indicate the width of the fuselage.



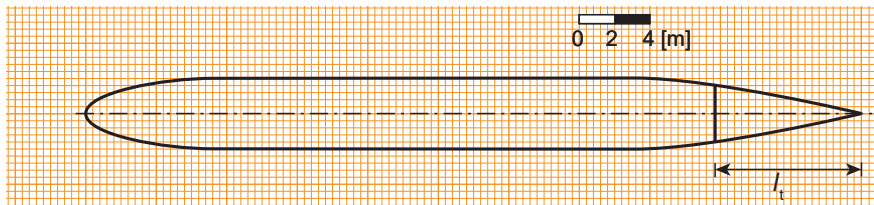
Step 6 We select a nose fineness ratio of 1.8. The resulting nose-cone length is $l_{nc} = 1.8 \cdot 4.0 = 7.2$ m. We draw the bounds for the nose cone and tail cone in the drawing below.



Step 7 We construct the fuselage perimeter in the top view in the drawing below. We make sure we have a blunt nose cone that is slightly elliptical and a tail cone that is tangent to the fuselage.



Step 8 With the tail length, we draw the aft cabin wall. Note that the resulting cabin resides partially in the nose and tail cone. Particularly in the tail cone, there is a noticeable decrease in the cabin's width within the tail cone. Since the standard six-abreast seats would no longer fit, this floor space could be effectively used for a galley and/or lavatory.



Examples 6.5 and 6.6 have shown that the step-by-step procedure can be used for dimensioning the fuselage in the top view, regardless of its actual size. Of course, you should still employ common sense when making choices. If you struggle with deciding what values to choose for the parameters of Table 6.5, you can consult your reference airplanes (see Section 3.4). By measuring the dimensions of their nose-cone and tail-cone lengths, you might get a better idea of acceptable values for these parameters.

ASSIGNMENT 6.3

In this assignment, you will design your fuselage in the top view.

- Choose a value for the following dimensional parameters of the nose and tail cone of the fuselage. Substantiate your choice in a single sentence.
 - nose length: l_n
 - nose-cone slenderness ratio: l_{nc}/d_{fus}
 - tail-cone slenderness ratio: l_{tc}/d_{fus}
 - tail-to-tail-cone length ratio: l_t/l_{tc}
- Use the sequence of the design steps at the beginning of this section to draw your fuselage in the top view.
- What is the resulting cabin length, l_{cabin} ?
- What is the resulting length of your fuselage, l_{fus} ?

6.5. DESIGN OF THE FUSELAGE IN SIDE VIEW

Now that you have designed the cross-section of the fuselage as well as its top view, it is time to design the fuselage in the side view. To be able to design the fuselage in the side view, we need to consider the impact of three requirement sets:

- emergency evacuation (Sec. 6.1.2))
- pilot visibility (Sec. 6.1.4)
- ground clearance (Sec. 6.1.5)

We will discuss what the effect of each of these requirements is on the fuselage design and how that affects the side view drawing of the fuselage.

The requirements on pilot visibility, ground clearance, and emergency evacuation influence the design of the fuselage in the side view. If we combine these requirements with the results from the design of the fuselage cross-section and the design of the fuselage in top view, we can design the fuselage in side view by performing the following design steps:

Step 1 Determine fuselage height from cross-section.

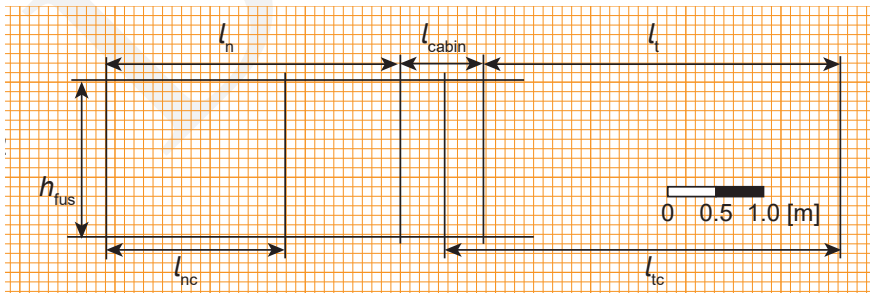
- Step 2* Copy nose cone and tail cone locations from the top view.
- Step 3* Determine flight deck location.
- Step 4* Draw main deck floor, lower deck floor (if applicable), and flight deck floor.
- Step 5* Determine the location of the pilot's eye and draw the field of view.
- Step 6* Choose an upsweep angle and determine the vertical position of the tail cone endpoint. Choose a vertical position of the nose point.
- Step 7* Construct crown and belly curves
- Step 8* Determine the type of passenger doors and their respective locations and draw them to scale.
- Step 9* Copy doors and windshield design to top view.

By following this step-by-step process, you arrive at a conceptual design of the fuselage in side view. The distribution of the emergency exits could still change at a later stage due to the integration of the wing and/or the propulsion system. In the following two examples, the presented procedure is applied to our two demonstration airplanes.

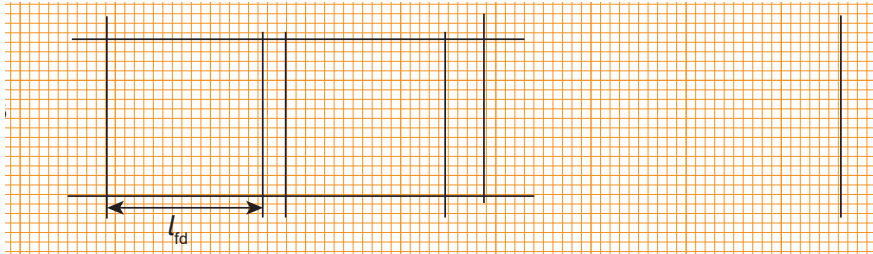
Example 6.7

In this example, we show how the step-by-step procedure can be used to design the fuselage of the four-seat airplane of Example 6.5 in side view.

- Step 1* We take the height of the fuselage (h_{fus}) from the design of the cross-section and draw two horizontal lines that mark the upper and lower sides of the fuselage.
- Step 2* We copy all the longitudinal dimensions from the top view and add them as vertical lines to our drawing.

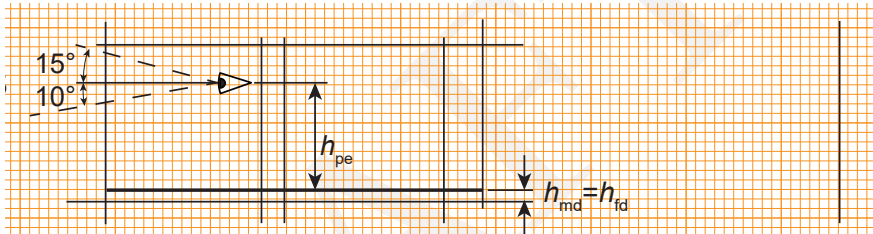


- Step 3* The two front seats are for the pilot and possibly a co-pilot. We term this part of the fuselage the “flight deck.” . Based on the anthropometrics, we estimate the length of the flight deck to be 1.6 meters from the beginning of the fuselage. We draw this dimension into the drawing.



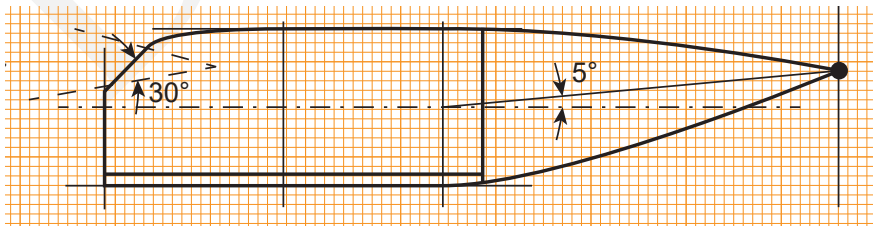
Step 4 In this small airplane, there is no real distinction between the main deck and the flight deck. We draw a line for the complete floor, 15 cm above the bottom curve of the fuselage, to allow for structure.

Step 5 Based on anthropometrics, we estimate that the pilot's eye is located 1.2 m behind the front of the fuselage and 1.1 m above the floor. We assume there is an over-nose requirement of 10 degrees and an upward-viewing requirement of 15 degrees. We draw the pilot's eye and field of view.



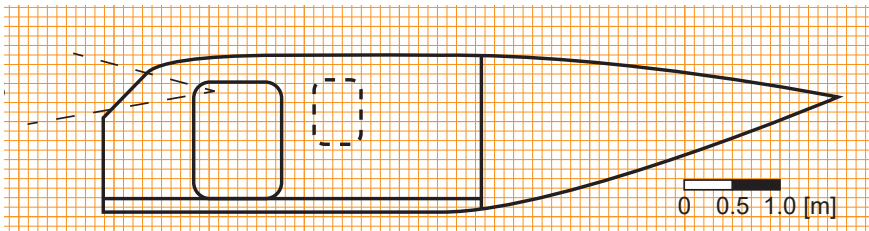
Step 6 We choose an upsweep angle of 5 degrees and construct a straight line from the beginning of the tail cone until the end of the fuselage. We place a dot at the resulting endpoint of the fuselage. We do not place a single point for the start of the fuselage, because we know that an engine still needs to be placed ahead of the fuselage.

Step 7 We construct the crown and belly curve of the fuselage by using all the points and lines that we have drawn so far as guides for our drawing. Note that construct a distinct cockpit shape, with a windshield that has a grazing angle that equals 30 degrees.

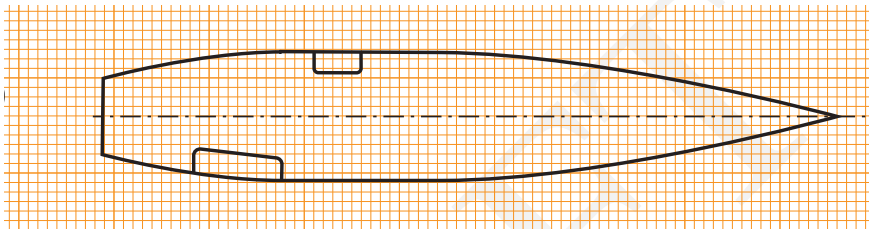


Step 8 Referring to the regulatory requirements regarding emergency evacuation of Example 3.15, we need a minimum of two exit doors, each measuring at least 48-by-66 cm. We choose to have a larger passenger door on the left-hand side of the airplane to enable easy boarding of the airplane. In addition, we choose a door of minimum size on the right-hand side of the airplane. The boarding door is

positioned close to the pilot's seat. The emergency exit is positioned in between the pilot seats and rear seats.



- Step 9** We copy the location of the two doors in the top view of the airplane to show on which side each of the emergency exits is located.



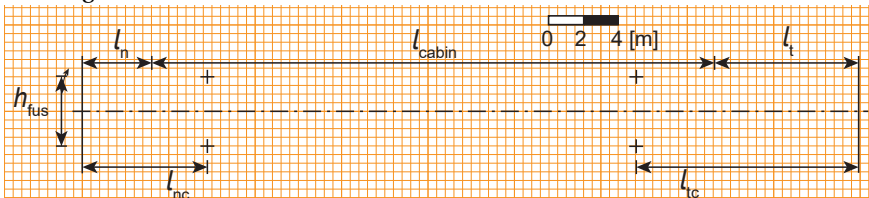
Let us briefly reflect on the design we have just constructed. The design fulfills the requirements in terms of pilot visibility and emergency evacuation. Regarding the clearance of the tail, we have already provided some upsweep in the tail cone. However, only when we integrate the landing gear will we know whether this is an adequate angle. Furthermore, the over-nose angle of 10 degrees shall also impact the shape of the engine cowling that is yet to be added ahead of the fuselage. The following example shows how the design sequence is applied to our 130-seater.

Example 6.8

In this example, we design the fuselage of the large passenger airplane of Example 6.6 in side view.

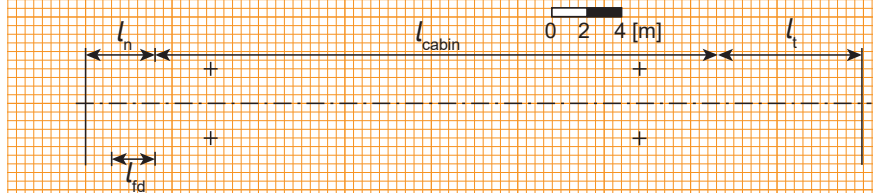
- Step 1** From Example 6.4, we know that the height of the fuselage is $h_{\text{fus}} = 4.00 \text{ m}$. We draw this height on our canvas.

- Step 2** We copy all fuselage dimensions from the top view design of Example 6.6 to our drawing in side view.



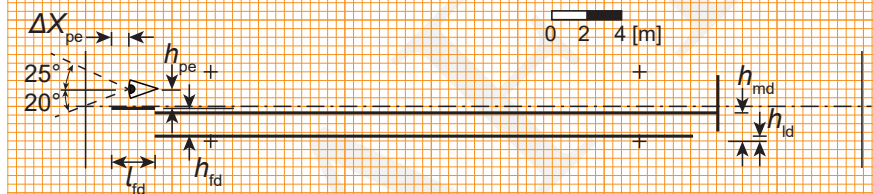
- Step 3** We decide that the cockpit of his airplane has a crew of two pilots and select a flight deck length of 2.5 m. The flight deck ends at the longitudinal location

where the cabin starts.



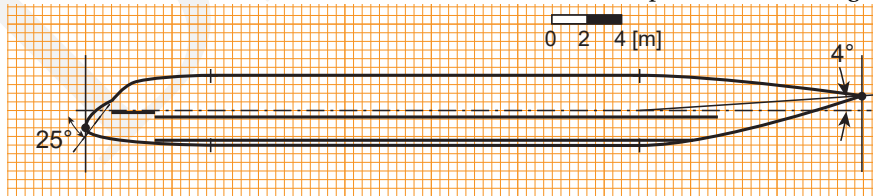
Step 4 From Example 6.4, the distance from the keel of the fuselage to the main deck is 1.63 m. The height of the lower deck is 0.29 m above the keel of the cross-section. We decide to raise the flight deck by 25 cm with respect to the cabin deck to enable more volume below the floor for stowage of the nose landing gear. We draw the main deck, lower deck, and flight deck in our drawing.

Step 5 The pilot's eye is located at 1.0 m behind the start of the flight deck and 1.1 m above the flight deck. We draw the position of the pilot's eye along with an over-nose angle of 20 degrees and an upward viewing angle of 25 degrees.

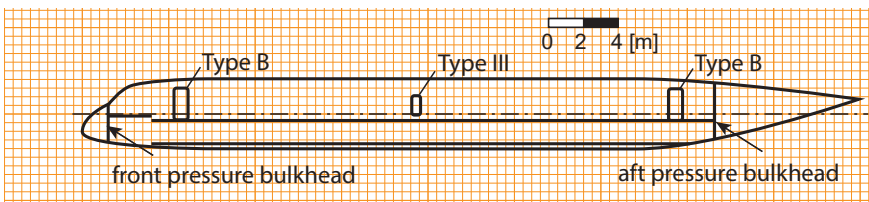


Step 6 We choose an upsweep angle of 4 degrees and draw the endpoint of the fuselage. We also draw the tip of the nose at a vertical location somewhere between the flight deck and the keel of the airplane.

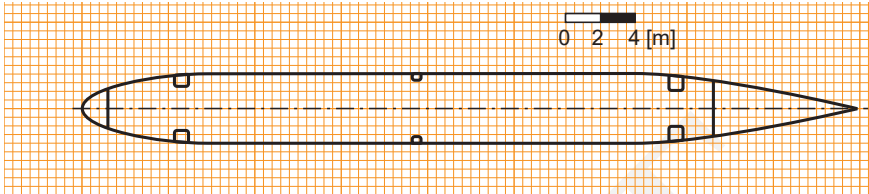
Step 7 Using all the guides that we have made so far, we draw the perimeter of the fuselage in the side view. We select a grazing angle of 25 degrees for the cockpit windshield. We make sure that the lines that we construct are smooth, except for the kink at the lower side of the windshield and the endpoint of the fuselage.



Step 8 Based on the maximum number of passengers (180) and the regulations provided in Example 3.16, we decide to use two pairs of Type B exits (150 passengers) and one pair of Type III exits (35 passengers). We position each pair of Type B exits on either side of the cabin, leaving some space for a galley. The pair of Type III doors is positioned between these exit pairs. The Type III doors are envisioned to become over-wing exits. Their longitudinal positions could, therefore, still change at a later stage of the design.



Step 9 We copy the doors from the side view of the airplane to the top view.



The previous examples have demonstrated that the design sequence presented at the beginning of this section can be used for both small and large airplanes. Note that for CS-25 airplanes, you are choosing how many *pairs* of emergency exits you need based on the number of seats. For example, if you would have 330 seats, this would mean you would have to install 3 pairs of Type A exits to facilitate emergency evacuation. This means 6 emergency exits in total, 3 on either side. In the following assignment, you will practice designing your fuselage in the side view.

ASSIGNMENT 6.4

In this assignment, you will design your fuselage in the side view.

- What upward view angle and over-nose angle do you choose for the pilot of your airplane and why?
- What upsweep angle do you choose for the tail cone of your fuselage and why?
- Follow the steps laid out at the beginning of this section and design your fuselage in the side view.
- Motivate why your decision on the distribution of the emergency exits.

7

WING AND PROPULSION SYSTEM SIZING

Many of the requirements that we have derived from the mission profile relate to the flight performance of your airplane (see Example 3.3). Also, many of the airworthiness regulations dictate flight performance minima (see Table 3.2). This includes requirements on the climb rate, the climb gradient, cruise speed, landing distance, take-off distance, approach speed, and sometimes stall speed. In this chapter, we use these requirements to *size* the wing and the propulsion system. Section 2.3 has explained how the sizing process works in general. In this chapter, we are going to make this more concrete. We employ flight mechanics relations to estimate the wing loading and power loading (or thrust-to-weight ratio) of your airplane. These, in turn, are required to compute the wing area and the power or thrust of the propulsion system at take-off.

Let us first define “wing loading,” “power loading,” and “thrust-to-weight” ratio. The wing loading is defined as the amount of weight (W) per unit of wing area (S_w). The weight is the mass of the airplane times the gravitational acceleration (g). During flight, fuel-burning airplanes become lighter. Therefore, their wing loading changes. However, in the context of the design of a fixed-wing airplane, when we talk about “wing loading,” we imply the maximum take-off weight per unit area, i.e.:

$$\frac{W_{TO}}{S_w} = \frac{m_{MTOG}}{S_w} \quad (7.1)$$

The power loading is a term that we associate with propeller-powered airplanes. The power (P) produced by electric motors is virtually independent of the altitude, ambient temperature, or flight speed. While the power produced by air-breathing engines is independent of speed, they produce less power with increasing altitude and temperature (see Section 7.4.2). When we mention “power loading” in the context of this textbook, we mean the maximum take-off weight per unit of available take-off power at mean sea-

level conditions, assuming an international standard atmosphere (ISA¹), i.e.:

$$\frac{W_{TO}}{P_{TO}} = \frac{m_{MTO}g}{P_{TO, SL}} \quad (7.2)$$

The thrust-to-weight ratio is a term that we associate with jet-powered airplanes. For pure turbojet engines, the thrust (T) is (virtually) independent of the speed, which makes it easy to work with in calculations. For the turbofan engines, the thrust lapses with increasing speed, increasing altitude, and increased temperature (see Section 7.4.2). Therefore, turbofan engines are typically rated according to their sea-level static (SLS) thrust under ISA conditions. To be able to select an engine, we need to find the required thrust-to-weight ratio of the airplane, which is defined as follows:

$$\frac{T_{TO}}{W_{TO}} = \frac{T_{TO, SLS}}{m_{MTO}g} \quad (7.3)$$

7.1. FLIGHT PERFORMANCE REQUIREMENTS

In this section we are going to size the wing and the powerplant of a jet-powered airplane and a propeller-powered airplane such as they fulfill requirements on:

1. Stall speed (V_s) or approach speed (V_{app})
2. Landing field length (LFL, \mathcal{L}_{LF})
3. Cruise speed (V_{CR}) or cruise Mach number (M_{CR})
4. Climb rate (c)
5. Climb gradient (G)
6. Take-off field length (TOFL, \mathcal{L}_{TO})

Each of these requirements can be related to the wing loading and thrust-to-weight ratio or power loading of the airplane. We can construct a diagram with on the horizontal axis the wing loading and on the vertical axis the thrust-to-weight ratio or power loading such that each requirement can be represented as a curve in this axis system (see Figure 7.1). These so-called constraint curves bound a two-dimensional area in the diagram representing the “feasible design space.” In other words, each point in this area represents a combination of wing loading and thrust-to-weight ratio that fulfills all performance requirements. We then go on to select the *best* point according to our stated design objective. In the subsequent paragraphs, we show how you can construct this diagram and select the appropriate design point.

As the flight performance of airplanes is related to their aerodynamic performance, the drag polar (Section 5.2.1) is required. Furthermore, the *maximum lift coefficients* also needs to be assumed along with the assumed propeller efficiency (if necessary).

The following example introduces the two airplanes and associated aerodynamic characteristics that are used throughout the remainder of this section.

Example 7.1

In this section, we consider the design of a propeller-powered airplane and a jet airplane. Based on the TLARs, we know that the propeller airplane is going to be certified

¹The international standard atmosphere defines the pressure, density, and temperature as a function of altitude above mean sea level (SL). See wikipedia.org.

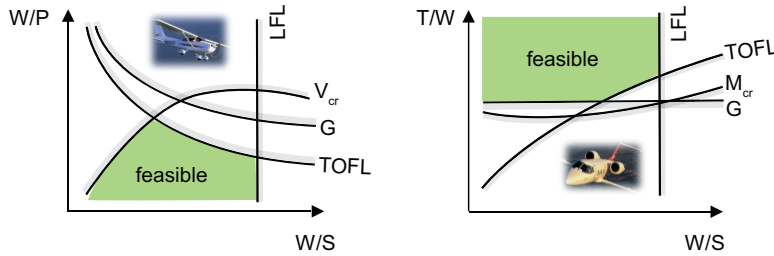


Figure 7.1: Schematic examples of the constraint diagrams for propeller-powered airplanes (left) and jet-powered airplanes (right). Each line represents a flight performance requirement and imposes a constraint on the feasible design space.

according to CS/FAR-23 and the jet airplane according to CS/FAR 25. We have made the following design decisions for each of them:

	propeller	jet
energy carrier	battery	kerosene
Number of engines/motors (N_e)	1	2
aspect ratio (\mathcal{R})	9.0	8.0
landing gear	fixed	retractable
Bypass ratio (B)	-	10
Cruise altitude (h_{CR}) [m]	1800	10,000

For the **propeller airplane**, the performance requirements are listed below. Note that all but one requirement is to be evaluated at sea-level (SL) altitude assuming ISA conditions and at maximum take-off mass. Requirements include engine operative (EO) and engine inoperative (EI) conditions as well as three configurations regarding the flap settings: cruise (CR), take-off (TO), and landing (L).

requirement	alt. (m)	temp (K)	eng.	flaps	gear	m/m_{MTO}	value
V_{S0} (m/s)	0	T_{ISA}	EI	L	↓	1.0	31
\mathcal{L}_{LF} (m)	0	T_{ISA}	EI	L	↓	1.0	750
V_{CR} (m/s)	1800	T_{ISA}	EO	CR	↓	1.0	70
c (m/s)	0	T_{ISA}	EO	CR	↓	1.0	2.0
G (%)	0	T_{ISA}	EO	TO	↓	1.0	8.3
\mathcal{L}_{TO} (m)	0	T_{ISA}	EO	TO	↓	1.0	750

The requirements for the **jet airplane** are a bit more elaborate and are shown in the table below. Here, we also consider “hot” conditions for two requirements, where the temperature is 15° higher than standard ISA conditions. Also, we have two one-engine inoperative (OEI) requirements: one for the climb gradient and one for the take-off field length. Furthermore, we also consider “hot-and-high” conditions for the take-off field length. Furthermore, the landing gear (gear) can either be up or down, which is indicated by an arrow in the table below. Finally, the ratio m/m_{MTO} is lower than one for some of the requirements as we assume that part of the fuel has been burned when this requirement needs to be satisfied.

requirement	alt. (m)	temp. (K)	eng.	flaps	gear	m/m_{MTO}	value
V_{APP} (m/s)	0	T_{ISA}	AEI	L	↓	0.85	68
\mathcal{L}_{LF} (m)	1600	$T_{ISA} + 15^\circ$	AEI	L	↓	0.85	1800
M_{CR} (-)	$10 \cdot 10^3$	T_{ISA}	AEO	CR	↑	0.95	0.81
c (m/s)	$10.5 \cdot 10^3$	$T_{ISA} + 15^\circ$	AEO	CR	↑	0.95	0.50
G (%)	0	T_{ISA}	OEI	TO	↑	1.0	2.4
\mathcal{L}_{TO} (m)	1500	$T_{ISA} + 15^\circ$	OEI	TO	↓	1.0	2500

The requirements presented in Example 7.1 are made specific and measurable according to the guidelines provided in Section 3.2. The cruise altitude, h_{CR} , needs to be assumed at this stage. In Chapter 10, we will show how the optimal altitude can be computed. If the optimal altitude is known, this should be used instead of the assumed altitude we use here. The elevated temperature and altitude of the jet airplane lead to a reduction in air density. The lift and drag directly depend on the density. The available shaft power of piston engines and turboprops also scales with density according to (7.24). Depending on the bypass ratio, the thrust of a turbofan engine scales with ambient pressure, temperature, and Mach number according to Eqs. (7.35)-(7.38).

To evaluate the requirements, we introduce the mass ratio β as follows:

$$\beta = \frac{m}{m_{MTO}} \quad (7.4)$$

where m is the mass at which the requirement needs to be evaluated. For example, a landing field length requirement might specify a landing mass below the maximum take-off mass. At this stage of the design, we therefore use the mass ratio. However, we need to be careful that $1 - (m_f/m_{MTO}) < \beta \leq 1$ as the reduction in mass is due to the fuel that is burned off. Many transport airplanes are designed with a maximum landing mass (MLM) that is significantly lower than the maximum take-off mass. When such an airplane needs to land right after take-off in an emergency situation, it has to quickly dump fuel to arrive at its MLM. On the other hand, for full-electric airplanes that use batteries as their energy carrier, $\beta \equiv 1$ for all requirements.

7.2. MINIMUM SPEED

A minimum speed requirement can be specified in terms of a stall speed requirement or an approach speed requirement. In this section, we show how the minimum speed requirement translates into a wing loading requirement, what maximum lift coefficient you should select, and how to draw the constraint line in the matching diagram.

7.2.1. FLIGHT MECHANICS

The first requirement that we investigate is the stall speed requirement for the propeller airplane. V_{S0} is the stall speed in landing configuration, which is obtained when the angle of attack of the wing is increased until the lift coefficient reaches its maximum. In Figure 7.2, it is shown how the lift coefficient of a wing varies with the angle of attack. At low angles of attack, the lift coefficient changes linearly with the angle of attack. At a particular angle of attack, the flow starts to separate. This is the onset of the stall. Increasing the angle of attack further increases the stall region, while outside of the stall

region, the lift still increases with the angle of attack. At the stall angle-of-attack, the *maximum lift coefficient* is reached, beyond which the lift coefficient decreases with the angle of attack.

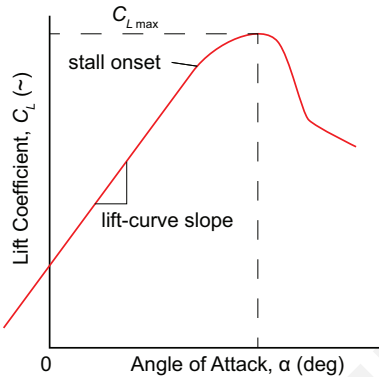


Figure 7.2: Lift curve with maximum lift coefficient.

If we examine the lift equation (5.7), substitute $V = V_{S0}$ and $C_L = C_{L\max}$ and know that $L = \beta W_{TO}$, we can interpret this requirement as a constraint on the wing loading:

$$\frac{W_{TO}}{S_w} < \frac{1}{\beta} \frac{\rho}{2} V_{S0}^2 C_{L\max} \quad (7.5)$$

For the jet airplane, we have an approach speed requirement, which, according to CS/-FAR 25.125, should be higher or equal to 1.23 times the reference stall speed. In other words, for the jet airplane, the wing loading should not be higher than:

$$\frac{W_{TO}}{S_w} < \frac{1}{\beta} \frac{\rho}{2} \left(\frac{V_{app}}{1.23} \right)^2 C_{L\max} \quad (7.6)$$

As you can see, for either requirement, we need a value for the maximum lift coefficient in order to evaluate the constraint. Many airplanes feature so-called *high-lift devices* to increase the maximum lift coefficient of the wing. As you can see, from the equations above, increasing the maximum lift coefficient leads to a higher wing loading for the same speed requirement. In the subsequent section, we explain how you can estimate the maximum lift coefficient.

7.2.2. ESTIMATING THE MAXIMUM LIFT COEFFICIENT

Flaps are an example of high-lift devices that are installed to increase the maximum lift coefficient of the airplane and thereby improve the overall field performance. How effective high-lift devices are, depends on a variety of factors, including the sweep angle of the wing, the size of the high-lift devices, and whether they act on the leading edge or trailing edge of the wing. None of these aspects are known at this stage. Therefore, we need to make an (informed) assumption on how much lift we can obtain from the wing with and without high-lift devices deployed. Table 7.1 provides some guidance in

selecting the value for $C_{L_{\max}}$ in cruise, take-off, and landing configuration for a variety of airplane types. Note, that minimum and maximum values are given that are typically found on the types of airplanes that are listed. In Chapter 10, you will design the high-lift system for your airplane, and the assumption that you make here will be updated with a value based on the actual flap design of your airplane.

Table 7.1: Tabulated minimum and maximum values for $C_{L_{\max}}$ for various airplane types. Data from [13]

airplane type	$C_{L_{\max, CR}}$	-	$C_{L_{\max, TO}}$	$C_{L_{\max, L}}$	-	$C_{L_{\max, L}}$	-	$C_{L_{\max, L}}$	
homebuilts	1.2	-	1.8	1.2	-	1.8	1.2	-	2.0
single engine/motor props	1.3	-	1.9	1.3	-	1.9	1.6	-	2.3
twin engine props	1.2	-	1.8	1.4	-	2.0	1.6	-	2.5
business jets	1.4	-	1.8	1.6	-	2.2	1.6	-	2.6
regional turboprops	1.5	-	1.9	1.7	-	2.1	1.9	-	3.3
transport jets	1.2	-	1.8	1.6	-	2.2	1.8	-	2.8

The maximum lift coefficient in landing configuration is usually the highest. The maximum lift coefficient in cruise configuration is the lowest. The take-off flap setting is usually somewhere in between the cruise configuration and the landing configuration. This is done to strike a balance between the increase in lift and the decrease in lift-to-drag ratio due to the deployment of high-lift devices. In the subsequent assignment, you will make assumptions on the maximum lift coefficient of your airplane. The questions will guide you in making the assumptions.

ASSIGNMENT 7.1

In this assignment, you make explicit assumptions about the maximum lift coefficients of your airplane.

- a. Considering Table 7.1, what airplane type does your design fall under?
- b. In the cruise configuration, i.e., with all high-lift devices stowed, what value of $C_{L_{\max, CR}}$ do you assume?
- c. Do you envision your airplane to have high-lift devices on the trailing edge?
- d. Do you envision your airplane to have high-lift devices on the leading edge?
- e. Based on your answers above, make an assumption on $C_{L_{\max, L}}$. When making the assumption, make sure that $C_{L_{\max, L}} \geq C_{L_{\max, CR}}$.
- f. Based on your answers above, make an assumption on $C_{L_{\max, TO}}$. When making the assumption, make sure that $C_{L_{\max, CR}} \leq C_{L_{\max, TO}} \leq C_{L_{\max, L}}$.

7.2.3. CONSTRUCTING THE CONSTRAINT LINE

Now that we have made an assumption on the maximum lift coefficients, we can proceed to construct the landing constraint line in the matching diagram. In the subsequent discussion, we use the maximum lift coefficient in landing configuration: $C_{L_{\max}} = C_{L_{\max, L}}$. We first show how the landing constraint is produced for our two example airplanes.

Example 7.2

We use the requirements, specified in Example 7.1. Furthermore, we use the following assumptions for the maximum lift coefficients:

	flaps	gear	$C_{L_{\max}}$
propeller	L	↓	2.1
jet	L	↓	2.5

PROPELLER AIRPLANE For the propeller airplane, we utilize the stall speed requirement in landing configuration (V_{S0}), given at sea-level conditions assuming standard ISA temperature. The wing loading required to fulfill this requirement is readily obtained by substituting all relevant data from Example 7.1 into (7.5). We then find:

$$\frac{W_{TO}}{S_w} < 1200 \text{ N/m}^2$$

As you can see, the wing loading is independent of the power loading of the airplane, as this requirement is evaluated assuming the engine is inoperative (EI). We now are going to set up the matching diagram. We set the bounds for this diagram at $W_{TO}/S_w = 1900$ [N/m²] and $W_{TO}/P_{TO} = 0.5$ [N/W]. For minimum and maximum power loading, we then have:

W_{TO}/S_w [N/m ²]	W_{TO}/P_{TO} [N/W]	1200	1200
		0	0.5

Obviously, this becomes a straight vertical line in the matching diagram. This is shown in Figure 7.3, where the hash markings indicate the side of the boundary for which the stall-speed constraint is not satisfied.

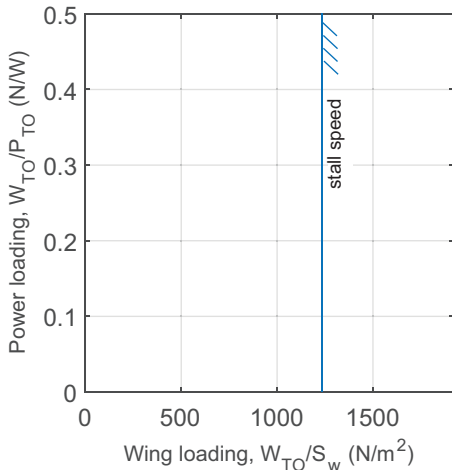


Figure 7.3: Stall-speed requirement for propeller airplane.

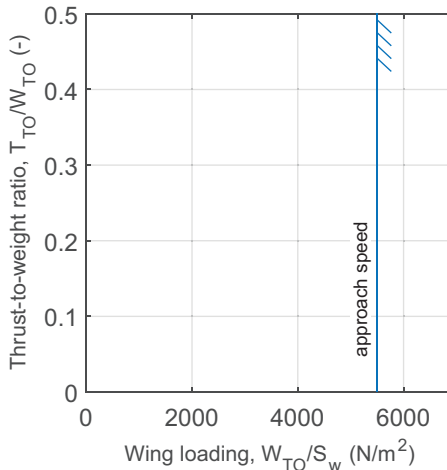


Figure 7.4: Approach-speed requirement for jet airplane.

JET AIRPLANE For the jet airplane, we have an approach speed of 68 m/s specified at sea level conditions and a landing mass which is 85% of the take-off mass (i.e., $\beta = 0.85$).

We compute the required wing loading by evaluating (7.6):

$$\frac{W_{TO}}{S_w} < 5500 \text{ N/m}^2$$

To construct the diagram, we set the bounds of this diagram to $W_{TO}/S_w = 7000 \text{ N/m}^2$ and $T_{TO}/W_{TO} = 0.5$. For the approach speed constraint, we have:

W_{TO}/S_w	[N/m ²]	5500	5500
T_{TO}/W_{TO}	[-]	0	0.5

In the matching diagram, this constraint becomes a straight line again. This is shown in Figure 7.4, where the hash marking indicates the infeasible side of the approach-speed boundary.

ASSIGNMENT 7.2

In this assignment, you will add a minimum-speed requirement to the matching diagram.

- Given your minimum speed requirement of Assignment 3.6, state the stall speed (V_{S0}) or approach speed (V_{app}) along with the following specified values: h , ΔT , β .
- Compute the maximum take-off wing loading of your airplane according to the minimum speed constraint of the previous step.
- Choose your wing-loading bound for the matching diagram along with a bound for the wing-loading or thrust-to-weight ratio, whichever one applies.
- Setup your matching diagram
- Draw your minimum-speed constraint in the matching diagram.

If a minimum speed requirement is given at a nonzero altitude or at a non-standard temperature, the corresponding density needs to be computed. The density is a function of the temperature and pressure. In the next section, we show how the variation in altitude and temperature can influence the maximum wing loading.

7.3. LANDING FIELD LENGTH

Now that we have made a start with creating the matching diagram, we continue with the second requirement on our list: the landing field length. For that, we first need to understand what constitutes a landing and what factors play a role in the distance. Since a landing distance can be specified at a certain altitude and temperature, we also need to investigate the effect of these variations on the density at the landing condition. We can then proceed to draw the line corresponding to the landing requirement in our matching diagram.

7.3.1. FLIGHT MECHANICS

The landing maneuver is explained in CS/FAR 23 and CS/FAR 25 and schematically shown in Figure 7.5. The landing field length starts when the airplane flies over an obstacle with

a height of 15 m (50 ft) and ends when the airplane has come to a standstill. It, therefore, comprises an air distance, \mathcal{L}_{AIR} , from obstacle to touchdown, as well as ground-roll distance, \mathcal{L}_{GR} , from touchdown till standstill. While CS/FAR 23 specifies the landing field length simply as the addition of the two components, the LFL of CS-25 airplane is extended by 2/3 of that distance for safety reasons:

$$\mathcal{L}_{\text{LF}} = \mathcal{L}_{\text{AIR}} + \mathcal{L}_{\text{GR}} \quad \text{for CS/FAR-23} \quad (7.7)$$

$$\mathcal{L}_{\text{LF}} = \frac{1}{0.6} (\mathcal{L}_{\text{AIR}} + \mathcal{L}_{\text{GR}}) \quad \text{for CS/FAR-25} \quad (7.8)$$

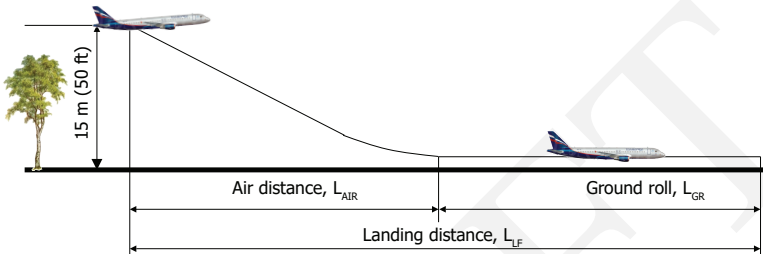


Figure 7.5: Definition of the landing field length, \mathcal{L}_{LF} , according to CS/FAR 23.

The total landing field length depends on the final approach speed V_{APP} that the airplane has when flying over the obstacle height as well as on the deceleration in the air and on the ground. While there is not much deceleration in the air, the air distance is dominated by the glide slope during the landing maneuver. Most of the deceleration takes place on the ground when the brakes are applied. The total landing distance is, therefore, largely dependent on the number of wheels and tire pressure, the runway type (grass, gravel, tarmac), the runway condition (dry, wet, icy), the available brake power, the application of lift dumpers (e.g. spoilers), the application of aerodynamic brakes (e.g. spoilers), pilot technique, and weather conditions. All of these aspects make it unavoidable to use statistics to estimate the landing field length.

Based on References [13] and [18], we relate the stall speed of the airplane in landing configuration to its landing distance on a dry runway as follows:

$$\mathcal{L}_{\text{LF}} = C_{\text{LFL}} V_{\text{S0}}^2 \quad (7.9)$$

where V_{S0} is the stall speed in landing configuration and C_{LFL} is the landing-field-length coefficient. We assume $C_{\text{LFL}} \approx 0.60$ [s^2/m] for CS/FAR-23 airplanes and $C_{\text{LFL}} \approx 0.45$ [s^2/m] for CS/FAR-25 airplanes. These numbers are subject to statistical validation and should be used with caution. The lower value of C_{LFL} for CS/FAR-25 airplanes implies that while their LFL is 67% longer than the sum of the air distance and ground roll distance, the combination of automated lift dumpers, strong wheel brakes and (supposedly) superior pilot technique results in a shorter field length per unit of stall speed.

Airplanes with variable-pitch propellers or turbofan engines often apply thrust reversing to reduce the landing field length and/or to reduce the wear on the wheel brakes.

According to the regulations, these are not to be included in the computation of the minimum landing distance on a dry runway. This is because an engine-inoperative condition should not impact the minimum landing distance.

Now, that we have explained the mechanics of a landing maneuver, let us return to the landing distance requirement. Apart from the landing distance measured in meters, the requirement can specify the altitude and temperature conditions at which this landing distance requirement needs to be met. A landing in so-called *hot and high* conditions happens at a lower density than at sea level. Therefore, we need to compute the density at which the landing requirement is given.

7.3.2. ATMOSPHERIC TEMPERATURE, PRESSURE AND DENSITY

The temperature, pressure, and density change as a function of altitude and weather conditions. Here, we limit our analysis to the effect of altitude and temperature on these properties, while we assume the International Standard Atmosphere (ISA).

The static temperature in Kelvin at altitude (h) can be computed using a simplified version of the international standard atmosphere:

$$T = T_{\text{SL ISA}} + \Delta T + \lambda h \quad \text{for } 0 \leq h < 11 \text{ km} \quad (7.10)$$

$$T = T_{\text{TP ISA}} + \Delta T \quad \text{for } 11 \leq h < 20 \text{ km} \quad (7.11)$$

where $T_{\text{SL ISA}} = 288 \text{ K}$ is the sea-level temperature, $T_{\text{TP ISA}} = 217 \text{ K}$ is the temperature at the tropopause, $\lambda = -0.0065 \text{ K/m}$ is the temperature lapse rate with altitude, and ΔT represents a change in temperature due to weather conditions. The latter allows us to evaluate the flight performance of airplanes on a hot day, i.e., when $\Delta T \geq 15 \text{ K}$. We make the simplified assumption that the temperature lapse rate of $-6.5^\circ/\text{km}$ is independent of the temperature conditions.

The atmospheric pressure (p) in the troposphere and in the stratosphere can be related to the altitude (h) using the following formulas, respectively:

$$p = p_{\text{SL ISA}} \left(1 + \frac{\lambda h}{T_{\text{SL ISA}}} \right)^{-\frac{g}{\lambda R}} \quad \text{for } 0 \leq h < 11 \text{ km} \quad (7.12)$$

$$p = p_{\text{TP ISA}} \exp \left(\frac{-g(h - h_{\text{TP ISA}})}{R T_{\text{TP ISA}}} \right) \quad \text{for } 11 \leq h < 20 \text{ km} \quad (7.13)$$

where $p_{\text{SL ISA}} = 101 \text{ kPa}$ is the sea-level pressure under ISA conditions, $p_{\text{TP ISA}} = 22.6 \text{ kPa}$ is the ambient pressure at the tropopause, $h_{\text{TP ISA}} = 11 \text{ km}$ is the altitude of the ISA tropopause, and $R = 287 \text{ J/kg/K}$ is the gas constant for air. To compute the density, we employ the equation of state for an ideal gas:

$$\rho = \frac{p}{RT} \quad (7.14)$$

These equations allow us to compute the temperature, pressure, and density as a function of altitude (h) and temperature deviation (ΔT).

The pressure and temperature variation with altitude is depicted in Figure 7.6. In addition, the icons depict the typical altitude where various types of airplanes cruise efficiently. Between an altitude of 5 km and 6 km, the low pressure can cause hypoxia, a

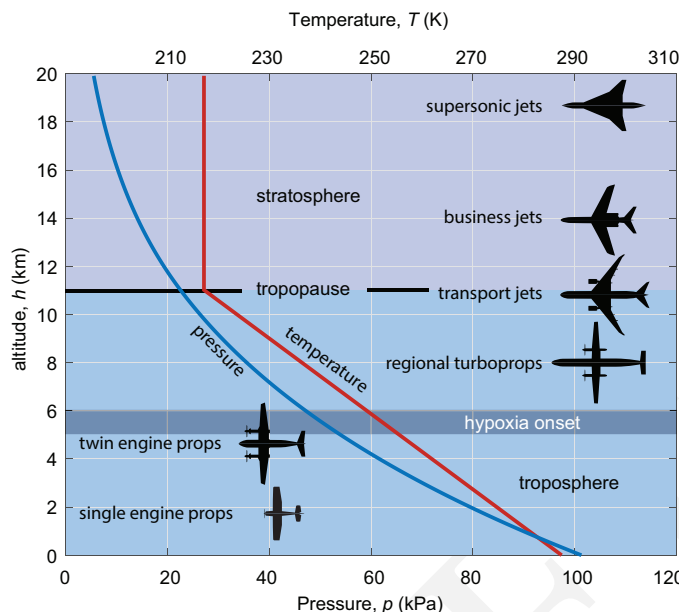


Figure 7.6: Relation between altitude and atmospheric pressure in International Standard Atmosphere. The airplane icons indicate a typical cruise altitude for various types of airplanes.

state where there is insufficient oxygen in the blood leading to a loss of consciousness. Therefore, a pressurized cabin is required when flying above these altitudes.

Example 7.3

In this example, we compute the density at an altitude of 1600 m and a temperature of $T + T_{ISA} + 15^\circ\text{C}$. These values correspond to the landing field length requirement for the jet airplane from Example 7.1.

Using the temperature lapse in the troposphere ($\lambda = -0.0065^\circ\text{C}/\text{m}$), the temperature at the landing condition can be computed as follows:

$$T = -0.0065 \cdot 1600 + 15 = 293\text{ K}$$

Using (7.12), the pressure at the landing altitude is:

$$p = 101 \cdot 10^3 \left(1 + \frac{-0.0065 \cdot 1600}{288} \right)^{-\frac{9.81}{-0.0065 \cdot 287}} = 84 \text{ kPa}$$

Using the Equation 7.14, we compute the density for the landing condition:

$$\rho = \frac{84 \cdot 10^3}{287 \cdot 293} = 0.99 \text{ kg/m}^3$$

7.3.3. CONSTRUCTING THE CONSTRAINT LINE

Now that we have computed the density, we now employ the lift equation to relate the maximum wing loading to the minimum landing distance:

$$\frac{W_{TO}}{S_w} < \frac{1}{\beta} \frac{\mathcal{L}_{FL}}{C_{LFL}} \frac{\rho C_{Lmax}}{2} \quad (7.15)$$

where $\beta = m_{ML}/m_{MTO}$ and C_{Lmax} is the maximum lift coefficient in landing configuration. The following example shows how this can be included in the matching diagram.

Example 7.4

We use the requirements and design decisions as specified in Example 7.1. We use the same values for the maximum lift coefficients as in the Example 7.2:

	flaps	gear	C_{Lmax}
propeller	L	↓	2.1
jet	L	↓	2.5

PROPELLER AIRPLANE For the propeller airplane, we have a landing field length of $\mathcal{L}_{LF} = 750$ m at sea level conditions. Assuming $C_{LFL} = 0.6$ and knowing that $\beta = 1$, we find with (7.15):

$$\frac{W_{TO}}{S_w} < 1600 \text{ N/m}^2$$

The corresponding constraint line is added to the matching diagram in Figure 7.7.

JET AIRPLANE For the jet airplane, we have a landing field length of $\mathcal{L}_{LF} = 1800$ m, a temperature of $T_{ISA} + 15^\circ\text{C}$, $\beta = 0.85$, and $C_{LFL} = 0.45$. Because the landing altitude is not zero, we first need to compute the density. We use the calculations from Example 7.3 to have $\rho = 0.99 \text{ kg/m}^3$. Employing (7.15), we find:

$$\frac{W_{TO}}{S_w} < 5840 \text{ N/m}^2$$

The corresponding constraint line is added to the matching diagram in Figure 7.8.

In the previous example, you can see that neither for the propeller airplane nor for the jet airplane does the landing distance become a sizing constraint. The stall speed and approach speed constraint result in a lower maximum wing loading, respectively. In the next assignment, you will add the constraint line corresponding to the landing field length to your matching diagram.

ASSIGNMENT 7.3

In this assignment, you will add the landing-field-length constraint to your matching diagram.

- Given your landing-field-length requirement of Assignment 3.4, state \mathcal{L}_{LF} , h , ΔT , and β .
- Compute the ambient density, ρ , for this requirement.

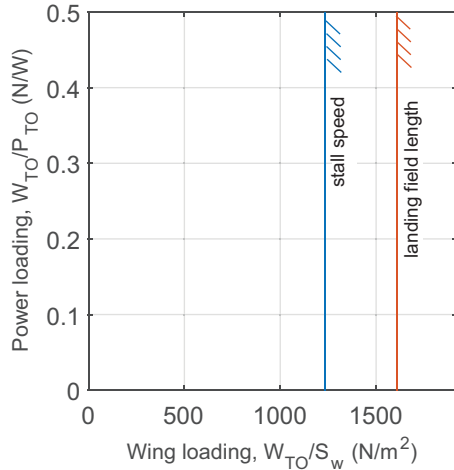


Figure 7.7: Matching diagram with added landing field length requirement for propeller airplane

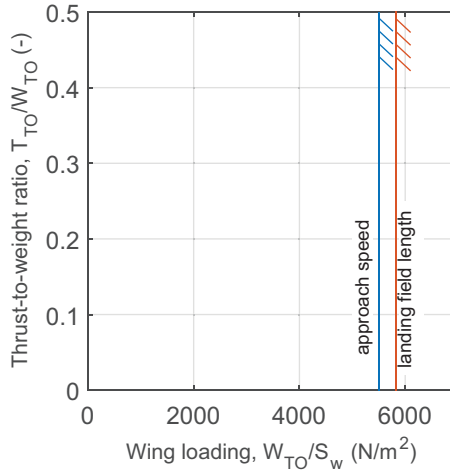


Figure 7.8: Matching diagram with added landing field requirement for jet airplane

- c. Compute the maximum wing loading of your airplane.
- d. Add the landing-field-length constraint to your matching diagram.

7.4. CRUISE SPEED

While the previous two requirements were evaluated at zero power and thrust, we are now focusing on the flight performance requirements that do require thrust and power. The first one is the cruise speed or cruise Mach number.

7.4.1. FLIGHT MECHANICS

The cruise speed is treated as the maximum speed at which you want the airplane to be operated. We assume that the cruise speed is performed at the cruise altitude and that the airplane is in steady, symmetric level flight. In that scenario, the thrust of the airplane is balanced by the drag, and we have:

$$T = D = C_D \frac{1}{2} \rho V^2 S_w \quad (7.16)$$

We divide both sides by W and substitute the drag polar (5.9) for C_D :

$$\frac{T}{W} = \frac{C_D \frac{1}{2} \rho V^2}{W/S_w} = \frac{C_{D_0} \frac{1}{2} \rho V^2}{W/S_w} + \frac{W/S_w}{\pi \mathcal{R} e \frac{1}{2} \rho V^2} \quad (7.17)$$

For the propeller-powered airplane, we employ (5.20) to relate the power loading to the wing loading:

$$\frac{\eta_p P}{W} = \frac{C_{D_0} \frac{1}{2} \rho V^3}{W/S_w} + \frac{W/S_w}{\pi \mathcal{R} e \frac{1}{2} \rho V} \quad (7.18)$$

Equations (7.17) and (7.18) relate to a balance in thrust and drag at the cruise altitude. The thrust or power that is produced by air-breathing engines depends on the density of the air that they are taking in. In addition, the forward speed of the airplane also reduces the thrust that is produced by the propeller or fan. We refer to these reductions as a *thrust lapse* or *power lapse*. This lapse in thrust or power means that our engines need more thrust or power at sea level to make sure that there is enough left to meet the cruise speed requirement. The power lapse is therefore defined as:

$$\alpha_P = \frac{P}{P_{SL}} \quad (7.19)$$

where P_{SL} is the power available at sea level. For a jet engine, we define the engine thrust lapse, α_T , as the ratio between the thrust at altitude and Mach number and the thrust at sea level in static conditions:

$$\alpha_T = \frac{T}{T_{SLS}} \quad (7.20)$$

where TO is the abbreviation for “take-off” and SLS for “sea-level static,” implying the engine is at zero speed. Turbofans are rated by their value of $T_{TO, SLS}$, although the performance constraints need to be evaluated at nonzero speeds.

To find the relation between the wing loading and power loading at take-off conditions and maximum take-off mass, we have to include the lapse in power with altitude, α_P , according to (7.24) as well as the mass ratio, β . We take the reciprocal of (7.18) and substitute $V = V_{CR}$ to find:

$$\frac{W_{TO}}{P_{TO}} < \eta_p \frac{\alpha_P}{\beta} \left(\frac{C_{D_0} \frac{1}{2} \rho V_{CR}^3}{\beta W_{TO}/S_w} + \frac{\beta W_{TO}/S_w}{\pi \mathcal{A} Re \frac{1}{2} \rho V_{CR}} \right)^{-1} \quad (7.21)$$

For the jet-powered airplane, we take (7.17), adjust the thrust-to-weight ratio for the thrust lapse, α_T , and multiply the weight by the mass ratio, β :

$$\frac{T_{TO}}{W_{TO}} > \frac{\beta}{\alpha_T} \left(\frac{C_{D_0} \frac{1}{2} \rho V_{CR}^2}{\beta W_{TO}/S_w} + \frac{\beta W_{TO}/S_w}{\pi \mathcal{A} Re \frac{1}{2} \rho V_{CR}^2} \right) \quad (7.22)$$

In order to use these questions to draw the constraint curves, we first need to compute the power lapse and thrust lapse of the engine.

7.4.2. ESTIMATING THE POWER AND THRUST LAPSE

Various ambient conditions can reduce the power or thrust that is produced by a propulsion system. We call this *power lapse* or *thrust lapse*, respectively. The power lapse of an air-breathing engine is dependent on the temperature and the altitude. An increase in altitude and/or temperature reduces the density. Therefore, there is less oxygen available to combust the fuel, which reduces the power. Similarly, the thrust of a jet engine also depends on the air density. However, it is also dependent on the flight Mach number. In this section, we present the equations that you can use to estimate the power lapse and thrust lapse, respectively.

POWER LAPSE For *piston engines*, we use the empirical relation by Ruijgrok [16] that shows that the power lapse is linearly related to the ambient density at altitude, ρ , according to:

$$\alpha_P = 1.132 \frac{\rho}{\rho_{SL\text{ISA}}} - 0.132 \quad (7.23)$$

where $\rho_{SL\text{ISA}} = 1.225 \text{ kg/m}^3$ is the ambient density at sea level ISA. For *turboprop engines*, Ruijgrok defines the power lapse with altitude (α_P) as a function of the local density as follows:

$$\alpha_P = \left(\frac{\rho}{\rho_{SL\text{ISA}}} \right)^{\frac{3}{4}} \quad (7.24)$$

In Figure 7.9, the power lapse of an *aspirated* piston engine and turboprop are shown. An aspirated piston engine relies purely on the density of the ambient air to determine the maximum power output. You can see that the piston engine has a stronger power lapse than the turboprop engine and that both engine types lose a significant amount of power when operated at higher altitudes.

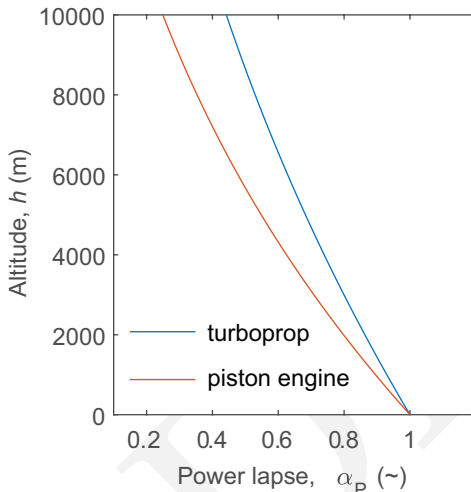


Figure 7.9: Power lapse for aspirated piston engines and turboprops

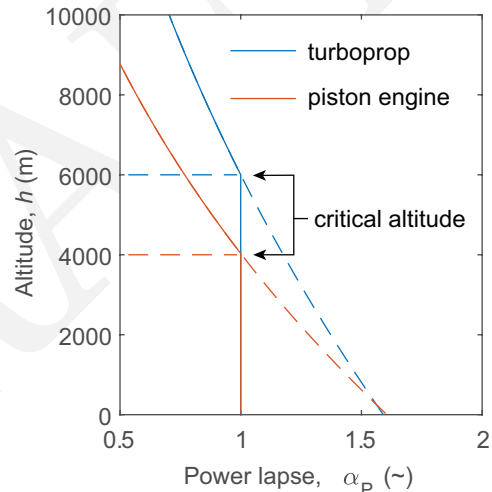


Figure 7.10: Power lapse for flat-rated piston engines and turboprops with assumed critical altitudes.

Because many airplanes cruise efficiently at higher altitudes, piston engines can be augmented with a supercharger or a turbocharger. A supercharger is a compressor connected to the engine's driveshaft and increases the air pressure before it enters the engine. This artificially increases the density and, therefore, the power that can be produced. A turbocharger has the same effect on the pressure increase but is driven by a turbine, which is placed in the exhaust of the piston engine. When a piston engine has a turbocharger or supercharger, it can be flat-rated. This means that below the so-called *critical altitude*, the engine throttle is limited to prevent damage to the engine or overheating as a result of too much power. Above the critical altitude, the throttle is fully

opened, and the engine power lapses due to the reduction in ambient density at altitude. Similarly, a turboprop engine is often flat-rated to prevent structural damage to the engine at low altitudes. The effect of flat-rating is a relatively high power-to-mass ratio of the aircraft engine that can provide sufficient power at cruise altitude.

In Figure 7.10, the power lapse of a flat-rated piston engine and turboprop are shown. The dashed lines for $\alpha_P > 1$ are added only to show the similarity to the power-lapse graphs of Figure 7.9. The graph for the piston engine has been drawn for an assumed critical altitude of 4,000 m. Up to that altitude, the shaft power is constant, and the reduction in ambient density is compensated with a higher throttle setting. For the turboprop engine, a critical altitude of 6,000 m is assumed. Above this altitude, the reduced air density is no longer compensated by a higher throttle setting, and the power reduces with altitude.

The power lapse of a *piston engine* can be computed for an assumed critical altitude, h_{crit} by modifying Equation (7.23) as follows:

$$\text{for } h \leq h_{\text{crit}} \quad \alpha_P = 1 \quad (7.25)$$

$$\text{for } h > h_{\text{crit}} \quad \alpha_P = \frac{1.132\rho - 0.132\rho_{\text{SL ISA}}}{1.132\rho_{\text{crit}} - 0.132\rho_{\text{SL ISA}}} \quad (7.26)$$

Similarly, for a *turpoprop engine* we modify (7.24) to compute the power lapse with altitude as follows:

$$\text{for } h \leq h_{\text{crit}} \quad \alpha_P = 1 \quad (7.27)$$

$$\text{for } h > h_{\text{crit}} \quad \alpha_P = \left(\frac{\rho}{\rho_{\text{crit}}} \right)^{\frac{3}{4}} \quad (7.28)$$

For *electric motors*, the maximal shaft power is independent of the atmospheric properties. We, therefore, have:

$$\alpha_P = 1 \quad (7.29)$$

THRUST LAPSE A jet engine experiences a thrust lapse due to altitude and due to speed. Two primary factors influence the thrust lapse with speed. First of all, the increase in flight speed reduces the difference between the exhaust velocity of the air that is accelerated by the engine and flight speed. This reduces the thrust. Secondly, an increase in flight speed causes an increase in pressure in the engine's inlet, which increases the overall pressure ratio (OPR) of the engine and thereby causes the exhaust velocity to increase. This increases the thrust. These two effects oppose each other, and whether the thrust at a particular Mach number is higher or lower than static thrust depends, among others, on the bypass ratio B of the engine. Therefore, we need a model for α_T that is sensitive to B , M , and h .

Before we can present the model of α_T , we first need to introduce the total temperature and total pressure. Let us first define the Mach number:

$$M = \frac{V}{\sqrt{\gamma RT}} \quad (7.30)$$

As you can see, the Mach number is solely determined by the ambient temperature and is therefore a function of h and ΔT through Equations (7.10) and (7.11). The total temperature is the sum of the static temperature and the dynamic temperature. If the flow

is brought to a standstill under isentropic conditions² the kinetic energy is converted to heat, raising the temperature. The total temperature can be shown to be related to the Mach number, M , according to:

$$T_t = T \left(1 + \frac{\gamma - 1}{2} M^2 \right) \quad (7.31)$$

where γ is the ratio of specific heat coefficients for air, and T is the ambient temperature at the cruise altitude. With $\gamma = 1.4$, this simplifies to: $T_t = T(1 + 0.2M^2)$. Similarly, we can express the total pressure, p_t , as a function of Mach number (M) as follows:

$$p_t = p \left(1 + \frac{\gamma - 1}{2} M^2 \right)^{\frac{\gamma}{\gamma-1}} \quad (7.32)$$

where p is the ambient static pressure.

The static pressure (p) and temperature (T) are a function of the altitude (h) and weather-induced temperature change, ΔT . You can use Equations (7.10), (7.11), and (7.12) to compute T and p . We now introduce two new variables that relate the total properties of the air to the static properties at sea level:

$$\delta_t = \frac{p_t}{p_{\text{SL ISA}}} \quad (7.33)$$

$$\theta_t = \frac{T_t}{T_{\text{SL ISA}}} \quad (7.34)$$

With δ_t and θ_t properly defined, we can now dive deeper into the workings of a turbofan engine in order to properly model it. A turbofan comprises a fan, a compressor, a combustion chamber, and a turbine. Up to a threshold value of the total temperature, the maximum thrust of the turbofan is limited by the maximum pressure ratio that the compressor can provide. Beyond the maximum T_t threshold, the materials that are used to construct the turbine blades limit the performance of the gasturbine. The engine controls are therefore controlled in such a way that beyond a particular value of θ_t , the throttle is reduced to protect the turbine blades. This value is termed θ_t^{break} and is a design choice for engine designers. According to Ref. [6], modern engines have values of θ_t^{break} ranging between 1.06 and 1.08.

Mattingly provides the following empirically derived equations for the thrust lapse of turbofan engines [6]:

$$0 < B < 5 \quad \theta_t \leq \theta_t^{\text{break}} \quad \alpha_T = \delta_t \quad (7.35)$$

$$0 < B < 5 \quad \theta_t \geq \theta_t^{\text{break}} \quad \alpha_T = \delta_t \left(1 - 2.1 \frac{\theta_t - \theta_t^{\text{break}}}{\theta_t} \right) \quad (7.36)$$

$$5 \leq B < 15 \quad \theta_t \leq \theta_t^{\text{break}} \quad \alpha_T = \delta_t \left[1 - (0.43 + 0.014B) \sqrt{M} \right] \quad (7.37)$$

$$5 \leq B < 15 \quad \theta_t \geq \theta_t^{\text{break}} \quad \alpha_T = \delta_t \left[1 - (0.43 + 0.014B) \sqrt{M} - \frac{3(\theta_t - \theta_t^{\text{break}})}{1.5 + M} \right] \quad (7.38)$$

²An isentropic process is both reversible and adiabatic, i.e., without the addition or removal of heat.

You can see that for low-bypass-ratio turbofans, the thrust lapse is actually positive with Mach number as long as $\theta_t \leq \theta_{t\text{ break}}$ and h is small, which means the word “lapse” is perhaps not the most appropriate way to address the change in thrust due to Mach number. You can also observe that for higher bypass ratios, the thrust lapse with Mach number gets stronger, particularly when $\theta_t \geq \theta_{t\text{ break}}$. Finally, you should recognize that the thrust lapse gets stronger with increasing bypass ratio B .

ASSIGNMENT 7.4

In this assignment you will calculate the thrust or power lapse at cruise altitude for the engine of your airplane.

- What is the cruise altitude of your airplane?^a
- Compute the power lapse (α_P) or thrust lapse (α_T) of your engine in cruise conditions using the cruise altitude and the bypass ratio of your choice.

^aIf this has not been specified in the requirements, you have to choose it

7.4.3. CONSTRUCTING THE CONSTRAINT CURVE

Now that you have estimated the power lapse or thrust lapse, we can return to our flight mechanics relations. Equation (7.21) relates the wing loading to the power loading, while Equation (7.22) relates the wing loading to the thrust-to-weight ratio. These equations are employed in the subsequent example to draw the constraint curves in the two matching diagrams.

Example 7.5

We use the requirements as specified in Example 7.1. In addition, we assume a propeller efficiency of $\eta_p = 0.80$ for the propeller airplane and a $\theta_{t\text{ break}} = 1.08$ for the jet airplane. For the aerodynamic characteristics in the clean configuration, we assume the following values:

	flaps	gear	C_{D_0}	e
propeller	CR	arrow	0.026	0.71
jet	CR	↑	0.018	0.80

PROPELLER AIRPLANE For the propeller-powered airplane we have cruise speed requirement of $V_{CR} = 70$ m/s at an altitude of 1800 m. As this airplane has an electric motor, there is no power lapse with altitude, i.e. $\alpha_P = 1$. Also, the mass of the airplane is constant: $\beta = 1$. At an altitude of 1800 m, we employ (7.12) and (7.10) to find that $p = 81.5$ kPa and $T = 276$ K, respectively. With the equation of state (7.14), we then find that $\rho = 1.03$ kg/m³. With $C_{D_0} = 0.0260$, $e = 0.71$, $\mathcal{R} = 9$, and $\eta_p = 0.80$, we can compute the power loading as a function of wing loading using (7.21):

$$\frac{W_{TO}}{P_{TO}} < 0.8 \left[\frac{4577}{W_{TO}/S_w} + \frac{W_{TO}/S_w}{721} \right]^{-1}$$

With this equation, we can substitute a range of values for W_{TO}/S_w and find the corresponding constraint value for W_{TO}/P_{TO} :

W_{TO}/S_w	[N/m ²]	500	1000	1500	2000
W_{TO}/P_{TO}	[N/W]	0.081	0.134	0.156	0.158

We can plot these points in the matching diagram to form a curve that bounds the maximum power loading as is done in Figure 7.11.

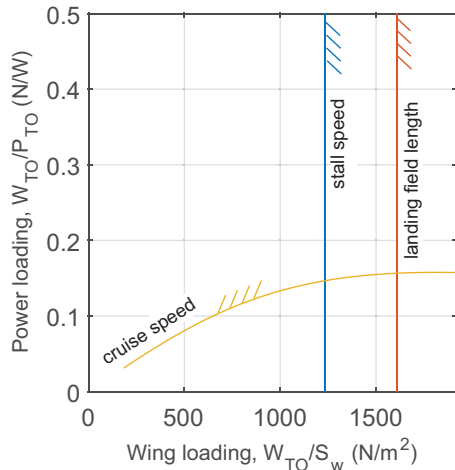


Figure 7.11: Matching diagram with added cruise speed requirement for propeller airplane

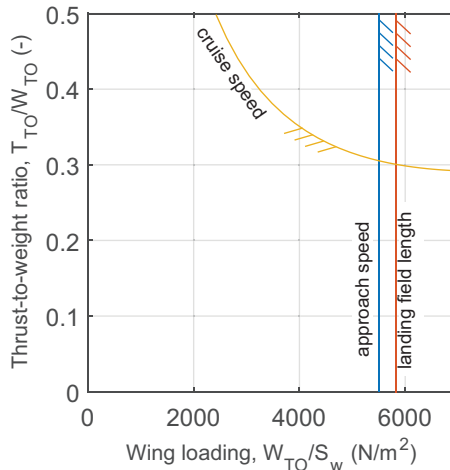


Figure 7.12: Matching diagram with cruise speed requirement for jet airplane

JET AIRPLANE For the jet airplane we have $M_{CR} = 0.8$ at an altitude of $h_{CR} = 10$ km. The mass ratio for which this requirement is investigated is $\beta = 0.95$. We compute the pressure and temperature with (7.12) and (7.10) with $\Delta T = 0$, respectively, to find: $p = 26$ kPa and $T = 223$ K. With (7.14) we find an ambient density at the cruise altitude of $\rho = 0.41$ kg/m³. Using the value of M_{CR} and T , we can compute the total temperature and total pressure in cruise conditions using (7.31) and (7.32), respectively, to find $p_t = 40$ kPa and $T_t = 252$ K. With (7.34) and (7.33), we can compute the total pressure ratio and total temperature ratio, respectively: $\delta_t = 0.40$ and $\theta_t = 0.87$. Realizing that $\theta_t < \theta_{t\text{ break}}$, we can now employ (7.37) for $B = 10$ to find the thrust lapse in cruise conditions is $\alpha_T = 0.19$. Finally, we use (7.30) to compute the cruise speed at $M_{CR} = 0.80$ and $h_{CR} = 10$ km: $V_{CR} = 240$ m/s. With $C_{D_0} = 0.0180$, $e = 0.80$, and $\mathcal{R} = 8$, we can compute the thrust-to-weight ratio as a function of wing loading using (7.17):

$$\frac{T_{TO}}{W_{TO}} > 4.87 \left[\frac{192}{W_{TO}/S_w} + \frac{W_{TO}/S_w}{214 \cdot 10^3} \right]$$

With this equation, we can substitute a range of values for W_{TO}/S_w and find the corresponding constraint value for W_{TO}/P_{TO} :

W_{TO}/S_w	[N/m ²]	1000	3000	5000	7000
T_{TO}/W_{TO}	[N/W]	1.11	0.42	0.32	0.29

We can subsequently plot the corresponding constraint curve in our matching diagram (Fig. 7.12). To satisfy the cruise-speed constraint, the thrust-to-weight ratio for any wing loading should be above this curve.

The example above shows that the cruise-speed requirement translates to a power or thrust constraint for the airplane. We can see that for lower wing loading, more thrust or power is required to sustain the cruise speed at the cruise altitude. Through the altitude, also the atmospheric properties play an important role in the estimation of the thrust (or power) lapse of the engine. In the next assignment, you will add the cruise-speed constraint to your own matching diagram.

ASSIGNMENT 7.5

In this assignment, you will add the constraint curve for the cruise speed to your matching diagram.

- a. For the cruise altitude and cruise speed of Assignment 7.4, list the α_P or α_T of your airplane.
- b. If a cruise Mach number is specified, compute the cruise speed V_{CR} at your cruise altitude using (7.30).
- c. Tabulate the power loading or thrust-to-weight ratio^a as a function of wing loading, similar to Example 7.5.
- d. Plot the constraint curve of the cruise speed in your matching diagram.

^awhichever one is applicable

7.5. RATE OF CLIMB

The next requirement we are going to add to the matching diagram is a rate-of-climb requirement. We use the words “rate of climb” and “climb rate” interchangeably in this section. In Figure 3.8 on page 33, we define the rate-of-climb (c). Airplanes for which the rate-of-climb is an important requirement are typically military combat airplanes that are out of the scope of this textbook. However, also the service ceiling of an airplane is typically specified in terms of a climb rate. For example, the service ceiling of a transport jet is typically defined as the altitude where $c = 100 \text{ ft/min}$, which is approximately $c = 0.5 \text{ m/s}$. For multi-engine airplanes, a flight ceiling can be specified in order to enable flight over mountainous terrain in a one-engine-inoperative condition. Such a ceiling is typically specified in terms of the climb rate requirement at the ceiling altitude. So let us derive the constraint curve in our matching diagram that stems from the rate-of-climb requirement.

We start our derivation by looking at the climb rate c definition in Figure 3.8:

$$c = V \sin \gamma \quad (7.39)$$

We acknowledge that during a steady climb, there is no acceleration, and the forces on the airplane are balanced. This is notionally shown in the free-body diagram of the airplane in Figure 7.13. By equating the forces in the direction of flight, we find:

$$T - D - W \sin \gamma = 0 \quad (7.40)$$

Combining (7.39) and (7.40) gives us the following expression for the climb rate:

$$c = V \frac{T - D}{W} = \frac{\eta_p P}{W} - V \frac{D}{W} \quad (7.41)$$

where we employ (5.20) to relate the thrust to the power.

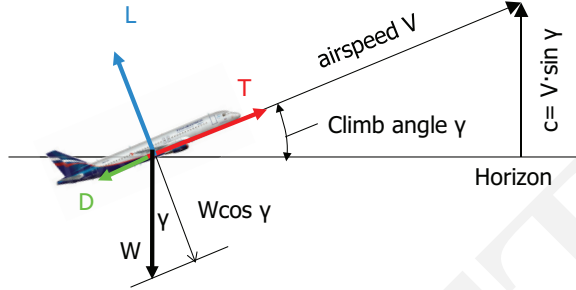


Figure 7.13: Free-body diagram of forces acting on an airplane in climbing flight.

Based on (7.41), we first investigate for which lift coefficient the climb rate of a propeller airplane is maximized. We consider the equilibrium of forces perpendicular to the flight direction:

$$L = W \cos \gamma \approx W \quad \text{for } \gamma \ll 1 \quad (7.42)$$

where γ is measured in radians. Since we have the lift equation, we can employ (5.7) such that V comes to the left-hand side of the equation:

$$V = \sqrt{\frac{W}{S_w \rho} \frac{2}{C_L}} \quad (7.43)$$

We can substitute this expression for V in (7.41) together with $D/W \approx D/L = C_D/C_L$ to find:

$$c = \frac{\eta_p P}{W} - \frac{C_D}{C_L^{3/2}} \sqrt{\frac{W}{S_w \rho} \frac{2}{C_L}} \quad (7.44)$$

By inspecting this equation, we can deduce that the climb rate is maximized when the fraction $C_D/C_L^{3/2}$ is minimized. We can analytically show that this fraction is minimized when:

$$C_L = \sqrt{3 C_{D_0} \pi \mathcal{R} e} \quad \text{and} \quad C_D = 4 C_{D_0}$$

Substituting this in (7.44) yields the equation for the maximum rate of climb:

$$c = \frac{\eta_p P}{W} - \frac{4 C_{D_0}^{1/4}}{(3 \pi \mathcal{R} e)^{3/4}} \sqrt{\frac{W}{S_w \rho} \frac{2}{C_L}} \quad (7.45)$$

To arrive at the function that relates the power loading to the wing loading in take-off conditions, we have to let $P = \alpha_P P_{TO}$ and $W = \beta W_{TO}$. We can rearrange (7.45) to express

the power loading constraint as a function of the wing loading as follows:

$$\frac{W_{TO}}{P_{TO}} < \eta_p \frac{\alpha_p}{\beta} \left(c + \frac{4C_{D_0}^{1/4}}{(3\pi A Re)^{3/4}} \sqrt{\frac{\beta W_{TO}}{S_w} \frac{2}{\rho}} \right)^{-1} \quad (7.46)$$

When we employ (7.46) we substitute for c_{max} the climb rate requirement. In order to evaluate this equation, we also need a value of the density, ρ . In other words, we need to specify an altitude along with a value for the climb rate.

Now, let us make a similar derivation but now for the jet airplane. Starting from (7.41), substituting (7.43), and approximating $D/W \approx D/L = C_D/C_L$ we have:

$$c = \left(\frac{T}{W} - \frac{C_D}{C_L} \right) \sqrt{\frac{W}{S_w} \frac{2}{\rho} \frac{1}{C_L}} \quad (7.47)$$

Contrary to the propeller airplane, we cannot analytically derive a lift coefficient that is independent of the thrust-to-weight ratio for which the climb rate is maximized. Ruijgrok shows that for a pure jet (i.e. $B = 0$), the lift coefficient for which the rate of climb is maximized is less than the lift coefficient for which the lift-to-drag ratio is maximized [16]. Since we consider a turbofan-powered jet airplane, we propose to use:

$$C_L = \sqrt{C_{D_0} \pi A Re} \quad \text{and} \quad C_D = 2C_{D_0}$$

If we substitute these values for C_L and C_D in (7.47) we can write:

$$c = \left(\frac{T}{W} - 2 \sqrt{\frac{C_{D_0}}{\pi A Re}} \right) \sqrt{\frac{W}{S_w} \frac{2}{\rho} \frac{1}{\sqrt{C_{D_0} \pi A Re}}} \quad (7.48)$$

With $T = \alpha_T T_{TO}$ and $W = \beta W_{TO}$, we can rearrange (7.48) and formulate the constraint curve for the rate-of-climb requirement:

$$\frac{T_{TO}}{W_{TO}} > \frac{\beta}{\alpha_T} \left(\sqrt{\frac{c^2}{\beta W_{TO}/S_w} \frac{\rho}{2} \sqrt{C_{D_0} \pi A Re}} + 2 \sqrt{\frac{C_{D_0}}{\pi A Re}} \right) \quad (7.49)$$

In the next example, we will show how the rate-of-climb constraint for the propeller airplane and the jet airplane appear in the matching diagram.

Example 7.6

We use the requirements and design decisions as specified in Example 7.1. For the aerodynamic characteristics in the clean configuration, we assume the following values:

	flaps	gear	C_{D_0}	e
propeller	CR	↑	0.026	0.71
jet	CR	↑	0.018	0.80

PROPELLER AIRPLANE For the propeller airplane we have $c = 2.0 \text{ m/s}$ at sea level. We perform the following steps:

1. Since we are at sea level, we obtain the density by evaluating (7.10), (7.12), and (7.14), knowing that $\Delta T = 0$. This results in $\rho = 1.23 \text{ kg/m}^3$.
2. We know that $\beta = 1$ and because we have electric motor $\alpha_P = 1$. So there is no need to compute the power lapse with altitude.
3. We can insert these values in (7.46) along with all the numerical values for the propeller airplane of Example 7.1. This results in the following constraint equation:

$$\frac{W_{\text{TO}}}{P_{\text{TO}}} > \frac{0.80}{2.0 + 0.095\sqrt{W_{\text{TO}}/S_w}}$$

4. We can now tabulate the values of power loading for a range of wing loading values:

W_{TO}/S_w	[N/m ²]	500	1000	1500	2000
$W_{\text{TO}}/P_{\text{TO}}$	[N/W]	0.19	0.16	0.14	0.13

5. The resulting constraint curve is added to the matching plot in Figure 7.14. You can see that the climb-rate curve is coincidentally crossing the stall-speed constraint at exactly the same point as the cruise-speed constraint. It is, therefore, not actively bounding the feasible design space in this example.

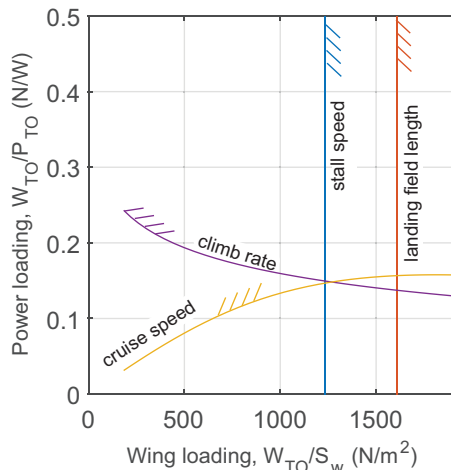


Figure 7.14: Matching diagram with added rate-of-climb requirement for propeller airplane

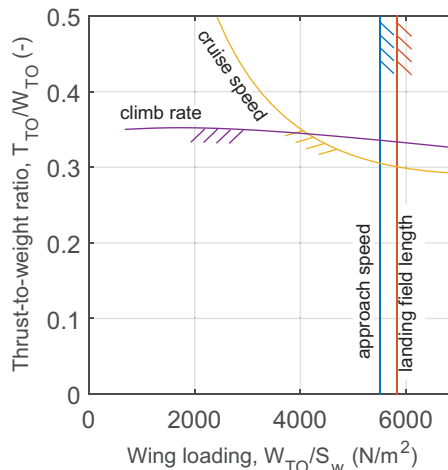


Figure 7.15: Matching diagram with added rate-of-climb requirement for jet airplane

JET AIRPLANE For the jet airplane, we have a climb rate requirement of $c = 0.5 \text{ m/s}$ at $h = 10,500 \text{ m}$ altitude. We perform the following steps:

1. We compute the atmospheric properties at $h = 10,500 \text{ m}$ by employing (7.10), (7.12), and (7.14), knowing that $\Delta T = 0$. We have: $T = 220 \text{ K}$, $p = 24.5 \text{ kPa}$ and $\rho = 0.39 \text{ kg/m}^3$.
2. We compute the lift coefficient for which we have the best rate of climb: $C_L = \sqrt{C_D 0 \pi \mathcal{R} e} = \sqrt{0.0180 \cdot \pi \cdot 8 \cdot 0.80} = 0.60$.

3. We compute the speed at which we have the best rate-of-climb using (7.43) as a function of wing loading, substituting $\beta = 0.95$ in accordance with the specification. Since the best speed varies with wing loading, we choose a range of wing loading values and tabulate the associated best climb speed for each wing loading (see table below).
4. Using (7.30), we compute the Mach number as a function of the wing loading and tabulate the best Mach number for a range of wing loading values (see table below).
5. Using (7.34) and (7.33), we compute the value of the total temperature ratio and total pressure ratio, respectively. We tabulate these values below.
6. Noting that $\theta_t < 1.08$ for all wing loading values, we employ (7.37) to compute the thrust lapse, α_T , corresponding to each wing loading value below.
7. We can now employ (7.49) to compute take-off thrust-to-weight ratio corresponding to each wing loading value. This is tabulated in the bottom row of the table below.

W_{TO}/S_w	(N/m ²)	Eq.	1000	3000	5000	7000
V	(m/s)	(7.43)	90	156	202	239
M	(-)	(7.30)	0.30	0.53	0.68	0.80
θ_t	(-)	(7.34)	0.78	0.81	0.83	0.86
δ_t	(-)	(7.33)	0.26	0.29	0.33	0.37
α_T	(-)	(7.37)	0.18	0.17	0.17	0.18
T_{TO}/W_{TO}	(-)	(7.49)	0.35	0.35	0.34	0.33

8. Using the tabulated values of wing loading and power loading, we add the constraint curve for the climb rate to the matching diagram of the jet airplane in Figure 7.15.

You can see that the climb-rate constraint cuts through the cruise-speed constraint in this example and is therefore actively constraining the minimum thrust-to-weight-ratio values for $W_{TO}/S_w > 4200 \text{ N/m}^2$.

The previous example shows that there are a few extra steps required to compute the constraint curve for the jet airplane compared to the propeller airplane. This is due to the more elaborate thrust-lapse relations that we employ for turbofan engines. In the following assignment, you will add the constraint curve to your matching diagram.

ASSIGNMENT 7.6

In this assignment, you will construct the constraint curve for the rate-of-climb requirement. For propeller airplanes, skip steps c through g as they only pertain to jet airplanes.

- a. State the climb rate requirement for your airplane and specify c , h , β , and ΔT .
- b. Compute the atmospheric properties T , p , and ρ for the given h and ΔT .
- c. Compute the lift coefficient for which the highest rate of climb occurs.
- d. For a chosen range of wing loading values, compute the speed for which

- the highest rate of climb occurs.
- e. For the chosen range of wing loading values, compute the Mach numbers for which the highest rate of climb occurs.
 - f. For the chosen range of wing loading values, compute the total temperature ratios (θ_t) and total pressure ratios (δ_T) corresponding to the Mach numbers of the previous step and the ambient pressure and temperature of step 2.
 - g. For the chosen range of wing loading values, compute the thrust lapse, α_T corresponding to the total temperature ratio and total pressure ratio of the previous step.
 - h. Compute the take-off power loading or take-off thrust-to-weight ratio^a versus take-off wing loading for a chosen range of take-off wing loading values.
 - i. Plot the rate-of-climb constraint in your matching diagram.

^aWhichever one is applicable

In the foregoing examples, we have considered the climb rate requirement assuming all engines are operative. A well-known climb rate requirement is the definition of a minimum flight altitude in case of a one-engine inoperative (OEI) situation. To assess this requirement, the power loading or thrust-to-weight ratio needs to be corrected for the inoperative engine. For the propeller airplane with OEI, (7.46) would be modified as follows:

$$\frac{W_{TO}}{P_{TO}} < \frac{N_e - 1}{N_e} \eta_p \frac{\alpha_P}{\beta} \left(c + \frac{4C_{D0}^{1/4}}{(3\pi \mathcal{A}Re)^{3/4}} \sqrt{\frac{\beta W_{TO}}{S_w} \frac{2}{\rho}} \right)^{-1} \quad (7.50)$$

where N_e is the number of engines (or motors) that you have chosen. For the jet airplane with OEI, (7.49) is modified according to:

$$\frac{T_{TO}}{W_{TO}} > \frac{N_e}{N_e - 1} \frac{\beta}{\alpha_T} \left(\sqrt{\frac{c^2}{\beta W_{TO}/S_w} \frac{\rho}{2}} \sqrt{C_{D0} \pi \mathcal{A}Re} + \sqrt{\frac{4C_{D0}}{\pi \mathcal{A}Re}} \right) \quad (7.51)$$

7.6. CLIMB GRADIENT

Closely related to the climb rate is the climb gradient of the airplane. In Figure 3.8, we already deduced that the climb gradient can be approximated by c/V when γ is small. In practical situations, this is usually the case for fixed-wing airplanes. As we can see in Section 3.3, the airworthiness regulations specify multiple climb gradient requirements for CS/FAR-23 and CS/FAR-25 airplanes. In this section, we only treat one climb gradient requirement. However, if your design requirements list multiple climb-gradient requirements, you have to evaluate each of the requirements individually to find out whether it is impacting the power loading or thrust-to-weight ratio of your airplane.

7.6.1. FLIGHT MECHANICS

To compute the constraint curves associated with the climb gradient requirement, let us start with the equilibrium of forces in steady climb according to Fig. 7.13, which is

denoted in (7.41). By dividing both sides of that equation by V , we have:

$$\frac{c}{V} = \frac{T - D}{W} = \frac{\eta_p P - DV}{VW} \quad (7.52)$$

Note that the fraction c/V is our climb gradient requirement. In other words, we leave this fraction intact in the following derivation and substitute a numerical value for it when we evaluate our constraint at the end of the process.

For the propeller airplane, we know that $D/W \approx D/L = C_D/C_L$. Therefore, (7.52) can now be written as:

$$\frac{c}{V} = \frac{\eta_p P}{W} \frac{1}{V} - \frac{C_D}{C_L} \quad (7.53)$$

We can insert (7.43) to substitute the speed to find:

$$\frac{c}{V} = \frac{\eta_p P}{W} \sqrt{\frac{\rho}{2} \frac{C_L}{W/S_w}} - \frac{C_D}{C_L} \quad (7.54)$$

The climb gradient is maximized when C_L is as high as possible. Practically, we are bound by the value of the maximum lift coefficient that we assume for the configuration that is chosen to evaluate the climb-gradient requirement. We apply a margin of 1.1 between the optimal climb speed and the stall speed. Given the quadratic relation between the lift coefficient and speed when weight equals lift, this translates into a factor of $1/1.1^2$ between the climb lift coefficient and the maximum lift coefficient. Therefore, the following lift coefficient and drag coefficient are chosen for the evaluation of the climb gradient requirement:

$$C_L = \frac{C_{L_{\max}}}{1.1^2} \quad \text{and} \quad C_D = C_{D_0} + \frac{C_{L_{\max}}^2}{1.1^4 \pi A Re} \quad (7.55)$$

Using the thrust lapse (α_P) and the mass ratio (β), we can rearrange (7.54) to find the constraint curve for the climb gradient requirement:

$$\frac{W_{TO}}{P_{TO}} < \eta_p \frac{\alpha_P}{\beta} \left(\frac{1}{c/V + C_D/C_L} \right) \sqrt{\frac{\rho}{2} \frac{C_L}{\beta W_{TO}/S_w}} \quad (7.56)$$

where C_D and C_L are given by (7.55). In case we wish to evaluate the climb gradient requirement of a multi-engine airplane in an OEI condition, (7.56) can be amended as follows:

$$\frac{W_{TO}}{P_{TO}} < \frac{N_e - 1}{N_e} \eta_p \frac{\alpha_P}{\beta} \left(\frac{1}{c/V + C_D/C_L} \right) \sqrt{\frac{\rho}{2} \frac{C_L}{\beta W_{TO}/S_w}} \quad (7.57)$$

where N_e is the number of engines (or motors).

For the jet airplane, we also start from (7.52). We apply $D/W \approx D/L = C_D/C_L$ and rewrite the climb-gradient equation as follows:

$$\frac{c}{V} = \frac{T}{D} - \frac{C_D}{C_L} \quad (7.58)$$

We can readily see that c/V is maximized when C_D/C_L is minimized. As we know by now, this happens for the following values of the lift and drag coefficients:

$$C_L = \sqrt{C_{D_0} \pi A Re} \quad \text{and} \quad C_D = 2C_{D_0}$$

We can substitute the expressions of the lift and drag coefficients in (7.58) to find:

$$\frac{c}{V} = \frac{T}{W} - 2\sqrt{\frac{C_{D_0}}{\pi A Re}} \quad (7.59)$$

By letting $W = \beta W_{TO}$ and $T = \alpha_T T_{TO}$, we can now express the take-off thrust-to-weight ratio as a function of the take-off wing loading:

$$\frac{T_{TO}}{W_{TO}} > \frac{\beta}{\alpha_T} \left(\frac{c}{V} + 2\sqrt{\frac{C_{D_0}}{\pi A Re}} \right) \quad (7.60)$$

We see that for the climb-gradient requirement, the take-off thrust-to-weight ratio seems to be independent of the wing loading. However, the thrust lapse, α_T , is dependent on the Mach number. Therefore, there is still a relationship with the wing loading through the equation relating velocity to lift (7.43). If we consider an OEI condition, we need to increase the required thrust-weight ratio according to:

$$\frac{T_{TO}}{W_{TO}} = \frac{N_e}{N_e - 1} \frac{\beta}{\alpha_T} \left(\frac{c}{V} + 2\sqrt{\frac{C_{D_0}}{\pi A Re}} \right) \quad (7.61)$$

where N_e is the number of engines.

As we learned from Example 3.13 in Chapter 3, various climb gradient requirements are specified in the certification documents. For many of them, the airplane is specified to be in take-off or landing configuration with either the landing gear up or down. For each configuration, the airplane has a different drag polar. You can imagine that when the flaps and landing gear are deployed, the airplane produces more drag. So, before we can compute the constraint curve in the matching diagram, we first need to estimate how the zero-lift drag coefficient and the Oswald factor change as a function of the flap deflection and landing gear deployment.

7.6.2. ESTIMATING THE DRAG POLAR FOR VARIOUS FLAP AND LANDING GEAR CONFIGURATIONS

So far, we have considered the Oswald factor for the cruise configuration of the airplane. When an airplane deploys its flaps (see Figure 7.16) to increase the maximum lift coefficient and thereby reduce its stall speed, the zero-lift drag coefficient of the airplane increases. In addition, the lift-dependent parasite drag parameter (ψ) increases while the span efficiency (φ) reduces. The net effect on the Oswald factor is that it typically increases with flap deflection for low-speed flight. Obert proposes the following change in Oswald factor as a function of flap deflection, δ_f [8]:

$$\begin{aligned} \Delta_{fe} &\approx 0.0046 \cdot \delta_f && \text{for airplanes with fuselage-mounted engines} \\ \Delta_{fe} &\approx 0.0026 \cdot \delta_f && \text{for airplanes with wing-mounted engines} \end{aligned} \quad (7.62)$$

where Δ_{fe} is the change in Oswald factor due to flap deflection (δ_f), with δ_f being measured in degrees. We can use this equation to estimate the Oswald factor for any flap deflection angle. To achieve the highest maximum lift coefficient, the maximum flap deflection is obtained in the landing configuration. So, in designing the airplane you should decide what flap deflection this will be. Secondly, you can choose intermediate flap deflection angles for the take-off of the airplane that range anywhere from zero deflection to maximum deflection.



Figure 7.16: Boeing 737 with flaps partially extended during approach. Photo: Manic Nirvana.

The zero-lift drag coefficient also depends on the flap deflection. The change in drag depends on the size of the flaps, the type of the flaps, and the amount of flap deflection. Since we do not have that information at the present time, we use a very rudimentary relation that assumes for every degree of flap deflection, we incur a 13-count³ drag penalty in zero-lift drag coefficient:

$$\Delta_f C_{D_0} \approx 0.0013 \cdot \delta_f \quad (7.63)$$

A final contributor that we would like to include at this stage is the change in drag due to landing-gear deployment. As the landing gear deployment has little impact on the lift-induced drag, we only include the change in zero-lift drag coefficient:

$$0.0100 < \Delta_{lg} C_{D_0} < 0.0250 \quad (7.64)$$

Naturally, the equations above are fairly crude, and in subsequent iterations of the design, many of these values are replaced by analysis results (see Chapter 10). However,

³A drag count is 1/10,000th of a drag coefficient

it allows you to construct a series of drag polars for the airplane, which you can use in subsequent steps of the design process.

Example 7.7

In this example, we produce the drag polars for one airplane in various configurations. This airplane has jet engines that are mounted on the fuselage (7.62). We have selected an aspect ratio of $\mathcal{R} = 8$, a take-off flap deflection of $\delta_{f, \text{take-off}} = 15^\circ$, and a landing flap deflection of $\delta_{f, \text{landing}} = 35^\circ$. Furthermore, we have a zero-lift drag coefficient and Oswald factor in cruise configuration of $C_{D_0} = 0.0180$ and $e = 0.80$. We consider four configurations: cruise, take-off (1), take-off (2), and landing. For take-off (1), the landing gear is up, while for take-off (2) and landing configuration, the landing gear is down. We perform the following tasks: For each configuration, we compute the zero-lift drag coefficient and the Oswald factor. We employ (7.62),(7.63), and (7.64). The resulting values for the aerodynamic coefficients are tabulated below:

flap	gear	δ_f [deg]	C_{D_0}	e
CR	↑	0	0.0180	0.80
TO	↑	15	0.0375	0.87
TO	↓	15	0.0575	0.87
L	↑	35	0.0635	0.96
L	↓	35	0.0835	0.96

ASSIGNMENT 7.7

In this assignment, you will construct the drag polars for your airplane.

- Using Eq. 5.17, compute the Oswald factor of your airplane in cruise configuration.
- What is the maximum amount of flap deflection that you choose for your airplane in the landing condition?
- What intermediate flap deflection do you choose for the take-off condition?
- Using Eq. 7.63 and 7.64 compute the zero-lift drag coefficient in take-off configuration and in landing configuration.
- Using Eq. 7.62, compute the Oswald factor in the take-off configuration and in the landing configuration.
- Tabulate your drag polar coefficients similar to the table in Example 7.7 using the following template:

flap	gear	δ_f [deg]	C_{D_0}	e
CR	\uparrow^a
CR	\downarrow
TO	\uparrow^a
TO	\downarrow
L	\uparrow^a
L	\downarrow

^a only applicable if your airplane has a retractable landing gear

7.6.3. CONSTRUCTING THE CONSTRAINT CURVE

Now that the coefficients for the drag polar have been defined, we can return to the equations that define the constraint curves in our matching diagram, i.e., Equations (7.56) and (7.60). In the following example, we show the process of constructing the constraint curves for the propeller airplane and the jet airplane, respectively.

Example 7.8

We use the requirements as specified in Example 7.1. For the climb gradient requirement, the flaps of the airplane are in the take-off configuration. For the propeller airplane, the landing gear is fixed, so it is down. The jet airplane is able to retract the landing gear, and therefore, its climb gradient is evaluated in the gear-up configuration. The following coefficients apply for either airplane:

	flaps	gear	C_{D_0}	e	$C_{L_{\max}}$
propeller	TO	\downarrow	0.049	0.75	1.7
jet	TO	\uparrow	0.038	0.87	2.1

PROPELLER AIRPLANE For the propeller, we have $c/V = 0.083$ at sea level ISA with the flaps in take-off configuration. To compute the constraint curve in the matching diagram, we perform the following steps:

1. We compute the density at sea level in ISA conditions: $\rho = 1.23 \text{ kg/m}^3$.
2. Knowing that the climb gradient is maximized when C_L is close to $C_{L_{\max}}$, we set $C_L = C_{L_{\max}}/1.1^2 = 1.7/1.1 = 1.4$.
3. We substitute C_L in the drag polar for the take-off configuration (i.e. $C_{D_0} = 0.049$ and $e = 0.75$) and find $C_D = 0.12$
4. With $\beta = 1$ and $\alpha_P = 1$, we can construct the relation between wing loading and power loading from (7.56):

$$\frac{W_{\text{TO}}}{P_{\text{TO}}} < \frac{4.0}{\sqrt{W_{\text{TO}}/S_w}}$$

5. Using this expression, we can tabulate the values of power loading versus wing loading:

W_{TO}/S_w	[N/m ²]	500	1000	1500	2000
$W_{\text{TO}}/P_{\text{TO}}$	[N/W]	0.18	0.13	0.10	0.090

6. We can now add the climb-gradient constraint curve to our matching diagram. This has been done in Figure (7.17).

You can see that the resulting climb-gradient constraint curve lies below the cruise-speed constraint curve for wing loading values above 1000 N/m^2 . This implies that this constraint is actively bounding the feasible design space for this propeller airplane.

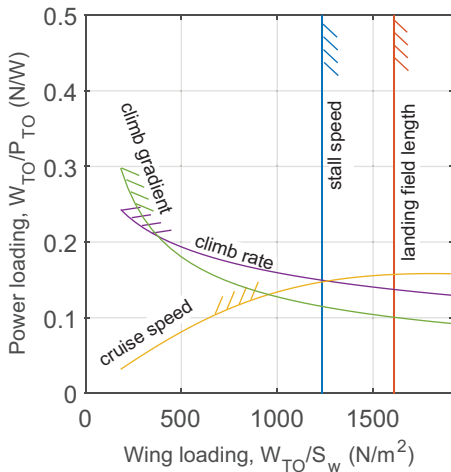


Figure 7.17: Matching diagram with added climb-gradient requirement for propeller airplane

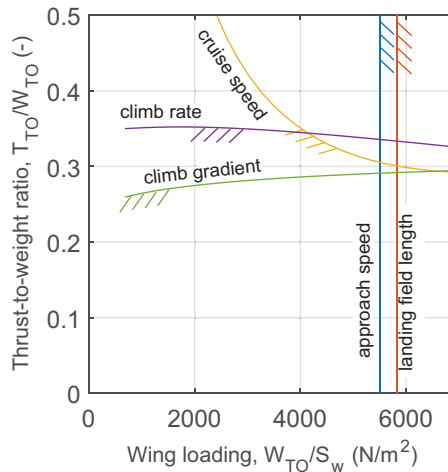


Figure 7.18: Matching diagram with added climb-gradient requirement for jet airplane

JET AIRPLANE For the jet airplane, we consider a more elaborate climb-gradient requirement: $c/V = 0.024$ at sea level but with a temperature increase of $\Delta T = 15^\circ$ above ISA conditions. Furthermore, we consider one engine to be inoperative, the mass equal to the maximum take-off mass, and the airplane to be in the take-off configuration. With the following steps, we construct the constraint curve:

1. First, we compute the density at sea level. We employ (7.10) and (7.12) to find that $T = 303 \text{ K}$ and $p = 101 \text{ kPa}$. Then, with (7.14), we compute the density to be $\rho = 1.16 \text{ kg/m}^3$.
2. We compute the value of the lift and drag coefficient for maximum climb gradient for the take-off configuration (i.e., $C_{D_0} = 0.038$ and $e = 0.87$):

$$C_L = 0.91 \quad \text{and} \quad C_D = 0.075$$

3. We compute the speed for which we have the best climb gradient by employing (7.43), for a range of wing-loading values and tabulate that in the table below.
4. Using (7.30), we compute the Mach number associated with each velocity value and ambient temperature and tabulate that below.
5. Using (7.34) and (7.32), we compute the total temperature ratio, θ_t , and total pressure ratio, δ_t associated with the Mach numbers computed in the previous step. We tabulate this below.

6. Acknowledging that $\theta_t < 1.08$ for all but the highest wing-loading value, we employ (7.37) and (7.38) to compute the thrust lapse for each Mach number. This is also tabulated below.
7. We can now employ (7.60) to compute the thrust-to-weight ratio as a function of wing loading:

W_{TO}/S_w	(N/m ²)	Eq.	1000	3000	5000	7000
V	(m/s)	(7.43)	44	75	97	115
M	(-)	(7.30)	0.12	0.22	0.28	0.33
θ_t	(-)	(7.34)	1.06	1.06	1.07	1.08
δ_t	(-)	(7.33)	1.01	1.03	1.06	1.08
α_T	(-)	(7.37), (7.38)	0.81	0.76	0.74	0.73
T_{TO}/W_{TO}	(-)	(7.61)	0.27	0.28	0.29	0.30

8. We plot the tabulated values above as a constraint curve in the matching diagram of Figure 7.18.

You can see that the curve that we drew for the climb-gradient constraint lies below the climb-rate constraint for all wing-loading values left to the approach-speed constraint. It is, therefore, not an active constraint in this example.

ASSIGNMENT 7.8

In this assignment, you will construct the constraint curve for the climb-gradient requirement. For propeller airplanes, skip steps f-i as they only pertain to jet airplanes and serve to compute the thrust lapse.

- a. State the climb gradient requirement of your airplane: c/V , h , β and ΔT . Also, state whether the requirement is to be fulfilled in AEO condition or in OEI condition and the configuration of the airplane.
- b. Based on the configuration, state the value of the zero-lift drag coefficient C_{D_0} and Oswald factor e that are applicable.
- c. Compute the ambient temperature and density that pertain to the climb gradient requirement.
- d. Compute the lift coefficient for which the climb gradient is maximized. Use an appropriate margin to the stall speed if this is applicable.
- e. Compute the drag coefficient for which the climb gradient is maximized.
- f. Using a chosen range of wing-loading values, compute the speed for which the climb gradient is maximized corresponding to each wing-loading value and the lift coefficient calculated above.
- g. For each speed value computed in the previous step, compute the associated Mach number.
- h. For each Mach number computed in the previous step, compute the value of θ_t and δ_t .
- i. Compute the value of the thrust lapse α_T corresponding to each wing-loading value. Make sure to check whether the computed value of θ_t surpasses the assumed value of $\theta_{t\text{ break}}$ such that you use the correct equation

- to compute α_T .
- For each wing loading value, compute the take-off power loading or take-off thrust-to-weight ratio^a such that the climb-gradient constraint is satisfied.
 - Plot the constraint curve for the climb gradient in your matching diagram.

^awhichever one is applicable

7.7. TAKE-OFF FIELD LENGTH

The take-off field length is the distance measured between the standstill location and the location where the airplane clears an obstacle of height h_2 (see Fig. 7.19). For normal, utility and aerobatic airplanes under CS/FAR-23, this obstacle height is 15 m (50 ft), and for commuter airplanes under CS/FAR-23 and all CS/FAR-25 airplanes this height is 11 m (35 ft). It consists of a ground roll distance (L_{RUN}) and an air distance (L_{AIR}) where the airplane is climbing. To be able to lift-off, the lift-off speed needs to be greater than the stall speed. We have seen in Example 7.2 that the stall speed is dependent on the maximum lift coefficient. Similarly, the ground-roll distance is also dependent on the maximum lift coefficient. The higher the maximum lift coefficient, the shorter the ground roll. We also know that the highest maximum lift coefficient is achieved when the flaps are fully deployed, i.e. when the airplane is in landing configuration. Secondly, the air distance is dependent on how steep the airplane is able to climb. In Example 3.13, we have seen that the climb gradient is dependent on the lift-to-drag ratio, and in Example 7.7, we have seen that the highest lift-to-drag ratio is achieved in clean configuration (i.e. with the flaps stowed). To minimize the combined ground-roll distance and air distance, the airplane therefore uses an intermediate flap setting that increases the maximum lift coefficient significantly but with an acceptable penalty in drag. This is what we refer to as the *take-off configuration*.

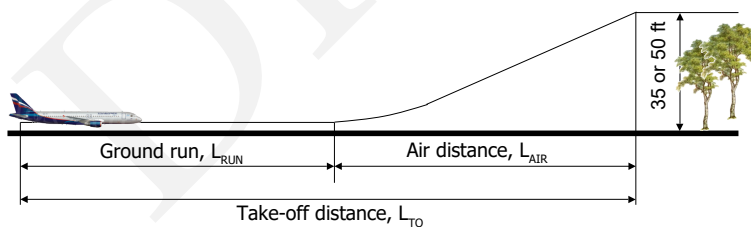


Figure 7.19: Definition of the take-off field length, L_{TO} , according to CS/FAR 23/25.

The take-off maneuver with associated distances, speeds, and climb angles is more elaborately explained in the airworthiness regulations (CS/FAR-23: paragraphs 51-61; CS/FAR-25 paragraphs 105-115). You can imagine that for multi-engined airplanes, the take-off distance in the OEI condition is different from the take-off distance in the AEO condition. For every multi-engined airplane, a decision speed (V_1) needs to be established. If an engine failure occurs below V_1 , the pilot needs to break and come to a

standstill. If an engine failure occurs beyond V_1 , the pilot needs to continue the take-off in OEI condition. So in the case of a continued take-off (CTO), the available thrust changes during the take-off maneuver. In our analysis of the take-off maneuver, we first consider the case for the AEO condition, which we subsequently augment to consider a CTO. The take-off safety speed at the obstacle height is termed V_2 . We will use V_2 and the associated C_{L_2} and T_{V_2} as the reference speed, lift coefficient and thrust, respectively.

Contrary to all of the previous flight performance requirements, the take-off maneuver is not steady, meaning the velocity changes with time. We follow the treatment by Torenbeek [18], who considers the take-off field length (\mathcal{L}_{TO}) to be the sum of the ground run (\mathcal{L}_{RUN}) and the air distance (\mathcal{L}_{AIR}) for jet airplanes:

$$\mathcal{L}_{\text{TO}} = \mathcal{L}_{\text{RUN}} + \mathcal{L}_{\text{AIR}} \quad (7.65)$$

The ground run is terminated at the lift-off speed, V_{LOF} . We assume that the difference between V_{LOF} and V_2 is small and can be neglected. If we assume a constant acceleration during the ground run due to an average acceleration force \bar{F}_{acc} (i.e., the resultant of thrust, ground friction, and drag), we can deduce that:

$$\mathcal{L}_{\text{RUN}} = \frac{W_{\text{TO}}}{2gk_T T_{V_2}} V_2^2 \quad \text{with} \quad k_T = \frac{\bar{F}_{\text{acc}}}{T_{V_2}} \quad (7.66)$$

The parameter k_T relates the thrust at V_2 to the average acceleration force. Its value is assumed to be 0.85 for jet airplanes. Applying the lift equation (7.43), we can substitute V_2 in (7.66) and find:

$$\mathcal{L}_{\text{RUN}} = \frac{W_{\text{TO}}^2}{\rho g S_w C_{L_2} k_T T_{V_2}} \quad (7.67)$$

where ρ is the density at the take-off altitude.

The air distance is measured from the point of lift-off to the obstacle height, h_2 . We assume that the airplane follows a circular take-off path during this maneuver ending with climb angle γ_2 at the obstacle height. The air distance that is covered during this maneuver is equal to the distance covered during a steady climb over twice the obstacle height, as is schematically shown in Figure 7.20. Knowing that the climb angle $\gamma_2 \ll 1$ when measured in radians, we can deduce the relation between the climb angle, the thrust-to-weight ratio, and the lift-to-drag ratio, similar to (7.52):

$$\mathcal{L}_{\text{AIR}} = \frac{2h_2}{\gamma_2} = 2h_2 \left[\frac{T_{V_2}}{W_{\text{TO}}} - \left(\frac{C_D}{C_L} \right)_{V_2} \right]^{-1} \quad (7.68)$$

The drag coefficient at V_2 can be found by substituting C_{L_2} in the drag polar of the airplane in take-off configuration (5.9). We then get:

$$\mathcal{L}_{\text{AIR}} = \frac{2h_2}{\gamma_2} = 2h_2 \left[\frac{T_{V_2}}{W_{\text{TO}}} - \left(\frac{C_{D0}}{C_{L2}} + \frac{C_{L2}}{\pi A Re} \right) \right]^{-1} \quad (7.69)$$

Substituting (7.67) and (7.69) in (7.65) gives the complete equation for the take-off field length:

$$\mathcal{L}_{\text{TO}} = \frac{W_{\text{TO}}^2}{\rho g S_w C_{L_2} k_T T_{V_2}} + 2h_2 \left[\frac{T_{V_2}}{W_{\text{TO}}} - \left(\frac{C_{D0}}{C_{L2}} + \frac{C_{L2}}{\pi A Re} \right) \right]^{-1} \quad (7.70)$$

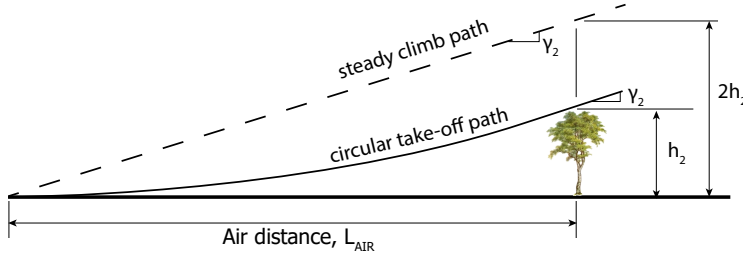


Figure 7.20: Approximation of air distance \mathcal{L}_{air} by means of steady climb angle γ_2 ,

For multi-engined airplanes performing a continued take-off with an inoperative engine, the available thrust-to-weight ratio during the climbing phase of the take-off is proportional to $(N_e - 1)/N_e$. Therefore, the CTO take-off field length becomes:

$$\mathcal{L}_{\text{TO}} = \frac{W_{\text{TO}}^2}{\rho g S_w C_{L_2} k_T T_{V_2}} + 2h_2 \left[\frac{N_e - 1}{N_e} \frac{T_{V_2}}{W_{\text{TO}}} - \left(\frac{C_{D_0}}{C_{L_2}} + \frac{C_{L_2}}{\pi \mathcal{A} Re} \right) \right]^{-1} \quad (7.71)$$

There exists one value of C_{L_2} for which this take-off field length is minimized. However, Torenbeek analytically derives that for high-aspect-ratio wings, the minimum take-off field length is insensitive to the actual value of C_{L_2} due to the trade-off between ground run and air distance [18]. The thrust-to-weight ratio at V_2 for a minimum take-off field length of \mathcal{L}_{TO} is then approximated as follows:

$$\frac{T_{V_2}}{W_{\text{TO}}} = 1.15 \sqrt{\frac{W_{\text{TO}}/S_w}{\mathcal{L}_{\text{TO}} k_T \rho g \pi \mathcal{A} Re}} + \frac{4h_2}{\mathcal{L}_{\text{TO}}} \quad (7.72)$$

It should be noted that in this expression, the Oswald factor e should be the one for the take-off configuration.

For jet airplanes, we now consider the thrust lapse due to speed, altitude and temperature to arrive at the take-off thrust-to-weight ratio constraint:

$$\frac{T_{\text{TO}}}{W_{\text{TO}}} > \frac{1}{\alpha_T} \left[1.15 \sqrt{\frac{W_{\text{TO}}/S_w}{\mathcal{L}_{\text{TO}} k_T \rho g \pi \mathcal{A} Re}} + \frac{4h_2}{\mathcal{L}_{\text{TO}}} \right] \quad (7.73)$$

For multi-engined jet airplanes, the take-off field length in OEI condition can be approximated as follows:

$$\frac{T_{\text{TO}}}{W_{\text{TO}}} = \frac{1}{\alpha_T} \left[1.15 \sqrt{\frac{N_e}{N_e - 1} \frac{W_{\text{TO}}/S_w}{\mathcal{L}_{\text{TO}} k_T \rho g \pi \mathcal{A} Re}} + \frac{N_e}{N_e - 1} \frac{4h_2}{\mathcal{L}_{\text{TO}}} \right] \quad (7.74)$$

You might have observed that with this derivation, we have reduced a complicated unsteady maneuver into a single equation relating the thrust-to-weight ratio to the wing loading. We therefore emphasize that this is an approximation and that (7.70) should be used to check whether the take-off constraint is actually met. Secondly, we still need to

choose a value of C_{L_2} in order to calculate V_2 as a function of wing loading and subsequently determine the value of α_T as a function of wing loading.

For propeller airplanes, we need to know V_2 in order to evaluate the required power at the obstacle height. Since the climb gradient of a propeller airplane is maximized when the lift coefficient is as high as possible, we choose C_{L_2} to be as high as possible as well. The airworthiness regulations give a lower bound to V_2 with respect to the stall speed in the take-off configuration. CS/FAR-23.51 specifies that $V_2 \geq 1.2V_{S1}$ and CS/FAR-25.107 specifies that $V_2 \geq 1.13V_{S1}$, where V_{S1} is the stall speed in a particular configuration (other than the landing configuration). In this case, V_{S1} is the stall speed in the take-off configuration. Using the ratios between the take-off safety speed and the stall speed, we can compute C_{L_2} as follows:

$$C_{L_2} = \left(\frac{V_{S1}}{V_2} \right)^2 C_{L_{\max}} \quad (7.75)$$

where we use the minimum value for the speed ratio specified by the regulations, i.e., 1.2 and 1.13 for CS-23 and CS-25 airplanes, respectively. Using the lift equation (7.43), we can relate V_2 to the wing loading and C_{L_2} . And, with the relation between power and thrust (5.20) and (7.72) we can establish the power loading constraint as follows:

$$\frac{W_{TO}}{P_{TO}} < \alpha_P \left[1.15 \sqrt{\frac{W_{TO}/S_w}{\mathcal{L}_{TO} k_T \rho g \pi A Re}} + \frac{4h_2}{\mathcal{L}_{TO}} \right]^{-1} \sqrt{\frac{C_{L_2}}{W_{TO}/S_w} \frac{\rho}{2}} \quad (7.76)$$

where α_P accounts for the power lapse of air-breathing engines with altitude. Note that we are implicitly assuming that $\beta = 1$ as we are considering the take-off constraint at maximum take-off weight. Similar to the multi-engined jet airplane, we can modify (7.76) to account for an OEI condition as follows:

$$\frac{W_{TO}}{P_{TO}} < \alpha_P \left[1.15 \sqrt{\frac{N_e}{N_e - 1} \frac{W_{TO}/S_w}{\mathcal{L}_{TO} k_T \rho g \pi A Re}} + \frac{N_e}{N_e - 1} \frac{4h_2}{\mathcal{L}_{TO}} \right]^{-1} \sqrt{\frac{C_{L_2}}{W_{TO}/S_w} \frac{\rho}{2}} \quad (7.77)$$

where N_e is the number of engines or motors that has been chosen. While the value of 1.15 in (7.76) and (7.77) stems from the analysis of jet airplanes in Ref. [18], we propose to also use it for propeller airplanes, for the lack of a better source. However, this number is subject to statistical validation. The following example demonstrates how the take-off constraint is added to the matching diagram.

Example 7.9

We use the requirements, design decisions, and assumptions as specified in Example 7.1. In addition, we estimate the following aerodynamic characteristics:

	flaps	gear	C_{D_0}	e	$C_{L_{\max}}$
propeller	TO	↓	0.049	0.75	1.7
jet	TO	↓	0.058	0.87	2.1

PROPELLER AIRPLANE Our battery-powered propeller airplane has a take-off field length requirement of 750 m at sea level. Since this is a single-motor airplane, the take-off distance can be computed with (7.70). We take the following steps to find the maximum power loading to satisfy the take-off field length constraint:

1. We know the density at sea level in ISA conditions is $\rho = 1.23 \text{ kg/m}^3$
2. The airplane is in take-off configuration, so the zero-lift drag coefficient, Oswald factor, and maximum lift coefficient are $C_{D_0} = 0.049$, $e = 0.75$, and $C_{L_{\max}} = 1.7$ respectively.
3. Using the 20% speed margin between the stall speed and the take-off safety speed from CS/FAR-23, we compute $C_{L_2} = 1.18$ with (7.75).
4. We employ (7.76) to compute the power loading values as a function of wing loading knowing that $\mathcal{A} = 9$ and assuming that $k_T = 0.85$:

$$\frac{W_{\text{TO}}}{P_{\text{TO}}} < \left(0.0029 \sqrt{W_{\text{TO}}/S_w} + 0.081 \right)^{-1} \frac{0.85}{\sqrt{W_{\text{TO}}/S_w}}$$

5. We substitute a range of values for W_{TO}/S_w in the equation above and tabulate the resulting values for $W_{\text{TO}}/P_{\text{TO}}$ in the table below:

W_{TO}/S_w (N/m ²)	500	1000	1500	2000
$W_{\text{TO}}/P_{\text{TO}}$ (N/W)	0.26	0.16	0.11	0.091

6. We plot the data points in the matching diagram of Figure 7.21.

The take-off constraint lies above the climb gradient constraint for all wing loading values below $W_{\text{TO}}/S_w < 1800 \text{ N/m}^2$. It is, therefore, not actively bounding the feasible design space for this propeller airplane.

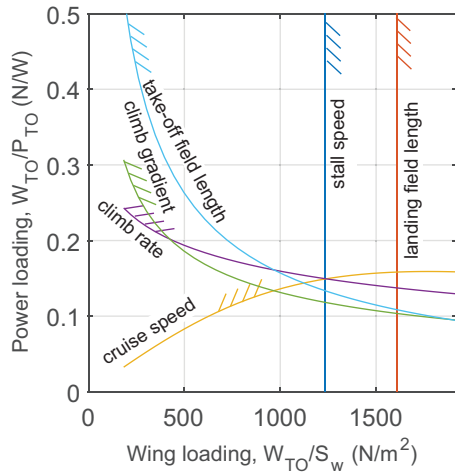


Figure 7.21: Matching diagram with added take-off field requirement for propeller airplane

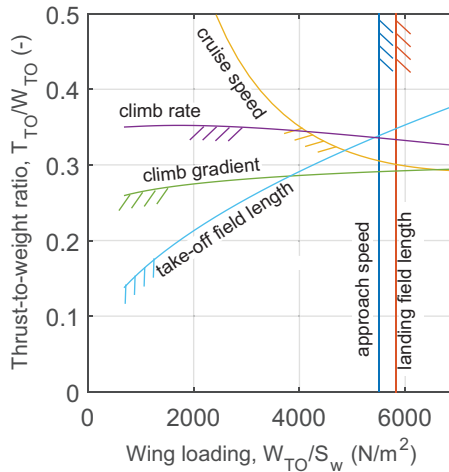


Figure 7.22: Matching diagram with added take-off field requirement for jet airplane

JET AIRPLANE Our jet airplane has a take-off field length requirement of 2500 m at an altitude of 1500 m and a temperature increase of 15° with respect to ISA conditions. We have a twin-engined airplane, and we consider the take-off field length to be equal to the continued take-off distance with one engine inoperative as given by (7.71). To compute the thrust-to-weight ratio constraint for the take-off field length, we perform the following steps:

- Using (7.10), (7.12), and (7.14) we compute the ambient temperature and density at the take-off condition: $T = 293 \text{ K}$, $\rho = 1.00 \text{ kg/m}^3$.
- The airplane is in take-off configuration with the landing gear down, so the zero-lift drag coefficient, Oswald factor, and maximum lift coefficient are $C_{D_0} = 0.058$, $e = 0.87$, and $C_{L_{\max}} = 2.1$ respectively.
- To compute the thrust lapse at V_2 , we need to choose a value of V_2 relative to the stall speed in the take-off configuration. We choose to use the minimal value allowed by CS/FAR-25: $V_2 = 1.13 V_{s1}$. We then compute $C_{L_2} = 1.6$ using (7.75).
- The take-off safety speed, V_2 depends on the wing loading according to (7.43). We substitute $C_L = C_{L_2}$ in this equation and tabulate the values of V_2 for a range of W_{TO}/S_w -values in the table below.
- We compute the Mach number at V_2 in the take-off condition using (7.30) and tabulate the resulting values in the table below.
- We subsequently employ (7.34) and (7.33) to compute the total temperature ratio θ_t and the total pressure ratio δ_t , respectively. They are both tabulated in the table below.
- Since $\theta_t < 1.08$ for all values of V_2 , we can employ (7.37) to compute the thrust lapse α_T for each value of V_2 . These values are tabulated in the table below.
- With $N_e = 2$, $\mathcal{R} = 8$, $h_2 = 11 \text{ m}$ and an assumed value of $k_T = 0.85$ we employ (7.74) to compute the minimal take-off thrust-to-weight ratio at each wing loading value. These values are tabulated in the bottom row of the table below.

W_{TO}/S_w	(N/m ²)	Eq.	1000	3000	5000	7000
V_2	(m/s)	(7.43)	35	60	78	92
M	(-)	(7.30)	0.10	0.18	0.23	0.27
θ_t	(-)	(7.34)	1.02	1.03	1.03	1.03
δ_t	(-)	(7.33)	0.84	0.85	0.86	0.88
α_T	(-)	(7.37)	0.69	0.65	0.63	0.62
$T_{\text{TO}}/W_{\text{TO}}$	(-)	(7.74)	0.16	0.26	0.32	0.38

- We construct the constraint curve for the take-off field length in the matching diagram of Figure 7.22.

The resulting constraint curve exceeds the constraint curve of the climb-rate requirement when $W_{\text{TO}}/S_w > 5400 \text{ N/m}^2$. So the take-off constraint actively bounds the feasible design space for the jet airplane. You might have also noted that the thrust lapse at V_2 can be rather large for this jet airplane. The combination of a 15-degree temperature rise, an altitude of 1600 m, and a speed of 79 m/s results in a thrust reduction of 37% ($\alpha_T = 0.63$) for a wing loading of 5000 N/m².

We have demonstrated how the take-off field length constraint can be added to the matching diagram. The mathematical formulation of the constraint curves is based on the optimization approach. To check if the constraint is actually satisfied, you can employ (7.70) or (7.71) once you have selected the take-off power loading or take-off thrust-to-weight ratio along with the wing loading. In the following assignment, you are going to construct the take-off constraint curve for your matching diagram.

ASSIGNMENT 7.9

In this assignment, you will construct the constraint curve for the take-off field-length requirement. For propeller airplanes, skip steps e-h as they only pertain to jet airplanes.

- a. State the take-off field length requirement and specify \mathcal{L}_{TO} , h , ΔT , and whether you consider the take-off distance in AEO condition or a continued take-off after an OEI condition has occurred.
- b. Based on the take-off configuration, state the values of the zero-lift drag coefficient C_{D_0} and Oswald factor e that are applicable.
- c. Compute the atmospheric properties for the take-off condition: T , p , and ρ .
- d. Using the minimal allowed margin to the stall speed, compute the value of C_{L_2} .
- e. For a chosen range of wing loading values, compute the associated take-off safety speed V_2 .
- f. For the computed values of V_2 , calculate the corresponding Mach numbers.
- g. Calculate the total temperature ratios θ_t and total pressure ratios δ_t associated with the Mach numbers computed in the previous step.
- h. For the chosen range of wing loading values, compute the thrust lapse α_T that corresponds to the values of θ_t and δ_t of the previous step.
- i. Compute the take-off power loading or take-off thrust-to-weight ratio^a for the take-off field length requirement for the chosen range of wing loading values.
- j. Plot the take-off field length constraint curve in the matching diagram.

^awhichever one is applicable

7.8. CHOOSING A DESIGN POINT IN THE MATCHING DIAGRAM

When all flight performance constraints have been transformed into constraint curves in the matching diagram, we need to select a single point in this diagram which determines the size of the wing as well as the power plant. We call this point the *design point*. The design point represents a combination of wing loading and power loading for a propeller airplane or wing loading and thrust-to-weight ratio for a jet airplane. In this section, we are going to demonstrate how you can select this design point.

With all the constraints plotted in the matching diagram, we need to make sure that the selected design point lies in the feasible design space as we have schematically shown in Figure 7.1. Secondly, we would like to choose a design point that optimizes our design objective. This is a bit problematic at this stage: we have not clearly defined how each possible design objective relates to the wing loading and power loading (or thrust-to-weight ratio). Generally speaking, we would like to select a design point that results in the smallest wing and smallest powerplant while still satisfying all constraints. This would imply the lowest mass and (friction) drag for the wing and propulsion system. For a propeller airplane, this implies the highest wing loading and highest power loading

permitted by the constraints. For the jet airplane, this implies the highest wing loading combined with the lowest thrust-to-weight ratio permitted by the constraints. This is visually shown in Figure 7.23. In the next example, we demonstrate how to choose a design point in the matching diagram.

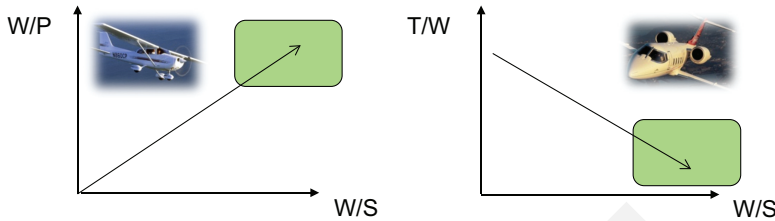


Figure 7.23: Notional representation of the design objective in the matching diagram of the propeller airplane (left) and jet airplane (right).

Example 7.10

We use the matching diagrams that have been constructed in the foregoing examples. The hash marks that we have added to each of our constraint curves now become important. They signify that any point on the hashed side of a particular constraint curve does not satisfy that constraint. Any point on the other side of the constraint does satisfy that particular constraint.

PROPELLER AIRPLANE For our propeller airplane, we first determine the feasible design space, which needs to be below all of the W_{TO}/P_{TO} curves and to the left of the constraining W_{TO}/S_w lines. This is marked by the green area in Figure 7.24. Based on this, we can see that the feasible design space is bounded by three constraints:

1. Stall speed
2. Cruise speed
3. Climb gradient

The other constraints are not actively bounding the design space for the chosen design parameters.

In order to minimize the design objective, we need to choose a point in the top-right corner of the feasible design space. Since there is no clearly defined top-right corner, we can select any point on the climb-gradient curve. We choose to go for a design point that results in the smallest wing at the junction of the stall-speed line and the climb-gradient line. This implies that the stall-speed constraint sizes the wing of the airplane while the climb-gradient constraint sizes the propulsion system. These are the two active constraints for the chosen design point. All other constraints are inactive.

JET AIRPLANE For our jet airplane, the feasible design space resides above all T_{TO}/W_{TO} curves and to the left of the W_{TO}/S_w lines. This is shown in green in Figure 7.25. The following constraints bound the design space:

1. Approach speed
2. Cruise speed
3. Climb rate
4. Take-off field length

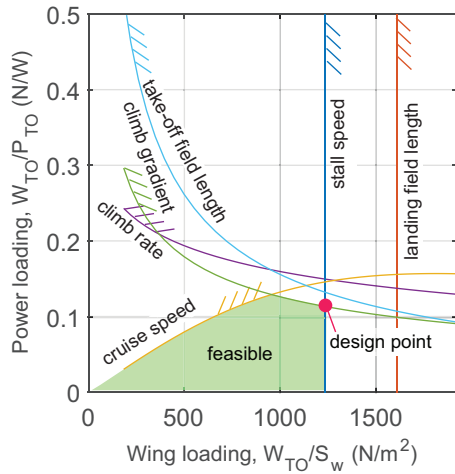


Figure 7.24: Matching diagram with feasible design space and chosen design point for the propeller airplane

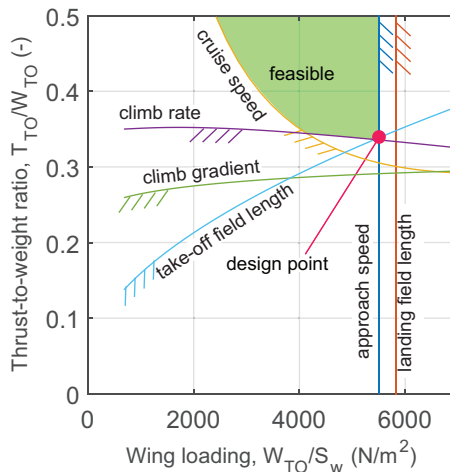


Figure 7.25: Matching diagram with feasible design space and chosen design point for the jet airplane

The other two constraints are not actively bounding the design space.

To minimize the design objective, we need to choose the design point in the bottom-right corner of the design space. Since the bottom right corner is not clearly defined, we can choose any design point on the take-off curve between the junction with the climb-rate curve and the junction with the approach-speed curve. We choose the design point at the junction between the take-off field length and the approach speed. For this choice, these two constraints are actively sizing the powerplant and wing of our jet airplane. All other constraints are inactive.

Now that we have chosen a feasible design point in our matching diagram, we can compute the power (or thrust) and wing area of the airplane, if we know the maximum take-off mass m_{MTO} . The wing area can be computed as follows:

$$S_w = \frac{m_{MTO}g}{W_{TO}/S_w} \quad (7.78)$$

For propeller airplanes, we can compute the take-off power as follows:

$$P_{TO} = \frac{m_{MTO}g}{W_{TO}/P_{TO}} \quad (7.79)$$

For jet airplanes, we can compute the sea-level static take-off thrust as follows:

$$T_{TO} = m_{MTO}g (T_{TO}/W_{TO}) \quad (7.80)$$

This is demonstrated in the following example.

Example 7.11

Consider the design points chosen for the propeller airplane and jet airplane in Example 7.10. We are going to calculate the required wing area for either airplane, along with the take-off power and take-off thrust, respectively.

PROPELLER AIRPLANE Assume that the battery-powered electric airplane has a maximum take-off mass of $m_{MTO} = 1,830$ kg. We can observe from the matching plot in Figure 7.24 that the design point corresponds to the following properties:

$$W_{TO}/S_w = 1230 \text{ N/m}^2 \quad W_{TO}/P_{TO} = 0.118 \text{ N/W}$$

By employing (7.78) and (7.79) we compute wing area, and take-off power:

$$S_w = 14.6 \text{ m}^2 \quad P_{TO} = 152 \text{ kW}$$

Since our jet airplane has a single electric motor, this motor should produce at least 152 kW of power.

JET AIRPLANE Assume that the jet airplane has a take-off mass of $m_{MTO} = 63.0$ t. We can observe from the matching plot in Figure 7.24 that the design point corresponds to the following properties:

$$W_{TO}/S_w = 5500 \text{ N/m}^2 \quad T_{TO}/W_{TO} = 0.34$$

By employing (7.78), (8.4), and (7.80) we compute the wing area and the take-off thrust at sea-level static conditions:

$$S_w = 112 \text{ m}^2 \quad T_{TO} = 210 \text{ kN}$$

Since the jet airplane has $N_e = 2$, each engine should have a take-off thrust of at least $T_{TO}/N_e = 105$ kN.

You can see that we have used six flight performance requirements to determine the required size of the wing and powerplant. This process is a *sizing* process as defined in Section 2.3. In this process we have been prompted to make assumptions as well as design choices. This implies that the resulting size of the wing and powerplant is dependent on these assumptions and choices. By making different choices, the result would be different. This is inherent to the design process. Some of the assumptions we have had to make are going to change once we analyze our airplanes. However, the result of the preliminary sizing process gives us an excellent starting point for the dimensioning of two of the most critical subsystems of an airplane: the wing and the powerplant. In Chapter 8, we will use the results from this preliminary sizing step as a starting point for determining the geometrical dimensions of the wing and powerplant. In the next assignment, you will determine the size of the wing and powerplant of your airplane.

ASSIGNMENT 7.10

In this assignment, you are going to determine the size of your wing as well as the power or thrust of your powerplant.

- In your matching diagram, indicate the feasible design space.

- b. List the constraints that are actively bounding the feasible design space.
- c. Based on your design objective, select a design point in your feasible design space. Report the value of W_{TO}/S_w and W_{TO}/P_{TO} or T_{TO}/W_{TO} , whichever one is applicable.
- d. Also plot the design points of your reference airplanes in the same diagram. Use the data from Assignment 3.9. How does your design point compare to those of your reference aircraft?
- e. Based on your design point, compute the value of S_w as well as P_{TO} or T_{TO} .
- f. If applicable, compute the take-off power or take-off thrust per engine or motor.

8

DESIGN OF WING AND PROPULSION SYSTEM

In this chapter, you are going to determine the design parameters of the wing and the propulsion system. At this point, we assume that you have determined the wing area (S_w) in a previous design step and that the aspect ratio of the wing has been chosen (see Chapter 7). In Chapter 4, you have chosen the type of propulsion system and the number of engines or motors for your design. Subsequently, in Chapter 2 you have estimated the required power (P_{TO}) or thrust (T_{TO}) that is required to meet the flight and field performance requirements.

In this chapter, you will learn how to determine the design parameters of your wing and propulsion system. For the wing, this includes determining the sweep angle, taper ratio, dihedral angle, and average thickness-to-chord ratio. All of these parameters will be properly introduced in the subsequent sections. We will also show how to position the main structural elements of the wing and how to compute the so-called mean aerodynamic chord (MAC). For the propulsion system, you will learn how to determine the dimensions of an engine or motor. If you have chosen propeller propulsion, you will learn how to determine the diameter of your propeller. Finally, we will show you how to integrate your propulsion system with the wing or fuselage.

This chapter is divided into three sections. In Section 8.1, we show you how to determine the geometrical design parameters that describe the wing shape. In Section 8.2, we show you how to size and integrate a propeller propulsion system. Here, we distinguish between electric motors, reciprocating engines, and turboshaft engines. In Section 8.3, we demonstrate how to determine the size of a turbofan engine and how to integrate it with the wing or the fuselage.

8.1. DESIGN OF WING GEOMETRY

The wing area and the wing aspect ratio are assumed to be known at this stage. However, that is not enough information to draw the wing in all three views. For that, we need

to estimate other geometric parameters. Together with the aspect ratio, the *sweep angle* and the *taper ratio* determine the *planform* shape of the wing, i.e the projection of the wing onto a horizontal surface. Based on the planform shape, we compute the location and dimension of the mean aerodynamic chord. The mean aerodynamic chord is the one-dimensional representation of the wing in the symmetry plane of the airplane. With the *dihedral angle* and the thickness-to-chord ratio, one can also draw the wing in side view and top view. How to determine each of these parameters is explained below.

8.1.1. SWEEP ANGLE

A wing can be swept forward or swept back for various reasons. Tailless airplanes require wing sweep to have adequate stability and control properties. However, most airplanes with tails use wing sweep to allow them to fly fast without a large penalty in drag. In the context of this book, we only consider wing sweep to be a function of the desired cruise speed.

Why does wing sweep allow for a higher cruise speed? That has to do with the formation of shock waves over the wing's upper surface that appear at high subsonic Mach numbers. These shock waves can cause flow separation, resulting in a large drag force. Without going into too much detail, the shock waves can form when the flow over the wing is sped up to supersonic conditions. Imagine that an airplane increases its Mach number during accelerated flight. For a given speed, the flow over the wing's upper surface has an even higher peak Mach number due to the wing's thickness and the lift it generates. Therefore, there exists a flight Mach number where the local Mach number reaches a value of 1: sonic flow somewhere on the wing. The flight Mach number where this occurs is called the critical Mach number. Beyond the critical Mach number, part of the wing experiences supersonic flow, and shock waves may occur. Introducing sweep increases the critical Mach number and, therefore, postpones shock wave formation. [24]

To understand how the critical Mach number is increased by wing sweep, have a look at Figure 8.1. Here, we have decomposed the Mach vector into a component parallel to the quarter-chord sweep line of the wing and a component perpendicular to it. Now, the effect that the parallel Mach vector has on the velocity distribution over the wing is negligible because in this direction, the wing is flat. On the contrary, the flow perpendicular to the sweep line experiences the airfoil curvature. Therefore, we can conclude that the perpendicular Mach vector is responsible for the flow acceleration over the wing and the maximum local Mach number reached. However, the magnitude of the perpendicular Mach vector is reduced by a factor $\cos \Lambda_{c/4}$, where $\Lambda_{c/4}$ is the quarter-chord sweep angle. In other words, the larger the sweep angle, the higher can be the critical flight Mach number.

This theory of how wing sweep can increase the critical flight Mach number is called *simple sweep theory* and is a simplification of the complicated interaction between geometrical parameters, such as wing sweep and wing thickness, and the mixed subsonic and supersonic flow that exists around the wing at high subsonic Mach numbers. However, simple sweep theory captures the most important effect that we are after: increasing the wing sweep can allow airplanes to fly at high subsonic Mach numbers with a relatively low drag penalty. We need a method that can relate the cruise speed to the

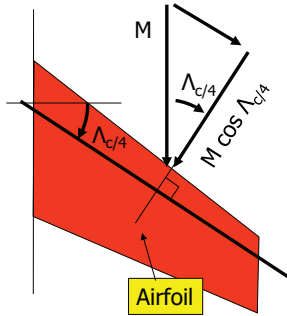


Figure 8.1: Definition of the quarter-chord sweep angle and decomposition of the Mach vector.

sweep angle.

In Ref. [10], the following method is presented to determine the quarter-chord sweep angle of the wing:

$$\Lambda_{c/4} = \begin{cases} 0 & \text{if } M_{CR} < 0.66 \\ \arccos\left(\frac{1.16}{M_{CR} + 0.5}\right) & \text{if } M_{CR} \geq 0.66 \end{cases} \quad (8.1)$$

where M_{CR} is the cruise Mach number that is related to the cruise speed V_{CR} through the local speed of sound according to (7.30). You can see that for airplanes that have a cruise Mach number below 0.66, we propose to have no sweep angle at all. It is implicitly assumed that with modern airfoils and the present sweep-Mach-number correlation, it is possible to obtain a wing geometry with adequate thickness to accommodate a lightweight structure and sufficient volume to store fuel and systems. For cruise Mach numbers higher than 0.66, the sweep angle increases gradually. For example, at $M_{CR} = 0.78$ the proposed quarter-chord sweep angle is $\Lambda_{c/4} = 25^\circ$.

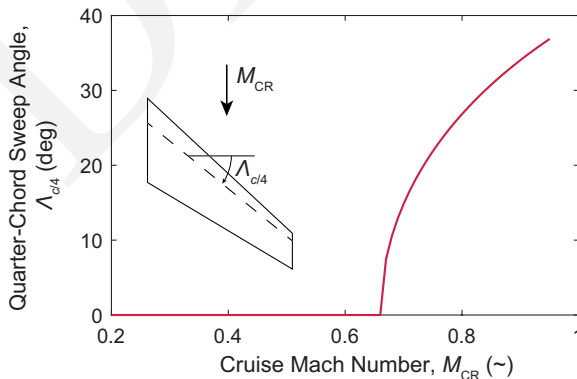


Figure 8.2: Proposed relationship between cruise Mach number and quarter-chord sweep angle.

ASSIGNMENT 8.1

In this assignment, you choose the quarter-chord sweep angle of your wing.

- What is the cruise Mach number of your airplane?
- What quarter-chord sweep angle do you choose for the wing of your airplane?
- Why do you choose this sweep angle for your wing?

8.1.2. TAPER RATIO

The taper ratio (λ) of the wing is defined as the ratio between the tip-chord length (c_t) and the root-chord length (c_r):

$$\lambda = \frac{c_t}{c_r} \quad (8.2)$$

As can be seen in Figure 8.3, the root chord of the wing is defined on the symmetry plane of the wing inside the fuselage. Also, note that both the root and tip chords are measured parallel to the airplane's longitudinal axis.

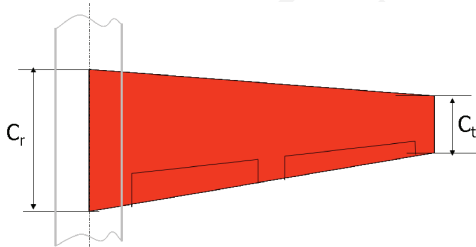


Figure 8.3: The taper ratio is the ratio of the tip chord over the root chord.

A wing with a taper ratio of 1 has the advantage of being easy to produce. The internal structure of a wing is often reinforced by positioning ribs in the chordwise direction at regular spanwise intervals. If the wing has no taper, each of the ribs has the same geometry. Also, all the connections between the wing skin and the ribs are the same at every rib station. This makes the manufacturing of ribs cheaper because you have fewer unique components. A tapered wing is, therefore, more expensive to produce but has advantages over an untapered wing.

Tapering the wing towards the tip affects the spanwise distribution of lift. You can imagine that a smaller chord length in the outboard wing also reduces the local lift. Vice versa, a larger wing chord at the root increases the lift. In other words, the value of the taper ratio influences how the lift is distributed. Figure 8.4 shows how the taper ratio changes the lift distribution for a wing with zero quarter-chord sweep angle. For a wing without tapering (i.e. $\lambda = 1$), there is relatively more lift over the outboard wing, while a taper ratio of $\lambda = 0$ causes more lift inboard. In Figure 8.5, we show that the sweep angle also affects the spanwise distribution of lift. Sweeping the wing rearwards results in more lift over the outboard wing and less lift inboard.

The redistribution of spanwise lift as a result of the taper ratio and the sweep angle has the following effects:

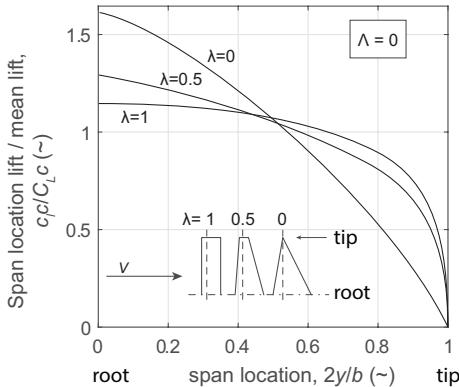


Figure 8.4: Effect of taper on spanwise lift distribution. Reproduced from Ref. [12].

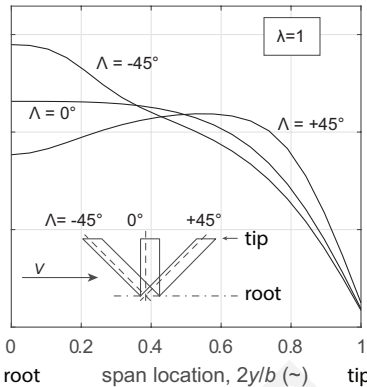


Figure 8.5: Effect of wing sweep on lift distribution on a wing without taper. Reproduced from Ref. [24].

1. **LIFT INDUCED DRAG.** The span efficiency factor (ϕ in Equation (5.17) of Section 5.2.1) is changed. The closer the lift distribution is to an elliptical lift distribution, the closer ϕ is to 1. An elliptical lift distribution minimizes the lift-induced drag of a wing. For a wing with zero quarter-chord sweep angle, a taper ratio of $\lambda = 0.4$ results in a lift distribution that is almost elliptical.
2. **WING MASS.** If more lift is generated outboard of the wing, this results in a higher bending moment in the wing structure. So tapering the wing can reduce the bending moments in the wing box. Secondly, a tapered wing results in a thicker airfoil at the wing root, which has a larger second moment of area about the chord line of the airfoil. This means that for a given bending moment and given allowable stress level in the material, a thinner skin or smaller spar cap is required to carry this moment. The lower bending moment and the larger second moment of area at the root of a tapered wing result in a lower mass of the wing structure compared to an untapered wing.
3. **TIP STALL** The taper ratio results in a lower chord length near the tip. The two-dimensional lift coefficient of an airfoil section has a dependency on the chord length. In general, airfoils with a smaller chord length have a lower maximum lift coefficient under the same aerodynamic conditions than the same airfoils with a larger chord length. This means stall on a tapered wing will likely start more outboard than on an untapered wing. A stall over the outboard wing might result in a reduction in roll control authority if an aileron is located in the stalled region of the wing. This effect is even stronger on tapered and swept wings.

You can choose a taper ratio anywhere between 0 and 1. Based on your design objective, you should qualitatively weigh the arguments above and come to a rational decision. To guide you in decision-making, we have reproduced a figure from Torenbeek [20] that plots the value of the quarter-chord sweep angle and taper ratio for various airplanes. You can see that for propeller airplanes, the taper ratio is scattered between 0.35 and 0.8. Also, you can see that when the quarter-chord sweep angle is increased, the taper ratio seems to decrease. Although there is quite some spread in the data, we propose

a simplistic trend line that relates the taper ratio to the sweep angle:

$$\lambda = 0.2 \left(2 - \Lambda_{c/4} \frac{\pi}{180} \right) \quad (8.3)$$

where $\Lambda_{c/4}$ is measured in degrees. You can see that this formula proposes a taper ratio of 0.4 when the quarter-chord sweep angle is zero. Naturally, you can deviate from this choice, as many airplane designers have done in the past.

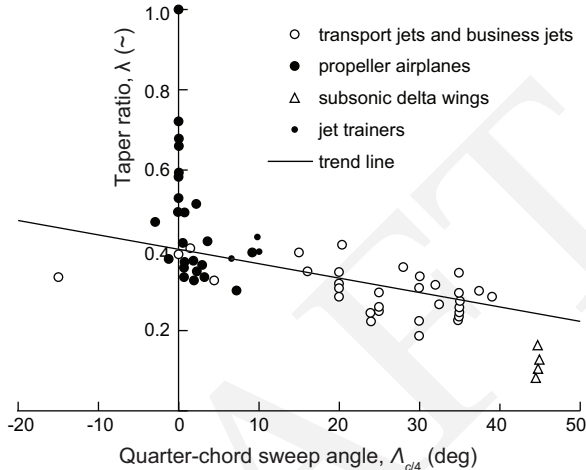


Figure 8.6: Sweep angle and taper ratio of various airplanes with notional trend line. Data from Ref. [20].

ASSIGNMENT 8.2

In this assignment, you choose the taper ratio of your wing.

- What taper ratio do you choose for your wing?
- Why do you choose this taper ratio?

8.1.3. WING PLANFORM AND MEAN AERODYNAMIC CHORD

In this section, we make the geometrical design of the wing planform, and we determine the so-called *mean aerodynamic chord*. The mean aerodynamic chord is a one-dimensional representation of the wing planform and is often used as a reference length. To construct the wing planform, we rely on the chosen values of aspect ratio (\mathcal{A}), sweep angle ($\Lambda_{c/4}$), and taper ratio (λ). Furthermore, we use the computed value of the wing area from Chapter 7. Finally, we assume a *straight-tapered wing*, i.e. a wing with a trapezoidal planform shape such as drawn in in Figure 8.1.

First, we estimate the span (b) of the wing using the definition of the aspect ratio (5.10):

$$b_w = \sqrt{\mathcal{A}_w S_w} \quad (8.4)$$

Secondly, we compute the root chord knowing that we have a trapezoidal wing planform:

$$c_r = \frac{2S_w}{(1 + \lambda)b} \quad (8.5)$$

Finally, using the definition of the taper ratio (8.2), we compute:

$$c_t = \lambda c_r \quad (8.6)$$

With all these geometric characteristics of the wing computed, it is now time to make a top-view drawing of our wing planform. In summary, we have the following design process for the wing planform design:

Step 1 Determine the quarter-chord sweep angle based on the cruise Mach number.

Step 2 Choose a taper ratio.

Step 3 Compute span, root chord, and tip chord.

Step 4 Draw a top view of the wing planform.

In the following example, we demonstrate how to do that.

Example 8.1

In this example, we design the wing planform for a turbofan airplane. We use the top-level airplane requirements from Example 7.1, which specify a cruise Mach number of $M_{CR} = 0.80$.

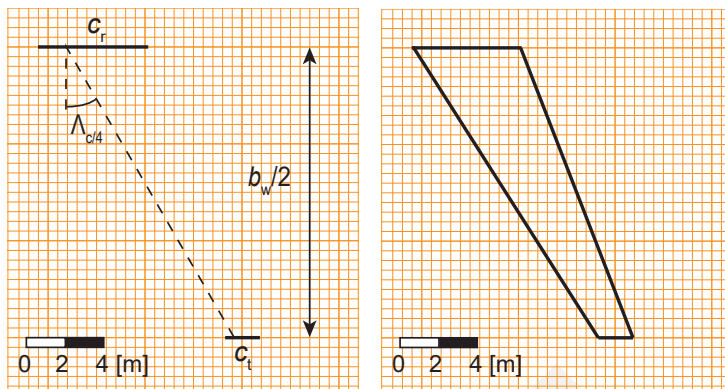
Step 1 We first determine the sweep angle. Since $M_{CR} = 0.80 > 0.66$, we decide to apply a sweep angle to our wing. We employ (8.1) to compute the quarter-chord sweep angle and report the value in the table below.

Step 2 Based on the sweep angle, we decide to use the linear relationship of (8.2) to compute the taper ratio and report the value in the table below.

Step 3 We subsequently employ Equations (8.4), (8.5), and (8.6) to compute the span, the root chord, and the tip chord. To do that, we use the wing area that we have determined in Example 7.11. We report the resulting values in the table below.

$\Lambda_{c/4}$ (°)	λ (-)	S_w (m^2)	b_w (m)	c_r (m)	c_t (m)
27	0.31	112	30	5.7	1.8

Step 4 We first draw the root chord and the span of the wing. Then, we draw the quarter-chord sweep line and the tip chord. Finally, we connect the leading and trailing edges of both wing sections, and we have the wing planform.


ASSIGNMENT 8.3

Draw the planform shape of your wing in the top view. You may also draw only one wing half, similar to the example above. Use the same scale as you used to draw your fuselage top view (Assignment 6.3) and side view (Assignment 6.4).

Now that we have defined the wing planform shape, we can graphically construct the mean aerodynamic chord (MAC), which is often written as \bar{c} . In Figure 8.7, the MAC, is drawn and the location of the leading edge of the MAC, i.e. the LEMAC, is indicated. The longitudinal location of the LEMAC and the length of the MAC are important properties of the wing. airplane properties such as the center-of-gravity or the neutral point are often expressed as a fraction of the MAC (See Section 9.1). To find the MAC and the LEMAC, we take the following steps:

Step 1 Draw the 50%-chord line

Step 2 From the trailing edge of the root, extend the root chord by a tip-chord length. Extend the tip chord by a root-chord length from the leading edge of the tip. Diagonally connect the points of the extended root and tip chords.

Step 3 At the intersection between the diagonal and the 50%-chord line, draw the mean aerodynamic chord line between the leading edge and trailing edge.

Step 4 Draw the MAC of the wing on the symmetry plane.

This graphical method works for all straight-tapered wings. However, technically, we have only constructed the MAC for only one-half of the wing. The MAC of the other wing half has the same longitudinal position but is mirrored in the symmetry plane. Therefore, the MAC of the full wing resides on the symmetry plane of the wing. You can perceive it as a one-dimensional representation of the wing. The following example shows how to construct the MAC using the steps above.

Example 8.2

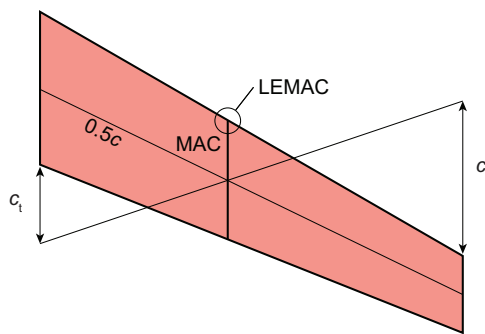
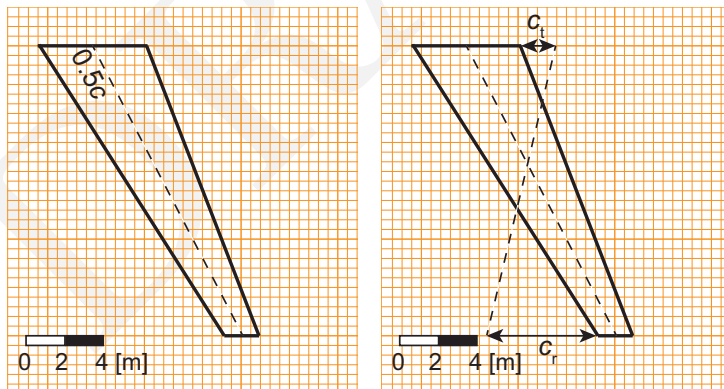


Figure 8.7: Geometric construction of the mean aerodynamic chord (MAC) on a straight-tapered half-wing planform.

In this example, we graphically construct the MAC for the wing of Example 8.1. We use the following steps:

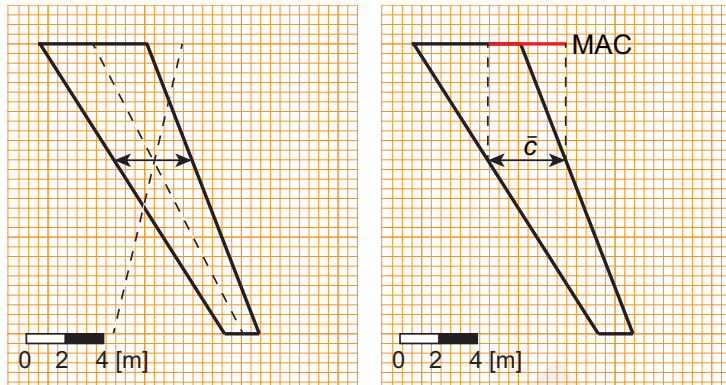
Step 1 First, we draw the 50%-chord line.

Step 2 Secondly, we extend the root and tip chords by the tip and root chords, respectively, and connect the tip points with a diagonal line.



Step 3 At the intersection of the two dashed lines, we draw the dimension of the MAC between the local leading and trailing edge.

Step 4 Finally, we draw the MAC on the symmetry line of the wing. We measure its length and find $\bar{c} = 4.1$ m.


ASSIGNMENT 8.4

Draw the mean aerodynamic chord on the symmetry line of your wing from Assignment 8.3.

8.1.4. POSITIONING OF SPARS

A typical wing structure comprises spars, ribs, and stiffeners. While it goes too far as to specify all of the elements in detail, in this section, we will present how to position the front spar and the rear spar. These structural elements are important for the integration of the landing gear (Chapter 9) and wing-mounted engines/motors (Section 8.2).

The spars are load-carrying components that transfer the wing lift to the fuselage. If a box structure is designed, the front and rear spar form the side edges of this box, while the wing skins form the top and bottom surfaces. To ensure a light-weight structure, it is important that this box forms a continuous load path between the fuselage and application point(s) of the load(s). Therefore, movable parts of the wing, such as ailerons and flaps, should be positioned behind the aft spar, while a movable leading edge should be positioned ahead of the front spar. The volume between the spars can be utilized for fuel storage. Therefore, the available fuel volume is also impacted by the location of the front and rear spar.

A wing can have a single spar, two, three, or even more spars. In the preliminary design phase (see Chapter 2), a more refined structural layout of the wing is made. In Figure 8.8, we show a wing profile with a front, mid, and rear spar. Here, we consider our wings to have a box structure with two spars: a front spar and a rear spar. In between the spars, we have volume for a fuel tank. We have a fixed leading edge or a leading-edge high-lift device such as a slat ahead of the front spar. Behind the rear spar, we can have a fixed trailing edge or volume for a flap or an aileron. In Chapter 11, we present how to size these wing movables. To allow for sufficient space for these high-lift devices, we

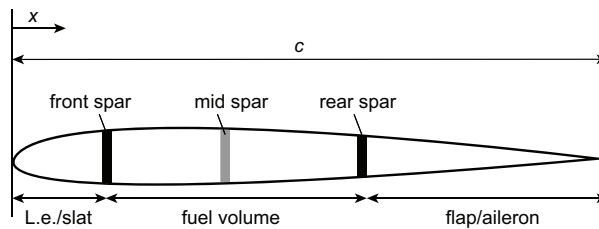


Figure 8.8: The chordwise location of the front and rear spar in a typical airfoil section.

propose the following positions of the front and rear spar, respectively:

$$\left(\frac{x}{c}\right)_{\text{front spar}} = 0.20 \quad (8.7)$$

$$\left(\frac{x}{c}\right)_{\text{rear spar}} = 0.70 \quad (8.8)$$

While it is likely that the exact positions of the spars change in the design process, they are important elements to position at this stage of the design process. The rear spar is important regarding the positioning of the main landing gear (Chapter 9), while the front spar is important for positioning a wing-mounted propulsion system such as a jet engine or an electric motor.

ASSIGNMENT 8.5

In this assignment, you position your wing's front and rear spar. You may assume that the spars are straight and are located at a constant chordwise location along the span of the wing.

- What is the chordwise location of your front and rear spar, respectively?
- Draw the spars in your wing planform from Assignment 8.3.

8.1.5. THICKNESS-TO-CHORD RATIO

The thickness of a wing has implications in several disciplines. First, the wing's thickness determines how much internal volume is available for storing fuel, integrating airplane systems, and positioning the wing structure. On the other hand, the thickness of a wing is limited by its aerodynamic characteristics.

The wing's structural mass contributes to the airplane's operating empty mass (OEM). A thicker wing leads to a lower structural wing mass. This is why. A high thickness-to-chord ratio results in a large second moment of area about the chord line of the airfoil. Since the wing lift is balanced by in-plane forces in the wing skin or spar caps, this implies that we can minimize the required skin thickness or spar cap area. This also gives us more internal volume to store wing systems such as (part of) the landing gear, fuel systems, and the fuel itself. So, a high thickness-to-chord ratio results in low wing mass and a large internal volume. However, aerodynamic considerations also need to be considered when selecting t/c .

First of all, the wing's drag is a function of the thickness-to-chord ratio. Generally speaking, the thicker the wing, the higher the so-called *form drag*. Form drag is drag associated with the shape of a body. Since the thickness-to-chord ratio of a wing affects the shape of the wing, it also impacts the form drag. The zero-lift drag of an airfoil can be correlated to the thickness-to-chord ratio using the following relationship:

$$c_{d0} \approx 0.0035 + 0.018 \left(\frac{t}{c} \right) \quad \text{for } 0.06 \leq \frac{t}{c} \leq 0.25 \quad (8.9)$$

The form drag of the airfoil contributes to the zero-lift drag coefficient (C_{D0}) that we have estimated in Chapter 5 based on the wetted-area-to-reference-area ratio (S_{wet}/S_w). The wetted area of the wing is approximately twice its wing area minus the part that is covered by the fuselage, i.e. $c_r \times w_{\text{fus}}$. We propose to select a thickness-to-chord ratio for which the two-dimensional zero-lift drag coefficient is:

$$c_{d0} < \bar{C}_f \left(2 - \frac{c_r w_{\text{fus}}}{S_w} \right) \quad (8.10)$$

where \bar{C}_f is the average friction drag coefficient of the airplane, which we introduced in Chapter 5.

If a wing is too thick, the flow might not be able to 'stick' to it and follow its curved surface all the way to the trailing edge. So, if airfoils are too thick, the flow might easily separate and cause the wing to stall. This can result in a low value of the maximum lift coefficient. On the other hand, if a wing is too thin, a sharp leading edge results, which can also cause premature separation and a relatively low maximum lift coefficient. This relationship is shown by means of bands for various two-dimensional airfoil families in Figure 8.9. While the maximum lift coefficient of an airfoil ($c_{l_{\max}}$) is not identical to that of a three-dimensional wing, it is correlated to it. The legend refers to various airfoil families that are further elaborated in Chapter 11. The band of each airfoil family is due to the fact that the maximum lift coefficient depends on the airfoil's size and the speed at which the airplane flies.

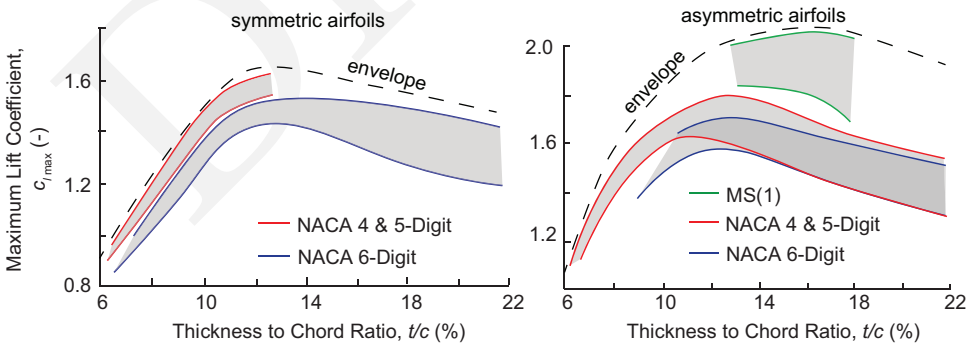


Figure 8.9: Relationship between thickness-to-chord ratio and maximum lift coefficient for various two-dimensional airfoil families. Modified from Ref. [15]

In Chapter 7, you made an assumption on the maximum lift coefficient, while in Chapter 11 you will further design the wing and estimate its maximum lift coefficient.

So at this stage of the wing design, you have to select a thickness-to-chord ratio that can support a wing shape with said $C_{L_{\max}}$. For swept wings with a moderate to high aspect ratio, it is known that the maximum lift coefficient deteriorates with increasing sweep angle. Therefore, we propose the following relation between the two-dimensional maximum lift coefficient of the airfoil ($c_{l_{\max}}$) and the quarter-chord sweep angle:

$$c_{l_{\max}} > 1.1 \frac{C_{L_{\max, CR}}}{\sqrt{\cos \Lambda_{c/4}}} \quad (8.11)$$

where $C_{L_{\max, CR}}$ is the maximum lift coefficient in the cruise configuration. The factor 1.1 accounts for three-dimensional effects as well as stall characteristics of the wing. We advise you to select a thickness-to-chord ratio for which the two-dimensional maximum lift coefficient is below the dashed envelope in the graphs of Figure 8.9.

If a wing is designed for Mach numbers higher than 0.65, it is likely to have wing sweep. Wing sweep allows airplanes to fly at high subsonic Mach numbers without a large drag penalty. However, that statement is only valid if the thickness-to-chord ratio is low enough to prevent the formation of strong shock waves at the combination of the cruise Mach number (M_{CR}) and the cruise lift coefficient ($C_{L, CR}$). Therefore, for swept wings, we follow Torenbeek [18] and propose:

$$\frac{t}{c} \leq \frac{\cos^3 \Lambda_{c/2} [0.935 - (M_{CR} + 0.03) \cos \Lambda_{c/2}] - 0.115 C_{L_{CR}}^{1.5}}{\cos^2 \Lambda_{c/2}} \quad (8.12)$$

where $\Lambda_{c/2}$ is the half-chord sweep angle and $C_{L_{CR}}$ is the cruise lift coefficient. This lift coefficient is computed from the lift equation (5.7), which can also be written in terms of M_{CR} and cruise pressure p_{CR} when we use the equation of state (7.14) and the Mach number definition (7.30):

$$C_{L_{CR}} = \frac{2}{\rho_{CR} V_{CR}^2} \frac{W_{TO}}{S_w} = \frac{2}{\gamma p_{CR} M_{CR}^2} \frac{W_{TO}}{S_w} \quad (8.13)$$

where W_{TO}/S_w is the wing loading, which we have estimated in Chapter 7 and γ is the ratio of specific heats, i.e. $\gamma = 1.4$ for air. Note that p_{CR} depends on the cruise altitude and can be computed using (7.12).

Figure 8.10 shows the relationship between the maximum thickness-to-chord ratio and the half-chord sweep angle for a range of cruise Mach numbers and two cruise lift coefficients. For a given lift coefficient and Mach number, a higher half-chord sweep angle allows for a higher thickness-to-chord ratio. Furthermore, you can observe that the allowable thickness-to-chord ratio is lower for $C_{L_{CR}} = 0.7$ compared to $C_{L_{CR}} = 0.3$.

In summary, to minimize the wing mass and maximize the internal volume, it is advised to choose a thickness-to-chord ratio that is as high as possible. However, aerodynamic constraints related to the profile drag, the maximum lift coefficient, and wave drag limit the thickness-to-chord ratio. Each of these can be perceived as a maximum lift *budget* that needs to be respected to arrive at a feasible design. This process consists of the following steps:

Step 1 Compute the maximum thickness-to-chord ratio to stay within the zero-lift-drag budget of the wing.

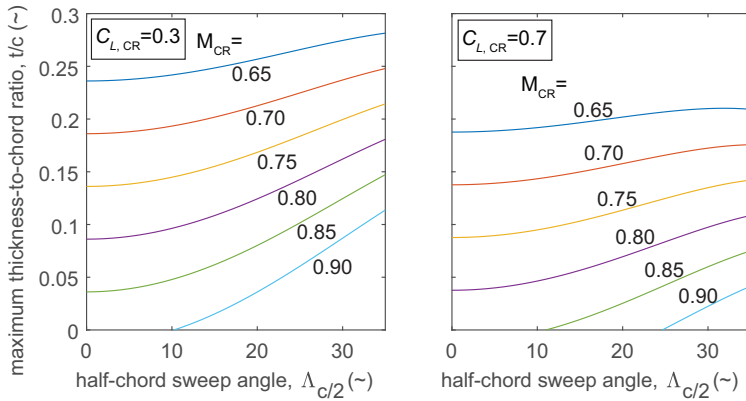


Figure 8.10: Relation between maximum thickness-to-chord ratio and half-chord sweep angle for various cruise Mach numbers and $C_{L,CR} = 0.3$ (left) and $C_{L,CR} = 0.7$ (right).

- Step 2* Compute the minimum and maximum thickness-to-chord ratio to stay within the maximum lift budget
- Step 3* For cruise Mach numbers over 0.65, compute the maximum thickness-to-chord ratio to stay within the wave drag budget.
- Step 4* select the highest thickness to chord ratio within the limitations set by the previous steps.

The next examples show how you can come to a robust choice for the thickness-to-chord ratio of your wing.

Example 8.3

In this example, we determine the thickness-to-chord ratio of the wing of Example 8.1.

- Step 1* Using (8.10) with $w_{\text{fus}} = 3.30 \text{ m}$ and $\bar{C}_f = 0.0030$, we compute that the two-dimensional, zero-lift-drag-coefficient budget for this wing is 55 drag counts. Using (8.9), we have $t/c \leq 0.111$.
- Step 2* Using (8.11), we compute that the airfoil should have a maximum lift coefficient that should be higher than 1.74. Using the envelope for asymmetric airfoils of Figure 8.9, we derive $0.094 \leq t/c \leq 0.245$.
- Step 3* Since the cruise Mach number is in excess of 0.65, we use (8.12) to compute: $t/c \leq 0.106$
- Step 4* Summarizing the previous steps, we have $0.094 \leq t/c \leq 0.106$. Therefore, we decide to select $t/c = 10.6\%$.

The previous example has shown that the difference between the minimum and maximum thickness-to-chord ratio can be quite small. You can imagine that in some cases,

the minimum thickness-to-chord ratio is higher than the maximum thickness-to-chord ratio. Then, you cannot choose a thickness-to-chord ratio that can satisfy all budgets. So, what do you do? In essence, you then have two options:

Option 1 You choose a thickness-to-chord ratio between the minimum and maximum values you have computed. This is advised if these two values are quite close to each other.

Option 2 You go back to an earlier step in the design process and lower the value for $C_{L_{\max, CR}}$ (see Assignment 7.1) or increase the value for the equivalent friction coefficient, \bar{C}_f (see Assignment 5.2). This option is advised if the minimum value is much higher than the maximum value.

If you choose option 2, you are essentially iterating on your design. You are updating a value that you estimated in an earlier design step. However, all the calculations that are performed downstream of the selection of these parameters need to be redone.

ASSIGNMENT 8.6

In this assignment, you will determine the thickness-to-chord ratio of your wing.

- a. What is the maximum zero-lift drag coefficient of the two-dimensional airfoil of your wing (c_{d_0}), and what is the corresponding maximum thickness-to-chord ratio?
- b. What is the minimum $c_{l_{\max}}$ of the airfoil? What is the associated minimum and maximum value of the thickness-to-chord ratio?
- c. If you have a cruise Mach number in excess of 0.65, what is the maximum thickness-to-chord ratio to minimize the wave drag?
- d. Based on the answers to the above questions, what is the minimum value of the thickness-to-chord ratio, what is the maximum value of the thickness-to-chord ratio, and what value of the thickness-to-chord ratio do you choose?
- e. Is there a need to revisit the assumptions on $C_{L_{\max, CR}}$ and/or \bar{C}_f based on your choice of the thickness-to-chord ratio?

8.1.6. DIHEDRAL

A wing's dihedral angle, Γ , is the angle the wing forms with the horizon when seen from the front and is shown in Figure 8.11. The dihedral angle impacts the lateral stability of the airplane, i.e. its rolling moment due to sideslip. . In Section 4.2.1, we explained what lateral stability means and why it is important for an airplane. We showed that a high-wing configuration increases the lateral stability while a low-wing configuration reduces the lateral stability. Lateral stability is also referred to as the *dihedral effect*. This is because an increase in dihedral angle increases the rolling moment due to sideslip.

The dihedral effect is explained in Figure 8.12. Here, it is assumed that the airplane experiences a small sideslip angle, β , which causes a side wind with respect to the airplane. The magnitude of the side wind is $V \sin \beta$. If we assume that the sideslip angle is small, we can approximate the side wind component with βV , where β is expressed

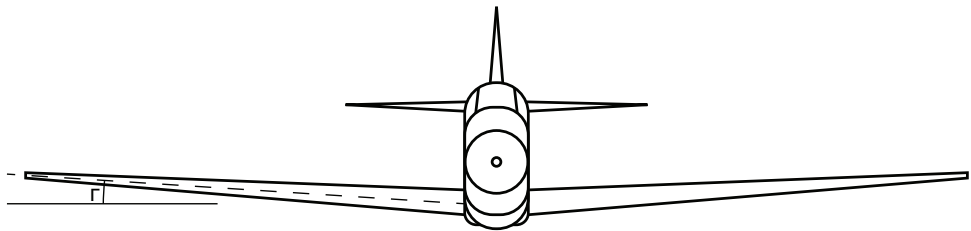


Figure 8.11: Definition of the dihedral angle of a wing

in radians. If we decompose the side wind velocity component into a component perpendicular to the wing and a component parallel to the wing, we observe that the port wing experiences a small increase in angle-of-attack, while the starboard wing experiences a decrease in angle-of-attack. Therefore, the port wing experiences an increase in lift, while the starboard wing experiences a decrease in lift. As a result, the airplane experiences a rolling moment in the counter-clockwise direction when seen from the front. This is a stabilizing rolling moment.

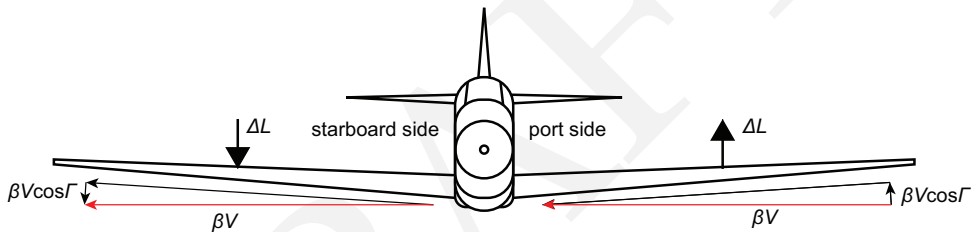


Figure 8.12: The dihedral angle Γ causes a change in lift on either wing half when subjected to a sideslip angle β .

Apart from the dihedral angle, also the sweep angle impacts the rolling moment due to sideslip. This is illustrated through vector decomposition in Figure 8.13. When we decompose the velocity vector V into a component perpendicular to the leading edge and a component parallel to the leading edge, we observe that the perpendicular component is smaller on the starboard side compared to the port side. If we assume that the perpendicular velocity component is responsible for the change in lift, we can deduce that the port-side wing produces more lift than the starboard-side wing. This causes a rolling moment in the counter-clockwise direction when seen from the front. In other words, an aft-swept wing produces a stabilizing rolling moment due to sideslip.

In summary, we have seen that there are three aspects that determine the lateral stability of the airplane:

1. Vertical wing position. A high-wing configuration increases stability.
2. Dihedral angle. The dihedral angle increases stability.
3. Wing sweep. Wing sweep increases stability.

When an airplane has a high-wing configuration, an aft-swept wing, and a positive dihedral angle, it could have too much lateral stability. That implies that the airplane produces a relatively large rolling moment when subjected to a side wind. This is, for

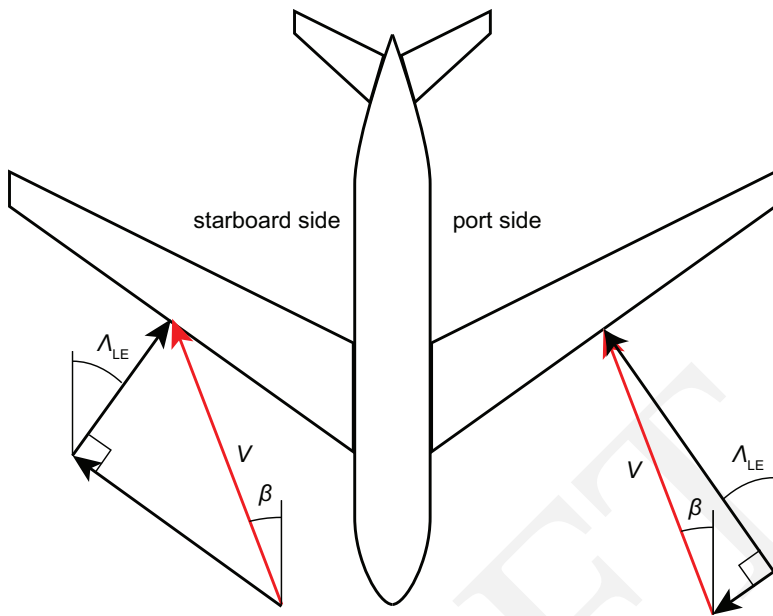


Figure 8.13: A sideslip angle causes a difference in the magnitude of the velocity vector perpendicular to the leading edge of the starboard wing and port wing, respectively.

example, problematic when performing a landing in cross-wind conditions. Therefore, airplanes with a high-wing configuration and wing sweep often apply *anhedral*, i.e. negative dihedral.. Applying anhedral to the wing reduces the lateral stability.

To determine the 'right' dihedral angle, we propose the following guidelines:

- Default: $\Gamma = 3^\circ$ for unswept wings at mid-wing location
- For every 10 degrees of quarter-chord sweep angle, reduce the dihedral angle by 1 degree.
- For high-wing or low-wing airplanes: subtract or add 2 degrees, respectively.

The following example shows how these guidelines can be applied.

Example 8.4

In this example, we determine the dihedral angle for the wing of Example 8.1, and we assume that this wing is made for an airplane with a low-wing configuration.

This wing has a quarter-chord sweep angle of 26° . If we follow our guidelines, we compute the following:

$$\Gamma = 3.0^\circ - 0.1 \cdot 27^\circ + 2.0^\circ = 2.3^\circ$$

The dihedral angle also has an effect on the clearance between the ground and the wing when the airplane is close to the ground and has a bank angle. Also, when an engine or a propeller is located on the wing, the dihedral of the wing affects its ground clearance. Figure 8.14 shows that the dihedral angle causes a vertical displacement of the propeller

and turbofan propulsion systems when mounted on the wing. It also raises the wing tip and provides adequate clearance when landing on one wheel with a bank angle of ϕ . Typically, a minimum clearance angle of eight degrees is required, i.e. $\phi > 8^\circ$, but more is desired to allow for operational maneuvering in proximity to the ground. Increasing the dihedral angle of a low-wing airplane can, therefore, result in lower landing-gear height and associated landing-gear mass. Therefore, choosing a dihedral angle that is a few degrees higher than suggested by the guidelines above can be justified.

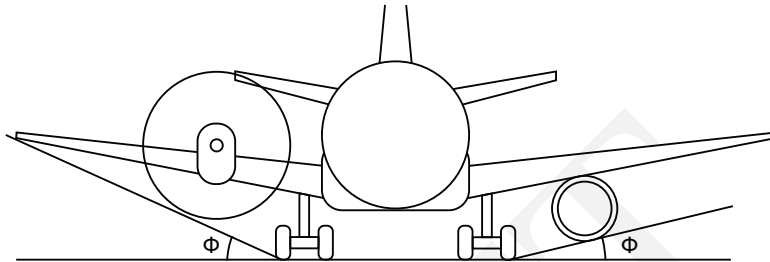


Figure 8.14: The wing's dihedral can increase the ground clearance of the wing and/or propulsion system when landing with a bank angle ϕ .

ASSIGNMENT 8.7

In this assignment, you are going to determine the dihedral angle for your airplane.

- Using the guidelines presented above, compute the dihedral angle, Γ .
- Based on ground-clearance considerations, would you increase the dihedral angle? If so, why? What dihedral angle would you then choose?

8.1.7. DRAWING THE WING IN FRONT AND IN SIDE VIEW

With the thickness-to-chord ratio and the dihedral angle defined, we can now draw the wing in the front and side views. We propose to use the American convention to prepare a three-view drawing of our wing. We propose the following steps to arrive at the front view and side view of the wing:

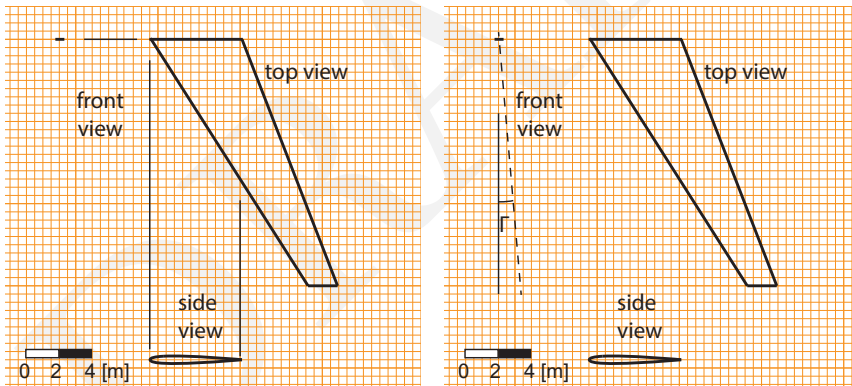
- Step 1* With the thickness-to-chord ratio, compute the wing thickness at the root of the wing. Draw the root of the wing in front view by means of a line. In the side view, draw an airfoil profile with the thickness and chord at the location of the root.
- Step 2* With a dashed line, draw the dihedral angle through the center of the root wing section with the same span as the wing.
- Step 3* Measure the vertical displacement of the tip section (Δz_t) with respect to the root section of the wing in the front view and draw the tip profile in the side view. With the thickness-to-chord ratio, compute the wing thickness at the tip and draw the tip section by means of a line.
- Step 4* Finish the side view of the wing by connecting the root and the tip airfoil by drawing lines between their respective leading and trailing edges.

In the following example, we show how this leads to a front view and side view of your wing.

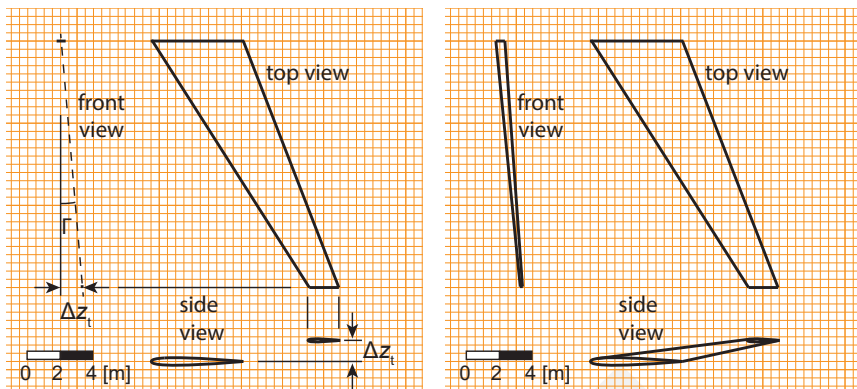
Example 8.5

In this example, we draw the wing of Example 8.1 in the front and top views.

- Step 1* With a thickness-to-chord ratio of 10.5%, we compute root thickness of 60 cm. We construct a generic profile shape in the side view of 60 cm and a line in the front view of the wing (below, left)
- Step 2* With a dashed line, we draw the dihedral angle in the front view (below right). Rather than using 2.3° , like in Example 8.4, we decide to use $\Gamma = 5^\circ$. This is due to the fact that turbofan engines are to be mounted to the wing. A somewhat higher dihedral angle could result in a somewhat shorter landing gear.



- Step 3* We compute a vertical displacement of the tip of $\Delta z_t = 1.3$ m, and we mark the location of the tip in the side view. With $t/c = 0.105$, we compute a tip thickness of 0.19 m. Subsequently, we draw the tip profile in the side view and a small line in the front view (below, left).
- Step 4* We finish the front view by connecting lines between the top and bottom of the airfoil profile, respectively. We finish the side view by connecting the leading and trailing edges of the root and tip profiles. This is shown below, right.


ASSIGNMENT 8.8

Using the steps presented above, add a front view and side view to the wing drawing you made in Assignment 8.3. Use the American convention to position your front and side views with respect to your top views, similar to Example 8.5. Use the same scale as in 8.3.

8.2. DESIGN AND INTEGRATION OF A PROPELLER PROPULSION SYSTEM

In Chapter 4, you have selected the type of propulsion system and the energy carrier for your airplane. If you have chosen propeller propulsion, this section explains how to dimension the propeller and the engine or motor. Propeller-powered airplanes can have three different types of powerplants: a reciprocating engine, a turboshaft engine, or an electric motor. Each of them is presented in an individual subsection. However, let us start with the propeller.

8.2.1. PROPELLER DIAMETER

The design of a propeller is complicated and involves many design steps. Decisions regarding the number of blades, the blade planform geometry, and the airfoils in the blade are beyond the scope of this text. Here, we only focus on the diameter of the propeller, which is important regarding the integration of the propulsion system within the airplane.

The function of the propeller is to transfer the shaft power to thrust. In order to produce that thrust, you need sufficient surface area of the propeller blades. The required diameter in order to achieve this disk area is dependent on the following factors:

- angular speed
- cruise speed
- engine power
- number of blades

- blade geometry
- tractor or pusher configuration

The angular speed and the cruise speed determine the *helical tip Mach number* of the blade. As the tip of the blade rotates, it also moves forward with respect to the flow. Therefore, the resultant velocity can be found by velocity vector triangulation. If this helical tip velocity is close to the speed of sound (i.e. the helical tip Mach number is close to one), the noise of the propeller can increase dramatically. As the tip speed is governed by the angular speed and the diameter, the implicit requirement to limit propeller noise affects the diameter of the propeller.

Statistically, a good first estimate for the diameter of a tractor propeller is given by:

$$D_p = 0.55 \sqrt[4]{\frac{P_{TO}}{1000 N_e}} \quad (8.14)$$

Where D_p is measured in meters, N_e is the number of engines (or motors), and P_{TO} is the take-off power that we determined in Chapter 7. Equation 8.14 is a modification of the method presented in Ref. [12]. A short survey among civil and military propeller airplanes showed that most propellers fall within a 5% accuracy of this estimation, while military propellers are underestimated in size up to 15%.

Example 8.6

For the battery-powered, four-seat airplane of Example 7.11, we determine the propeller diameter. We have $P_{TO} = 152$ kW and $N_e = 1$. Employing (8.14), we get: $D_p = 1.9$ m.

ASSIGNMENT 8.9

If your airplane has a propeller, use the methods presented above to determine the diameter of your propeller.

8.2.2. ENGINE AND MOTOR SIZING

As shown in Figure 4.2, there are three different systems that can provide shaft power to the propeller: a reciprocating engine, a turboshaft engine, or an electric motor. Also, hybrid-electric power trains can be conceived, but they are beyond the scope of this book due to the increased complexity [26]. With a known take-off power, you can choose an engine or motor from an online engine database. The characteristic dimensions, the engine mass, and the power-specific fuel consumption can then be used in the subsequent integration and analysis steps. However, in this section, we provide simple relations that define the dimensions of engines based on their take-off power, along with a volumetric *engine envelope* to account for adjacent systems.

RECIPROCATING ENGINE Many reciprocating engines are have an opposed piston configuration. That implies that two rows of pistons are opposite each other in the same plane. Such a reciprocating engine has the shape of a rectangular box with a height (h_e), a width (w_e), and a length (l_e). An example of a piston engine with the box dimensions

is shown in Figure 8.15. To estimate these dimensions we slightly modify the method of Ref. [12] and find:

$$h_e = 0.30 \left(\frac{P_{TO}}{1000N_e} \right)^{0.10} \quad w_e = 0.17 \left(\frac{P_{TO}}{1000N_e} \right)^{0.30} \quad l_e = 0.06 \left(\frac{P_{TO}}{1000N_e} \right)^{0.55} \quad (8.15)$$

where all the lengths are measured in meters. A small survey among opposed piston engines demonstrates that the predictions of Equation 8.15 to be within 10% of the measured values.

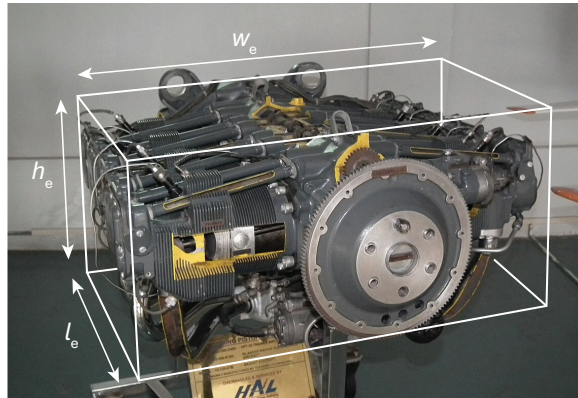


Figure 8.15: Example of a piston engine with rectangular box dimensions. Photo: Rameshng @①②

A reciprocating engine requires clearance to the adjacent airplane structure to add cooling systems, including an air intake, to fit auxiliary systems such as an alternator, and to fit the engine support structure. Therefore, we add 10% of engine width on all sides of the engine, except on the front side of the engine. We propose the following relations to define the dimensions of a rectangular box around the engine. We use the subscript 'ee' to refer to the engine envelope:

$$h_{ee} = h_e + 0.2w_e \quad w_{ee} = 1.2w_e \quad l_{ee} = l_e + 0.1w_e \quad (8.16)$$

Example 8.7

Assume that the airplane of Example 7.11 would have a reciprocating engine with the same take-off power. We determine the dimensions of the engine envelope for such an opposed-piston engine.

We have $P_{TO} = 152 \text{ kW}$ and $N_e = 1$. We first employ Equation 8.15 to find:

$$h_e = 0.50 \quad w_e = 0.77 \quad l_e = 0.95$$

We then employ (8.16) and find the dimensions of the engine envelope of this opposed-piston engine:

$$h_{ee} = 0.65 \quad w_{ee} = 0.92 \quad l_{ee} = 1.03$$

TURBOSHAFT We approximate the shape of a turboshaft engine as a circular cylinder with diameter D_e and length l_e . An example of a turboshaft engine with a cylinder drawn around it is shown in Figure 8.16. For the same engine dimensions, the shaft power can vary considerably for this engine. A good first estimate for the engine dimensions is given in Ref. [12]:

$$D_e = 0.20 \left(\frac{P_{TO}}{1000N_e} \right)^{0.18} \quad l_e = 0.10 \left(\frac{P_{TO}}{1000N_e} \right)^{0.40} \quad (8.17)$$

where P_{TO} is the take-off power and N_e is the number of engines.

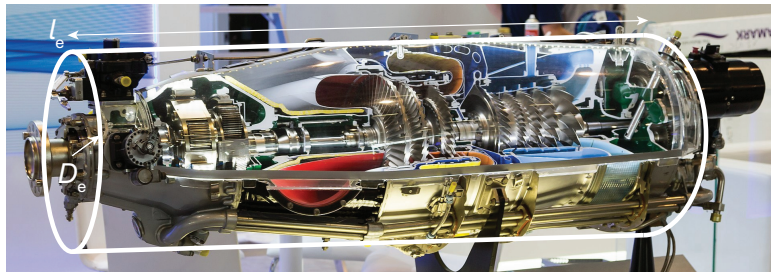


Figure 8.16: Example of turboshaft engine with circular tube dimensions. Photo: Matti Blume ©①②

An engine envelope is required to allocate volume for the support structure between the engine and the airframe. Moreover, volume is required for air ducting to and from the engine. Various shapes can be selected for engine envelopes. One of these shapes is a rectangular box that encompasses the engine and has an inlet located below the engine. The dimensions of the engine envelope for a turboshaft engine can be approximated with:

$$h_{ee} = 1.5D_e \quad w_{ee} = 1.1D_e \quad l_{ee} = l_e \quad (8.18)$$

Example 8.8

In this example, we size turboshaft engines for a commercial transport airplane of 50 passengers. In previous steps, we decided that this airplane has $N_e = 4$ turboshaft engines.

We perform the following steps:

- Step 1* Using Equation 8.14, we compute that the propeller diameter for each propeller is $D_p = 2.9$ m.
- Step 2* Using Equation 8.17, we compute that each turboshaft engine has the following dimensions: $D_e = 0.67$ m and $l_e = 1.46$ m.
- Step 3* Using Equation 8.18, we compute the following dimensions for the engine envelope: $h_{ee} = 1.00$ m, $w_{ee} = 0.73$ m, and $l_{ee} = 1.46$ m.

ELECTRIC MOTOR In Figure 8.17, we show an example of an electric motor that has been developed to drive a propeller. The motor itself can be approximated by a cylinder of

low fineness ratio, i.e. the ratio of the length over the diameter.. In addition, you can see two box-shaped items that are connected to the motor. These are so-called inverters. An inverter converts the direct current (DC) from the battery into alternating current (AC) for the motor. The inverter is connected to the cockpit motor controls and regulates the motor's rotational speed.

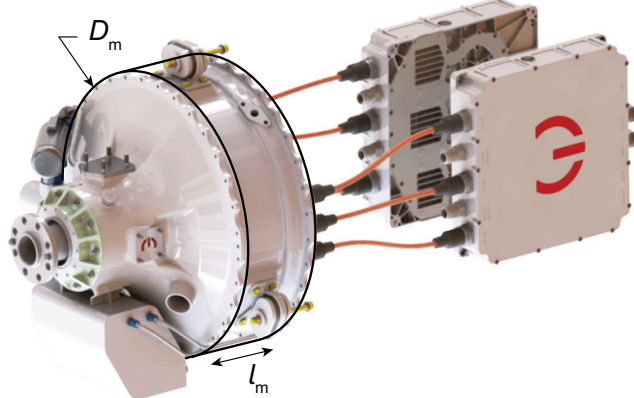


Figure 8.17: Example of an electric motor with circular tube dimensions and attached power electronics.
Photo: Magni-X

To determine the dimensions of the electric motor, we first establish the power density of the motor, i.e. the amount of power per unit volume. We call this parameter ρ_p , which has the unit W/m^3 . The subscript 'p' refers to power. The fineness ratio of the motor is indicated with f_m , and is defined as follows:

$$f_m = \frac{l_m}{D_m} \quad (8.19)$$

where D_m is the motor diameter and l_m is the motor length as shown in Figure 8.17. Using the geometrical relations of a cylinder, we determine the diameter of the engine as follows:

$$D_m = \sqrt[3]{\frac{4P_{TO}}{\pi f_m \rho_p}} \quad (8.20)$$

For a chosen motor fineness ratio, f_m , we can then use Equation 8.19 to compute the length of the motor, l_m .

With the motor dimensions established, we now determine the required engine envelope.¹ As you can see, the inverters in Figure 8.17 occupy quite some volume. This can also be seen in Figure 5.9, where an electric motor is integrated into the nose of a small airplane. We consider the volume that is occupied by the inverter and the cables between the motor and the inverter to be part of the engine envelope. On the other hand, the liquid cooling system that may be required for electric motors and inverters is not

¹We keep the terminology for the engine envelope the same as for the internal combustion engines, even though we have an electric motor.

considered to be part of the engine envelope. For the engine envelope, we propose a rectangular box around the engine with the following dimensions:

$$h_{ee} = 1.1D_e \quad w_{ee} = 1.1D_e \quad l_{ee} = l_m + (1 + k_{\text{cable}}) \sqrt[3]{\frac{\pi l_e D_m^2}{4}} \quad (8.21)$$

where k_{cable} is the ratio between inverter volume and the volume occupied by the cables between the motor and the inverter. If the inverter is attached to the motor, $k_{\text{cable}} = 0$. Note that we compute the volume required by the inverter by assuming its volume equals the volume of the electric motor and that it is shaped like a cube. In practice, various other motor-inverter configurations have been conceived, which are considered outside the scope of this textbook.

Example 8.9

In this example, we determine the dimensions of the electric motor for the propeller airplane of Example 7.11. From Example 7.11, we have a take-off power of $P_{TO} = 152 \text{ kW}$.

To determine the dimensions of the electric motor, we perform the following steps:

- Step 1* We choose a motor fineness ratio of $f_m = 0.5$ and assume a power density of $\rho_p = 7.0 \text{ MW/m}^3$.
- Step 2* We employ (8.20) and (8.19) to compute $D_m = 0.38 \text{ m}$ and $l_m = 0.19 \text{ m}$, respectively.
- Step 3* We choose $k_{\text{cable}} = 0.8$ and with (8.21) we compute: $h_{ee} = 0.42 \text{ m}$, $w_{ee} = 0.42 \text{ m}$, and $l_{ee} = 0.69 \text{ m}$.

ASSIGNMENT 8.10

If your airplane has a propeller, perform the following tasks:

- Determine the dimensions of your engine or motor.
- Determine the dimensions of your engine envelope.

8.2.3. INTEGRATION WITH THE FUSELAGE

When we have a propeller, an engine box, and an engine envelope, we can integrate the engine with the airframe. In the following examples, you can see how this can be done. First, we show the integration into the nose of an airplane (Example 8.10) and subsequently for integration with the wing (Example 8.12). When integrating the engine in the nose of the airplane, we follow these guidelines:

1 LATERAL POSITIONING

The engine is located on the symmetry plane of the airplane. This ensures that the thrust vector does not produce a yawing moment.

2 LONGITUDINAL POSITIONING

The engine envelope's rear is positioned against the front of the fuselage. This

ensures that we have the smallest cowling wetted area and also makes it easier for the pilot to see over the nose (i.e., the over-nose angle).

3 VERTICAL POSITIONING

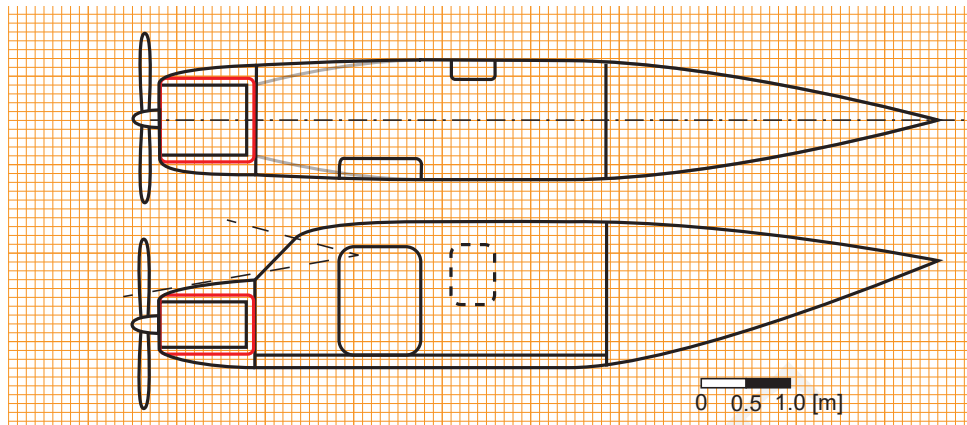
We would like to position the engine as close as possible to the center of the fuselage to minimize the thrust-induced pitching moment w.r.t. the center of gravity. However, the required over-nose angle limits the vertical position for which the engine can be installed.

The following example shows how a piston engine can be installed on the nose of a small airplane.

Example 8.10

The airplane of Example 6.7 is a four-seat airplane with a tractor propeller mounted on the nose. The fuselage is truncated at the front to leave room for an engine or motor. In this example, we show how the engine of Example 8.7 is integrated with the fuselage of Example 6.7. The figure below shows how the engine and the engine envelope (in red) are integrated with the fuselage. Here are the steps we take to position the engine with respect to the fuselage:

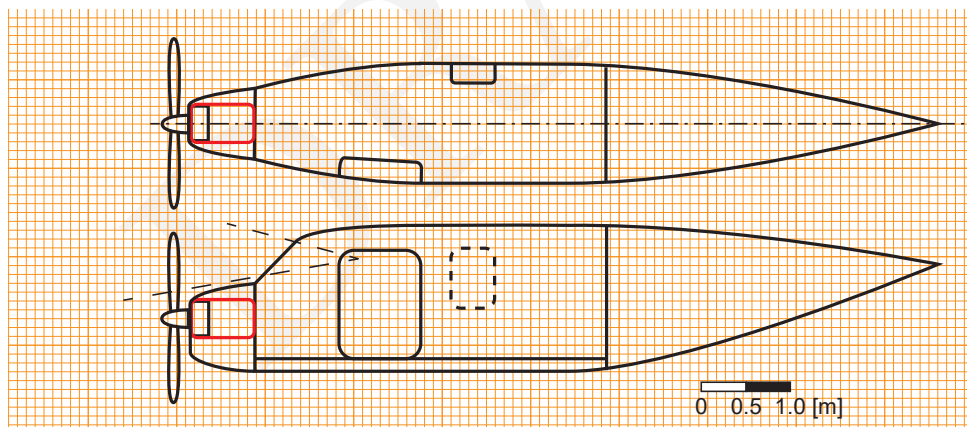
- Step 1* In the side view, we position the engine envelope against the front line of the fuselage. This line represents the *firewall*, a protective surface that separates the passenger cabin from the engine compartment. We try to position the engine as high as possible to minimize the pitching moment around the airplane's center of gravity. However, we are limited by the required over-nose angle.
- Step 2* We add the propeller and the spinner, i.e. the aerodynamic cover around the propeller hub.
- Step 3* We draw a notional engine cowling that gives the airplane its characteristic nose shape.
- Step 4* We draw the engine, the engine envelope, and the propeller in the top view of the airplane.
- Step 5* We add an engine cowling between the engine and the fuselage. In this example, the original fuselage design had some tapering towards the nose (still shown in gray). However, since the engine envelope is wider than the front of the original fuselage, we decide to modify the fuselage shape to better match the dimensions of the engine envelope.



Example 8.11

In this example, we integrate the electric motor of Example 8.9 with the fuselage of Example 6.7.

To integrate the motor of Example 8.9 we follow the same steps as laid out in Example 8.10 for integrating a piston engine in the nose of an airplane. Compared to the engine envelope of the piston engine, the volume of the engine envelope of the electric motor is considerably smaller. This allows for a smaller volume in the nose to house the motor and the inverters, as can be seen below.



ASSIGNMENT 8.11

If your airplane has propeller propulsion and you have chosen for integration in the nose of the airplane, perform the following tasks:

- a. Integrate the engine and propeller with the nose of your fuselage. Do this in the top view, side view, and front view.
- b. Add an appropriate engine cowling to ensure a smooth integration with the fuselage.

8.2.4. INTEGRATION WITH THE WING

In Example 8.10, we showed the integration of a reciprocating engine with a tractor propeller to the nose of a fuselage. However, we can also have engines mounted to the wing. When you are designing an airplane with wing-mounted reciprocating engines, we advise you to use the following guidelines:

1. LATERAL POSITIONING
 - i. Position the propeller as close as possible to the fuselage to minimize the one-engine-inoperative yawing moment.
 - ii. Keep between $0.1D_p$ and $0.3D_p$ of propeller clearance between the propeller tip and the fuselage to prevent acoustic fatigue on the fuselage structure and excessive cabin noise.
2. LONGITUDINAL POSITIONING
 - i. Minimize the risk of catastrophic failure in case of a blade-off event by ensuring that flight critical systems and the pilot compartment are outside the path of the propeller (see Example 3.19).
 - ii. Make sure the engine envelope is ahead of the front spar. For turboprop engines, this allows the fuel tank to be outside the hazard zone in case of turbine rotor burst. Additionally, this allows for easy installation and de-installation of the engine for maintenance purposes. Also, the wing's box structure remains uninterrupted, resulting in a maximal strength-to-mass ratio.
 - iii. Leave at least $0.5D_p$ between the propeller disk and the wing's leading edge to reduce the wing's aerodynamic effect on the propeller performance.
3. VERTICAL POSITIONING
 - i. Position the engine to minimize the thrust-induced pitching moment. This means that the arm between the thrust vector and the airplane's center of gravity should be minimized.
 - ii. Position the engine in such a way as to minimize the additional wetted area due to the engine. Positioning the engine axis in the middle of the wing results in the lowest wetted area of the engine cowling and, therefore, the minimum friction drag.
 - iii. Position the engine in such a way as to minimize the landing gear length. In the case of a low-wing airplane, the propeller clearance to the ground should be respected also in the case of deflated tires and compressed landing gear struts (see Example 3.17). Therefore, you may decide to raise the engine in favor of a shorter landing gear.

You might have noticed that information from other airplane components, such as the fuselage and landing gear, is required for some of these guidelines. Some of that information is not yet present in the first design iteration. Also, some of the guidelines might

be conflicting with each other. This means that you have to find a compromise when selecting the actual position of your engine with respect to your wing.

When you have positioned the engine and propeller on the wing, it results in a non-smooth geometry that is likely to create quite some pressure drag. Therefore, you need to add a fairing between the engine and the wing, just like a cowling was added to the engine in Example 8.10. In adding such a fairing, the following guidelines should be adhered to:

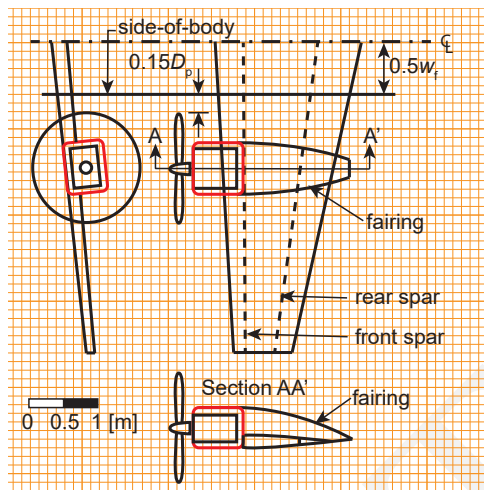
1. The fairing should go around the engine envelope
2. The fairing should be aerodynamically shaped (no sharp corners except for the trailing point)
3. The fairing should be long enough to position a structure within, which connects to the front spar and/or the rear spar.

Example 8.12

In this example, we integrate a reciprocating engine to a wing of a twin-prop airplane. The wing, propeller, and engine have been sized ahead of this example. Here we focus on how to integrate the engine. It is important to know that the wing has been sized for a low-wing configuration and has a dihedral angle of $\Gamma = 6^\circ$. We perform the following steps:

- Step 1* In the top view and side view of the wing, we draw the fuselage *side-of-body*, i.e. the junction between the wing and the fuselage
- Step 2* The longitudinal and lateral positions are determined simultaneously in the top view. We let the rear end of the engine envelope intersect with the front spar while the distance between the propeller disk and the side-of-body is $0.15D_p$.
- Step 3* We then draw the engine in the front view. We decide to let the bottom side of the engine be parallel to the lower surface of the wing. We also rotate the engine by 6 degrees to align with the wing's dihedral.
- Step 4* We make a section of the wing through the shaft of the propeller. Here, we add the engine and propeller in the side view, putting the rear end of the engine envelope against the front spar.
- Step 5* In the side view, we make a notional fairing between the engine envelope and a point behind the trailing edge.
- Step 6* In the top view, we make a notional fairing between the engine envelope and the trailing-edge point from the side view.

The steps result in an integrated engine with the wing, as shown below. The engine envelope is shown in red.



The previous example has shown that the creation of an additional fairing around the wing-mounted engines can result in quite a large volume behind the engine. It is up to the discretion of the designer to allocate functionality to this volume. This volume could, for example, be used to store luggage or fuel. Note that we have chosen to give the fairing a horizontal trailing edge. This makes sense because the engine envelope has a larger width than height. However, it is also an example of some artistic freedom in shaping this fairing.

Example 8.11 has demonstrated that the integration of the electric motor with the fuselage follows the same process as for the piston engine. The same applies to the integration of electric motors on the wing. All the guidelines provided on page 212 with respect to the integration of propellers with a wing should be adhered to. Due to the smaller engine envelope for electric motors, you must take care that the distance between the leading edge and the propeller disk is respected. Regarding the integration of turboshaft engines, we can also follow the same guidelines as for piston engines. The following example shows how the turboshaft engine can be integrated into a large passenger transport airplane.

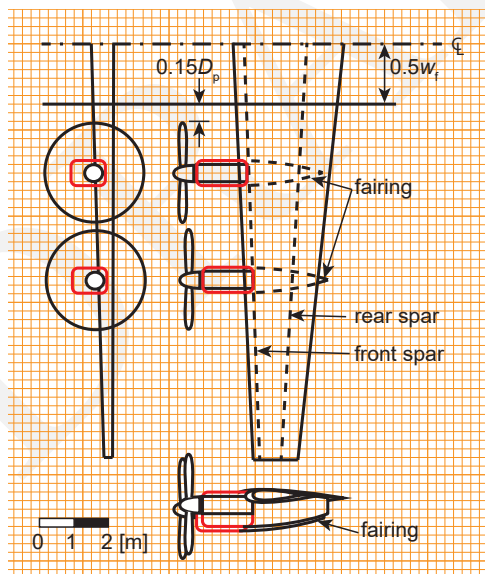
Example 8.13

In this example, we integrate turboshaft engines of Example 8.8 to a wing of a commercial transport airplane for 50 passengers. In previous steps, we designed the wing, the fuselage, and we decided to have two engines per wing half. Furthermore, this airplane has a high-wing configuration.

The figure below shows a three-view drawing of the integrated propellers and engines. We construct this drawing by performing the following steps:

- Step 1* We position the inboard engine and engine envelope (in red) in the top view. We let the end of the engine envelope touch the front spar while we keep $0.15D_p$ of clearance between the fuselage side-of-body and the tip of the propeller.

- Step 2** We position the second engine and its envelope in the top view by placing the engine envelope against the front spar and letting a very small spacing between the two propeller disks.
- Step 3** We draw the engines, their envelopes, and propellers in the front view. We decide to let the top of the engine envelopes be aligned with the middle of the wing section such that most of the engine is below the wing. Because this is a high-wing airplane, this vertical position brings the thrust line of the propeller closer to the expected center of gravity of the airplane. Furthermore, this position also brings the engine closer to the ground, making inspection, servicing, and maintenance easier. Finally, because this is a high-wing configuration, the ground clearance of the propeller is expected to be easily maintained with a short landing gear.
- Step 4** In the top view, we add a fairing behind the engine envelope. Because the entire fairing exists below the wing, we draw it as a dashed line in the top view. We add a fairing behind the engine envelope with the same shape as the first engine. Due to the smaller chord of the wing at the spanwise location of the outboard engine, part of the fairing sticks out behind the wing.
- Step 5** Based on the front and top views, we construct the side view of the wing with the two propellers, engines, engine envelopes, and fairings. We decide to construct a vertical trailing edge of the engine fairing.



The previous example has demonstrated how multiple propellers can be fitted to the wing. You can see that there is some design freedom in deciding on the exact spacing between the propellers. In this case, we decided to keep the propellers relatively close to each other such that the yawing moment in case of a one-engine-inoperative condition

is relatively small. Also, in shaping the fairings, we took some freedom in creating a shape that ‘looks good.’ While this is not a quantifiable design objective, it does help in defining shapes that bring realism to the design. If you want to get inspiration for how to shape such components, it might be instructive to review the pictures of your reference airplanes (see Assignment 3.9).

ASSIGNMENT 8.12

If your airplane has propeller propulsion and you have chosen wing-mounted propellers, perform the following tasks:

- a. Integrate the engine(s) and propeller(s) with your wing. Do this in the top view, side view, and front view.
- b. Add appropriate fairings to ensure a smooth integration with the wing.

8.3. DESIGN AND INTEGRATION OF A JET PROPULSION SYSTEM

If you have chosen a jet engine to propel your airplane, this section explains how to dimension your engine and nacelle and how to integrate them with the airframe. Here, we only consider jet engines of the turbofan configuration, i.e. a turbojet engine with an additional fan. A turbojet engine consists of three basic components: the compressor, the combustion chamber, and the turbine. The thrust of the engine is limited by the amount of compression that the compressor can achieve and the temperature that can be achieved in the combustion chamber. We call the ratio between the inlet (total) pressure and the total pressure at the exit of the compressor the *overall pressure ratio* (OPR). The maximum temperature that can be achieved in the combustion chamber is limited by the materials and cooling systems used in the turbine. Therefore, the *turbine inlet temperature* is an important design parameter of a turbojet or turbofan engine.

In a turbofan engine, part of the ingested air passes only through the fan before exiting the engine through a nozzle. We call this the *bypass* flow. The other part passes through the fan *and* through the core of the engine, i.e. the part with compressor, combustion chamber, turbine, and nozzle. We call this the *core* flow. The ratio of the bypass flow over the core flow is called the *bypass ratio*. A turbofan engine is typically installed in a *nacelle*, which is a streamlined casing around the engine. The dimensions of the nacelle are required for the integration of the engine with the airframe.

We first explain how a turbofan engine and its nacelle can be sized based on the thrust requirement and a handful of design choices. Then, we show how turbofan engines can be integrated with a wing. Finally, we show how to integrate a turbofan engine with the fuselage.

8.3.1. SIZING THE NACELLE

The maximum thrust a turbofan engine can deliver depends on the mass flow of air through the engine, the bypass ratio, the overall pressure ratio of the compressor, and the temperature at which the fuel can be combusted. Combustion occurs in the engine’s combustor or *gas generator*. The maximum temperature is typically limited by the material properties of the turbine blades that are located right behind the gas generator. The

turbine inlet temperature (TIT) is, therefore, another important design parameter of the engine. To determine the required size of the turbofan, we follow the method of Torenbeek and Berenschot [22], who size the turbofan based on these parameters along with the required take-off thrust, T_{TO} .

At take-off conditions, the thrust of a jet engine is proportional to the exhaust mass flow (\dot{m}) and the average jet velocity. Because the mass flow is an important parameter for the size of the engine, we compute it first:

$$\dot{m} = \frac{T_{TO}}{N_e a_0} \frac{1 + B}{\sqrt{5\eta_{noz} G(1 + \eta_{tf}B)}} \quad (8.22)$$

where N_e is the number of engines, a_0 is the speed of sound at sea level, η_{noz} is the nozzle efficiency, G is the gas generator function, η_{tf} is the combined efficiency of the turbine and fan, and B is the bypass ratio.

Let us go through the parameters in Equation 8.22. The number of engines N_e is a design parameter that you already selected in Assignment 4.3. The speed of sound at sea level (ISA) is 340 m/s. The bypass ratio is the ratio between the mass flow through the bypass duct and the mass flow going through the core of the engine. The nozzle efficiency is the average value of the nozzle efficiency of the bypass nozzle and the core nozzle. This efficiency typically ranges between 97% and 99%, depending on the aerodynamic design of the nozzles. The turbine and fan efficiency, η_{tf} , is the product of the turbine efficiency η_t and the fan efficiency, η_f . A typical value of $\eta_{tf} = 0.75$ can be assumed. Finally, G is the gas generator performance expressed in non-dimensional form. The gas generator function G is statistically related to the turbine inlet temperature according to [22]:

$$G \approx \frac{T_{t4}}{600} - 1.25 \quad (8.23)$$

where T_{t4} is the TIT measured in Kelvin. The higher T_{t4} , the lower the mass flow per unit of thrust and the smaller the engine. It is therefore desired to let the TIT be as high as possible if you wish to minimize the mass, size, and drag of the engine. To increase the TIT, turbine blades are therefore made out of heat-resistant metals and are often actively cooled from the inside. Modern jet engines (in 2023) have a TIT somewhere between 1830 K and 1970 K.

The combustion temperature also influences the emissions of the engine. Combusting fuel produces carbon dioxide (CO₂), which is a greenhouse gas. The amount of CO₂ is linearly correlated to the fuel consumption and independent of the TIT. The formation of nitrogen oxides, on the other hand, is dependent on the TIT. Nitrogen oxides (NO_x) are formed when nitrogen and oxygen molecules, which naturally occur in air, are exposed to the high temperature and pressure of the combustion chamber. When emitted at high altitudes, NO_x has an indirect global warming effect, similar to CO₂. The higher the TIT, the more NO_x is produced. Therefore, modern engines feature combustion chambers that allow for a lean mixture of air and fuel to be combusted. This reduces the peak temperatures within the combustion chamber and reduces the formation of NO_x with respect to rich combustion. More information on the effect of the various combustion species on global warming can be found in Ref. [11].

ASSIGNMENT 8.13

In this assignment, you will size the mass flow of your jet engine.

- What bypass ratio, B , did choose for your engine in Assignment 5.4?
- What turbine inlet temperature, T_{t4} do you choose for your gas generator?
- What values do you assume for the combined turbine and fan efficiency, η_{tf} , the nozzle efficiency, η_{noz} , and the gas generator property, G ?
- Compute the mass, \dot{m} flow through your jet engine.

Now that we have shown how to determine the mass flow of your jet engine, let us start sizing the nacelle. The nacelle of the jet engine is similar to the engine envelope that we defined for the turboprop, electric motor, and piston engine. However, here we distinguish two types of nacelle geometries:

- Type B: the nacelle completely covers the bypass flow and gas turbine core. The bypass flow and core flow are mixed ahead of the exhaust. This forced mixing results in lower thrust-specific fuel consumption and reduced noise. However, the nacelle has a relatively large wetted surface.
- Type C: The nacelle consists of a fan cowling and a cowling for the gas turbine core. The fan cowling spans part of the nacelle length. This reduces the wetted area of the nacelle compared to Type B.

In Figure 8.18, nacelle Type B is shown while Figure 8.19 shows Type C. Note that the inlet is slightly drooped downward for both nacelle designs. This is to emphasize that a practical nacelle design is not axisymmetric. However, in the context of this textbook, we will approximate the nacelle by an axisymmetric body. Type A nacelles are reserved for turbojet engines, which are outside the scope of this textbook.

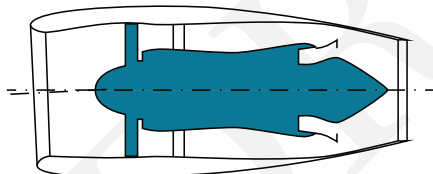


Figure 8.18: Turbofan installation Type B, after [22]

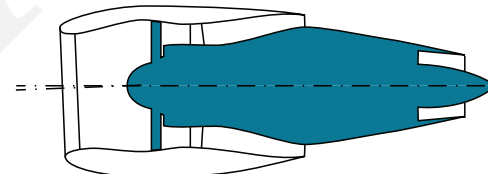


Figure 8.19: Turbofan installation Type C, after [22]

ASSIGNMENT 8.14

Which type of nacelle do you choose for your turbofan engine? Explain your decision.

In Figure 8.20, you can see a schematic nacelle geometry of Type C with all relevant dimensions labeled. Ahead of the turbofan engine is the inlet. The function of the inlet is to reduce the speed of the incoming flow such that the fan can compress it with high efficiency. The inlet's highlight is the leading edge perimeter, and the highlight plane is the imaginary plane through the highlight perimeter. Like a propeller, the engine fan has a spinner that guides the flow towards the fan blades. The bypass flow (or fan flow)

is enclosed by the fan cowling. For a Type B nacelle, the fan cowling would extend to the end of the nacelle, and the engine core would be inside it. However, in this example, part of the engine core is visible and has its own cowling. Finally, a cone (sometimes referred to as *plug*) is located behind the core nozzle.

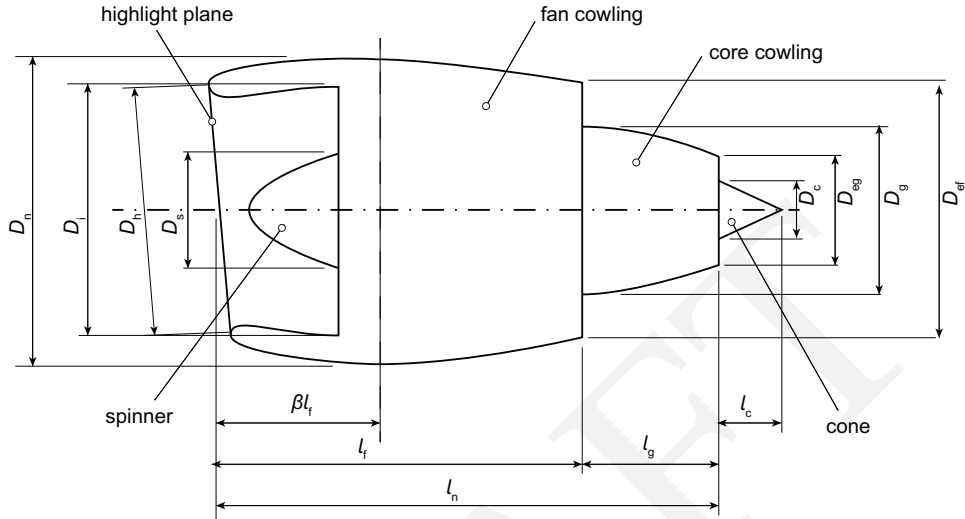


Figure 8.20: Definitions of the dimensions of a jet engine nacelle. After Ref. [22].

Based on the computed mass flow (Equation 8.22), we are now going to compute the value of each of the nacelle dimensions of Figure 8.20 following Ref. [22]. The spinner-to-inlet ratio can be computed as follows:

$$\frac{D_s}{D_i} \approx 0.05 \left(1 + 0.1 \frac{\rho_0 a_0}{\dot{m}} + \frac{3B}{1+B} \right) \quad (8.24)$$

The inlet diameter, D_i , is:

$$D_i = 1.65 \sqrt{\frac{\frac{\dot{m}}{\rho_0 a_0} + 0.0050}{1 - \left(\frac{D_s}{D_i}\right)^2}} \quad (8.25)$$

We assume that the highlight diameter and the inlet diameter are the same, i.e.:

$$D_h = D_i \quad (8.26)$$

The nacelle length (excluding the cone), can be computed according to:

$$l_n = C_l \left(\sqrt{\frac{\dot{m}}{\rho_0 a_0} \frac{1+0.2B}{1+B}} + \Delta l \right) \quad (8.27)$$

where C_l is a dimensionless coefficient and Δl is length measured in meters. Both values are statistically obtained and dependent on the type of nacelle. Table 8.1 provides typical

Table 8.1: Statistically-obtained parameters for dimensioning turbofan nacelles.

Type	C_l	Δl	β
B	9.8	0.05	0.35
C	7.8	0.1	$0.21 + \frac{0.12}{\sqrt{\varphi - 0.3}}$

values for either nacelle type. Based on the provided values, you can see that nacelle Type B is 20%-25% longer than nacelle Type C. This allows for the integration of a mixer behind the turbine of the engine.

The nacelle length equals the fan cowl length for Type B nacelles. For Type C nacelles, the fan cowl length is shorter. You have to choose how much shorter the fan cowl is by specifying a value for φ , the ratio between fan cowl length and nacelle length. A long cowl length allows for the integration of an acoustic liner on the inside of the nacelle to reduce the jet noise. However, it also increases the contact area between the flow through the bypass duct as well as the external flow around the cowling. The latter contributes to the friction drag of the airplane. Typically, a value of $0.5 < \varphi < 0.8$ is selected. The fan cowl length is, therefore:

$$l_f = \varphi l_n \quad (8.28)$$

Independent of the nacelle type, the maximum nacelle diameter is computed as follows:

$$D_n = D_i + 0.06\varphi l_n + 0.03 \quad (8.29)$$

The location of the maximum nacelle thickness is a fraction, β , of the nacelle length. The value of β is dependent on the cowl type and typical values are suggested in Table 8.1. The length between the highlight and the position of maximum thickness is βl_f as shown in Figure 8.20.

The exit diameter of the fan cowl is:

$$D_{ef} = D_n \left(1 - \frac{1}{3}\varphi^2\right) \quad (8.30)$$

For Type B nacelles (i.e. $\varphi = 1$), the diameter of the fan exit is the same as the exit diameter of the nacelle. For Type C nacelles, we can continue to compute the dimensions of the exposed cowling of the gas turbine:

$$l_g = (1 - \varphi) l_n \quad (8.31)$$

The cowling diameter of the exposed gas-turbine core at the fan cowling exit is:

$$D_g = D_{ef} \left(\frac{0.089 \frac{\dot{m}}{\rho_0 a_0} B + 4.5}{0.067 \frac{\dot{m}}{\rho_0 a_0} B + 5.8} \right)^2 \quad (8.32)$$

The exit diameter of the gas-turbine cowling can be approximated as follows:

$$D_{eg} \approx 0.55 D_g \quad (8.33)$$

Finally, the cone diameter can be related to the gas-turbine exit diameter:

$$D_c \approx 0.55D_{eg} \quad (8.34)$$

The length of the cone is approximately:

$$l_c = 1.5D_c \quad (8.35)$$

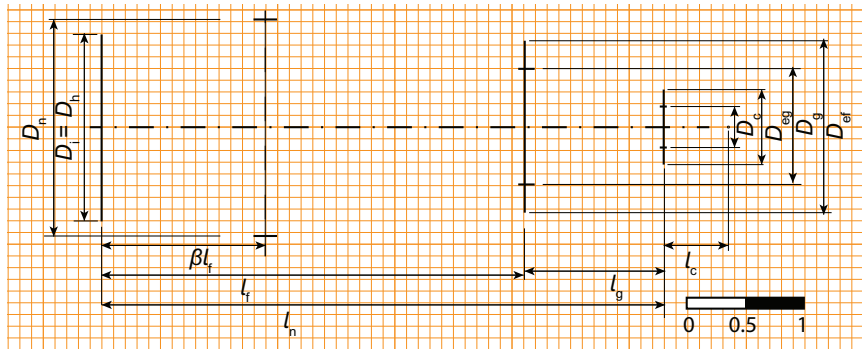
With all the nacelle dimensions computed, we can now proceed to draw the nacelle. In the following example, you see the step-by-step procedure that is followed to draw the nacelle.

Example 8.14

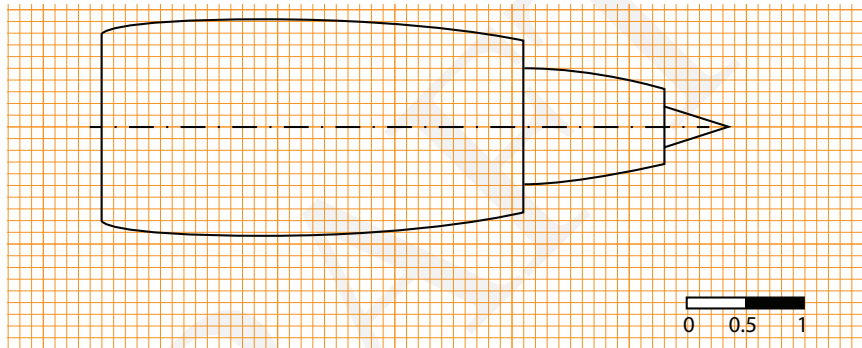
In this example, we draw the nacelle for the jet airplane of Example 7.11. We choose the nacelle to be of Type C and to have a fan cowl fraction of $\varphi = 0.75$. Selecting a TIT of $T_{t4} = 1680$, we compute $\dot{m} = 380$ kg/s per engine when it produces maximum thrust at sea level. Based on this mass flow, we size the nacelle according to the following steps.

- Step 1* Compute inlet diameter from the mass flow. Using (8.24) and (8.25), we compute $D_s/D_i = 0.19$ and $D_i = 1.6$ m.
- Step 2* Draw highlight diameter (neglect droop). Assuming the highlight diameter and inlet diameter are the same, we have $D_h = 1.6$ m.
- Step 3* Compute nacelle length. Using (8.27) and using the values from Table 8.1 under Type C, we compute $l_n = 4.8$ m.
- Step 4* Compute fan cowling length. With (8.28) we compute $l_f = 3.6$ m.
- Step 5* Compute position of maximum diameter. We compute $\beta = 0.39$ using the formula in Table 8.1. The maximum diameter of the nacelle is therefore found at $\beta l_f = 1.4$ meters from the highlight plane.
- Step 6* Compute maximum diameter. The maximum diameter is computed using (8.29) and is $D_n = 1.9$ m.
- Step 7* Compute fan cowling diameter at the exit. We employ (8.30) to find $D_{ef} = 1.5$ m.
- Step 8* Compute gas turbine diameter at fan cowling exit.² By employing (8.32) we find $D_g = 1.0$ m.
- Step 9* Compute gas turbine diameter at exit. Using (8.33), we have $D_{eg} = 0.56$ m.
- Step 10* Compute cone dimensions. Using (8.34) and (8.35), we have $D_c = 0.36$ and $l_c = 0.54$ m.
- Step 11* Using all the computed dimensions, draw an outline of the nacelle.

²Only applicable for Type C nacelles



Step 12 Connect all points.



In the previous example, you saw how a nacelle can be drawn. Note that we use the symmetry line (dash-dotted) as a starting point for the drawing because we assume the nacelle is axisymmetric. In the following assignment, you can practice with the design steps of Example 8.14

ASSIGNMENT 8.15

In this assignment, you will calculate the dimensions of your turbofan nacelle and make a drawing of it.

- Choose a cowl fraction, φ for your nacelle.^a
 - Using the steps from Example 8.14, compute all the relevant dimensions of your nacelle and fill out the following table:
- | D_h | l_n | l_f | βl_f | D_n | D_{ef} | D_g | D_{eg} | D_c | l_c |
|-------|-------|-------|-------------|-------|----------|-------|----------|-------|-------|
| ... | ... | ... | ... | ... | ... | ... | ... | ... | ... |
- Produce a drawing of your nacelle. Use the same scale as you used for your fuselage (Assignments 6.3 and 6.4) and wing (Assignments 8.3 and 8.8).

^aIf you have chosen nacelle Type B in Assignment 8.14, $\varphi \equiv 1$

8.3.2. INTEGRATION WITH THE WING

Turbofan engines are connected to wing or fuselage by means of a *pylon*. The pylon is a structural element between the hard points of the jet engine and the structure of the airplane. For a wing-mounted jet engine, the pylon is structurally attached to the wing box. When positioning the jet engine on the wing, the following aspects should be considered:

1. LATERAL POSITIONING

When an engine is hung from a wing, it provides a bending moment opposite to the one introduced by the lift. This reduces the bending moment in the wing and can result in a lower structural mass of the wing. The more outboard the engine is positioned, the stronger the bending moment relief. However, an engine that is positioned too far outboard also produces a strong yawing moment. So, in case of an OEI condition, a (very) large vertical tail would be needed to balance the airplane around its vertical axis. These two opposing factors should be taken into account when selecting the lateral position for the engine.

- i. With one engine per wing half, a typical lateral position is 35% of the semi-span, i.e. $2y_e/b_w = 0.35$.
- ii. With two engines per wing half, a typical lateral position is $2y_e/b_w = 0.4$ and $2y_e/b_w = 0.7$.

2. LONGITUDINAL POSITIONING

- i. The engine should be positioned, such that rotor fragments have a less than 5% chance of causing a catastrophic failure in case of turbine disk failure (see Example 3.18). Since a fuel tank is often located behind the front spar, it is advised to keep the rotating parts of the engine ahead of the front spar. In the case of a Type B nacelle, it can be assumed that the aft 15% of the nacelle comprises the nozzle and the mixer. For Type C nacelles, it can be assumed that the last 10% of the nacelle length comprises the (core) nozzle. Alternatively, dry bays can be introduced in the wing to mitigate the risk of catastrophic failure in case of a turbine disk failure.
- ii. To reduce the aerodynamic interference between the nacelle, pylon, and wing, the engine should be positioned as far forward as possible.
- iii. To minimize the mass of the pylon, the engine should be positioned as close as possible to the wing box.

3. VERTICAL POSITIONING

- i. The closer the engine is positioned to the wing, the stronger is the aerodynamic interference between wing, pylon and nacelle.
- ii. A lower engine position reduces the ground clearance. Similar to Example 3.17, a minimal distance between the nacelle and the ground should be respected. A lower vertical position could therefore result in a taller landing gear to respect this ground clearance.
- iii. A higher engine position reduces the distance between the thrust vector and the center of gravity of the airplane, thereby reducing the thrust-induced pitching moment.

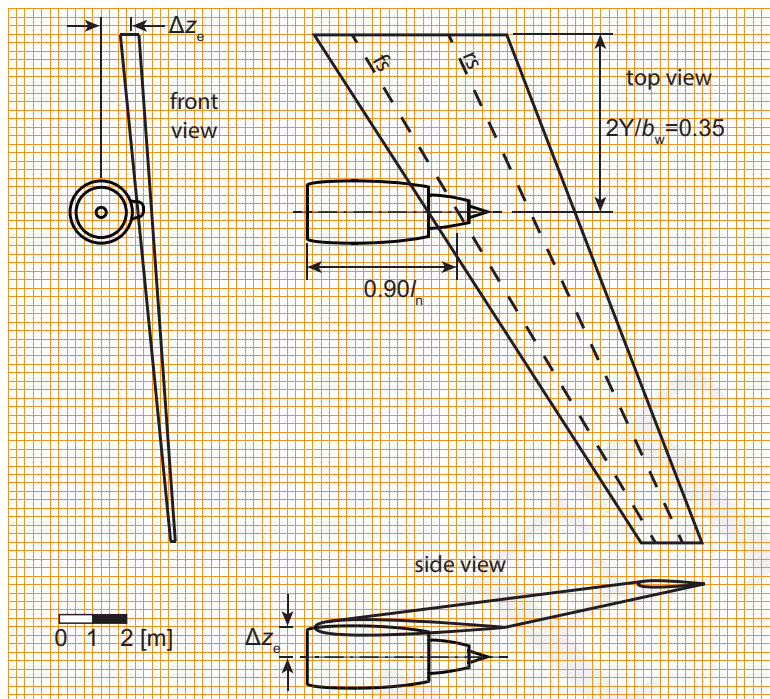
In the following example, we show how the nacelle of Example 8.14 can be integrated

with the wing of Example 8.5.

Example 8.15

In this Example, we integrate the nacelle of Example 8.14 with the wing of Example 8.5. We take the following steps:

- Step 1* We choose a location at 20% and 70% of the local chord for the front spar (fs) and rear spar (rs), respectively. We draw the spar locations in the top view of the wing by means of dashed lines (see below).
- Step 2* We choose the lateral location of the engine to be 35% of the semi-span of the wing, and we mark this location in the top view (see below).
- Step 3* We assume the last 10% of the nacelle length contains no rotating components, and we choose the position of the engine inlet to be 90% of the nacelle length ahead of the front spar (see below). This would allow a fuel tank between the front and rear spar to be sufficiently protected from turbine disk failure.
- Step 4* We draw the nacelle in the top view of the wing.
- Step 5* We draw the nacelle in the front view of the wing at the same lateral position as in the top view. We produce a circular nacelle shape and we choose to have the upper surface of the nacelle slightly below the lower surface of the wing in front view.
- Step 6* In the front view of our drawing, we measure the vertical offset of the engine with respect to the leading edge of the center airfoil: $\Delta z_e = 0.85 \text{ m}$.
- Step 7* We copy the longitudinal position of the engine from the top view to the side view, and we take the vertical position with respect to the leading edge of the center airfoil from the front view. We draw the engine in the side view of the wing.



The previous example has shown how you can integrate a nacelle with a wing. At multiple steps, you have to make a choice. For every choice that you make, you should be able to provide a justification. The content from the first paragraph of this section can be used to provide justification. However, you might have other reasons that guide your choice. In any case, each and every decision that you make throughout the design process should have some justification such that you can explain why you have made a certain choice.

ASSIGNMENT 8.16

If your airplane has jet propulsion and you have chosen your engines to be under the wing, perform the following tasks:

- Integrate the engine(s) with your wing. Do this in the top view, side view, and front view.
- Add lines to indicate the location of the pylon in the front view.

8.3.3. INTEGRATION WITH THE FUSELAGE

In Chapter 4, we showed that jet engines can be mounted to the fuselage. You can position an engine inside the tail cone of the fuselage as shown in Figure 4.11. Alternatively, you could mount the engines to the front of the fuselage, as shown on the left-hand side of Figure 8.21. However, the most common configuration is to position the engines at

the rear of the fuselage, as shown on the right-hand side of Figure 8.21. In this section, we focus on the latter configuration and present how you can integrate twin jet engines with the rear of the fuselage. This configuration is common for transport aircraft as well as for business jets.



Figure 8.21: Installation of jet engines at the front of the fuselage (left) and at the rear of the fuselage. Photos by: JuergenKlueser © ⓘ ⓘ and Lars Söderström © ⓘ ⓘ, respectively.

When we determine the position of jet engines on the rear fuselage, we take the following aspects into consideration:

1. LONGITUDINAL POSITIONING

- i. Rotor disk failure in the jet engine can cause a hazard to the fuselage. Rotor fragments can cause holes in the fuselage, which leads to depressurization. In addition, hazards to passengers might arise if they are seated between the engines. Therefore, it is desirable to position the engines aft of the cabin.
- ii. Cabin noise can be quite high when the engines are attached to the fuselage. The short structural path between the engine and the fuselage frames can cause the noise to travel through the structure into the cabin. The more aft the engines are positioned, the lower the cabin noise.
- iii. Emergency exits can be located at the rear of the fuselage. The engine should not block the emergency exit. The location of the emergency exit has been chosen based on the requirement to have the distribution as “uniformly as practical” (Example 3.16). If necessary, it is, therefore, possible to change the location of the aft-most pair of emergency exits to allow the integration of the jet engine.
- iv. The aerodynamic interference between the wing and the inlet should be considered. As the velocity over the wing increases, the inlet can be exposed to a (very) high Mach number when it is positioned over the wing. Therefore, it is desirable to have the inlet positioned behind the wing. We will see that for business jets, it can be inevitable to have the inlet slightly over the rear part of the wing.
- v. Jet engines are relatively heavy systems. If they are positioned on the rear of the fuselage, they cause a large center-of-gravity excursion during the loading of passengers and fuel (see Chapter 9). The center-of-gravity excursion affects the required size of the tail as well as the landing gear integration. It is therefore desired to have heavy systems, such as the engines, as close as possible to the center of gravity of the airplane. For rear-fuselage-mounted

engines, this would translate into the desire to position them as far forward as possible.

In the reference frame of the fuselage, we use capital X to denote the longitudinal position along the fuselage. X_h is the longitudinal position of the highlight plane of the engine inlet (see Section 8.3.1). Given these considerations, we propose to abide by the following guidelines regarding the longitudinal position of the engine. We want X_h to be as small as possible, subject to the following constraints:

$$X_h > X_{\text{apb}} - 0.5l_n \quad \text{and} \quad X_h > X_{\text{exit}} + D_h \quad \text{for transport jets} \quad (8.36)$$

$$X_h > X_{\text{apb}} + 0.5D_h \quad \text{for business jets} \quad (8.37)$$

where X_{apb} is the longitudinal location of the aft pressure bulkhead and X_{exit} is the location of the aft-most pair of emergency exits.

2. VERTICAL POSITIONING

- i. Position the engine, such that the thrust vector with respect to the center of gravity is as small as possible. This minimizes the (nose-down) pitching moment that is introduced by the thrust of the engine. In practice, this means positioning the engine close to the middle of the fuselage.
- ii. Make sure the engine inlet is (barely) above the wing. This ensures that the wing wake is not ingested by the engine.
- iii. Make sure that the exhaust does protrude below the belly curve of the fuselage. This prevents the engine from scraping the runway when the airplane rotates during the take-off roll.

3. LATERAL POSITIONING

- i. Since the engine is mounted to the fuselage, the one-engine-inoperative yawing moment is relatively small. The closer the engine is to the fuselage, the smaller the yawing moment.
- ii. The closer the engine is located to the fuselage, the smaller the pylon and the lower the structural mass of the pylon can be.
- iii. The inlet should be offset from the fuselage to prevent the boundary layer of the fuselage from entering the engine. This would cause a reduction in inlet efficiency and distortion
- iv. The fuselage and the nacelle both create an increase in velocity. If these two bodies are positioned close together, the velocity between them can become so high that shock waves can appear. To reduce the adverse aerodynamic interference, a spacing of at least $0.25D_n$ is proposed between the fuselage and the nacelle.

In the following example, the engine of Example 8.14 is integrated with the rear fuselage from Example 6.8.

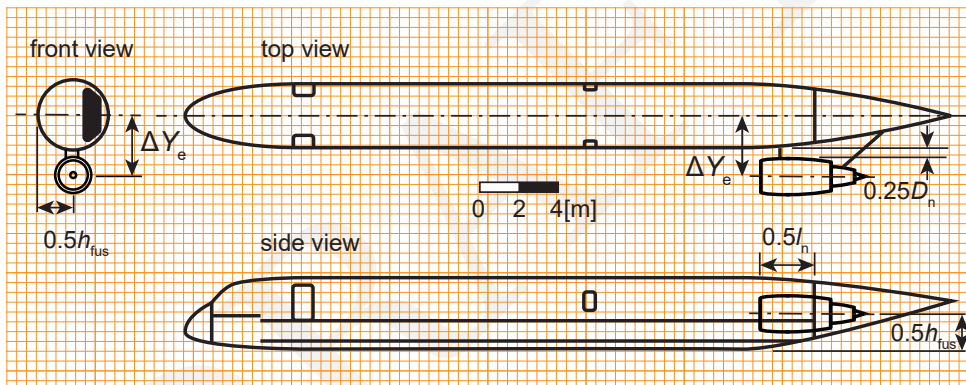
Example 8.16

In this example, we show how to integrate the engine of Example 8.14 with the fuselage of Example 6.8. We take the following steps:

Step 1 Since our airplane is a transport jet, we use Equation 8.36 to determine the lon-

itudinal location of the highlight. There is no emergency exit at the rear of the airplane, so the placement of the engine does not interfere with the exits.

- Step 2** To minimize the thrust-induced pitching moment, we propose to the vertical position to be in the middle of the fuselage. So the engine, is positioned $0.5h_{fus}$ above the bottom of the fuselage.
- Step 3** With the longitudinal and vertical position known, we draw the engine into the side view of the fuselage (see below). We verify that the nacelle does not protrude beyond the tail cone perimeter. This is not the case.
- Step 4** We determine the clearance between the engine and the fuselage to measure 25% of the nacelle diameter. We measure the resulting lateral displacement of the engine, which is $\Delta y_e = 3.1 \text{ m}$.
- Step 5** We draw the engine in the top view at the appropriate location and add a pylon geometry (see below).
- Step 6** We draw the engine in the front view and also add lines representing the pylon (see below).



Note that in the previous example, we only draw one engine in the top view and side view. Naturally, we there should also be an engine on the opposite side, as the airplane is symmetric. The motivation to draw only half of the airplane is to reduce the size of the drawing, such that we can use the available space on our paper most efficiently.

ASSIGNMENT 8.17

If your airplane has jet propulsion and you have chosen your engines to be attached to the fuselage, perform the following tasks:

- Integrate the engine(s) with your fuselage. Do this in the top view, side view, and front view.
- Add lines to indicate the location of the pylon in the top view and the front view.

9

DESIGN OF LANDING GEAR AND TAIL SURFACES

Before starting with the design of the landing gear and tail surfaces, you need to have finished the conceptual design of the fuselage, wing, and propulsion system. In addition, the propulsion system should already be integrated with the wing or the fuselage. Finally, you need to have chosen the landing gear and tail configuration. If these steps have been performed, you can proceed with the design of the landing gear and tail surfaces and follow the design methods laid out in this chapter.

The design of the landing gear and tail surfaces is all about the following three aspects:

1. **BALANCE** The airplane needs to maintain a state of equilibrium on the ground and in the air.
2. **STABILITY** The airplane needs to return to equilibrium after an upset on the ground or in the air.
3. **CONTROL** The airplane needs to be able to deviate from the equilibrium state to steer it on the ground and in the air.

Obviously, the landing gear provides this functionality on the ground, while the tail surfaces provide this functionality in the air. The landing gear and tail surface work together to provide this functionality during the landing and take-off maneuvers.

To achieve this functionality, three groups of forces play a major role. First, the airplane's mass and where its center of mass is located. This is important for the landing gear and the tail surfaces. Secondly, in the air, the aerodynamic forces on the airplane play an important role. These include the aerodynamic forces on the airframe and the changes in aerodynamic force when a control surface is deflected.

To balance, stabilize, and control an airplane on the ground and in the air, we propose the following design sequence in this chapter:

Step 1 Estimate the center of gravity excursion of the airplane

Step 2 Size and integrate the landing gear

Step 3 Size and integrate the tail surfaces

In the subsequent sections, these steps will be presented. We will present procedures and introduce methods to perform these steps. Through examples, we will demonstrate how this works in practice. Following the exercises, you will have a three-view drawing of your airplane by the end of this chapter.

9.1. ESTIMATING THE CENTER OF GRAVITY EXCURSION

In this Section, we introduce the concept of *center of gravity* and present a method to estimate how it shifts when loading payload or fuel. The center of gravity is the spatial representation of the aircraft as a point mass. Imagine that you are trying to balance an airplane on your fingertip. Then, the location of the center of gravity is that point on the airplane where it balances perfectly. The center of gravity is the point where the resultant weight force applies. It is also the pivot point of the airplane in the air. In other words, the airplane rotates about its center of gravity.

In steady rectilinear flight, the resultant aerodynamic force must apply in the center of gravity to balance the resultant weight force. The location of the center of gravity also influences the airplane's stability. If the center of gravity is located far forward, the airplane becomes very stable about its lateral and vertical axis. When the center of gravity shifts aft, the stability reduces, and the airplane can even become unstable. A center of gravity that is too far aft can also cause problems with the landing gear. For example, it could tip on its tail. A center of gravity that is too far forward on a tricycle landing gear could cause such a high nose-gear load during landing that it breaks. In summary, the location of the center of gravity needs to be limited between a forward and aft limit.

In Figure 9.1, we show schematically how the center of gravity can change when loading passengers and fuel. We start with the airplane at its operating empty mass, m_{OE} .¹ This results in the center of gravity position measured in the reference frame of the aircraft (X, Z). In this example, adding the payload mass to the operating empty mass ($m_{OE} + m_{pl}$) shifts the center of gravity forward. If we fill up the fuel tanks completely, we arrive at a mass of $m_{OE} + m_{pl} + m_f$ and a center of gravity position between the previous two. The sum of these three masses exceeds the maximum take-off mass (m_{MTO}) and is, therefore, a theoretical point in the loading diagram. When we remove the payload mass again, we arrive at a mass of $m_{OE} + m_f$ and the most aft center of gravity position in this example. When we connect these four points, we create a simplified loading diagram.

The wing's location on the fuselage has a large impact on the center of gravity position of the operating empty mass and on the center of gravity excursion when fuel and payload are added. Fuel tanks are often located in the wing, and their positions, therefore, influence the location of the center of gravity when fuel is added. Ideally, the four points in the loading diagram are as close as possible to each other regarding their X position. This yields the smallest center-of-gravity excursion and, therefore, the smallest tail surface. Therefore, the longitudinal (X) location of the wing on the fuselage needs to be chosen wisely.

¹For small airplanes, you can replace this with empty mass, m_E if this is more appropriate in the context of your airplane design.

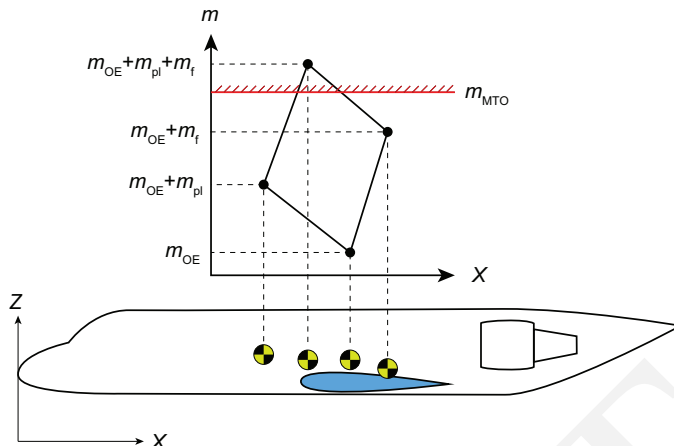


Figure 9.1: Example of the center of gravity excursion during loading of fuel and payload and associated loading diagram.

To create the loading diagram and determine the “right” wing position, we divide the airplane components that we have designed into two groups: a fuselage assembly and a wing assembly. This is visually shown in Figure 9.2. The fuselage assembly comprises all airplane components attached to the fuselage and the fuselage itself. In this example, the fuselage assembly consists of the fuselage, the engine, the tail, and the nose landing gear. The wing assembly comprises the wing and all the components attached to it. In the example of Figure 9.2, the wing assembly consists of the wing and the main landing gear. The landing gear and the tail surfaces have been drawn with dashed lines because we have not yet designed them. Note that if your airplane has its engines attached to the wing, they belong to the wing assembly instead of the fuselage assembly.

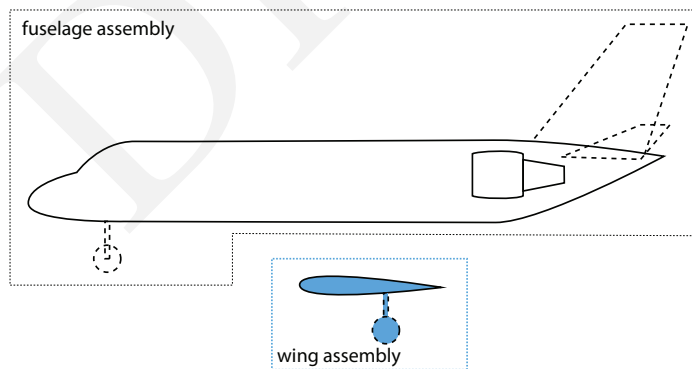


Figure 9.2: Visual definition of a wing assembly and a fuselage assembly of airplane components.

We now need to find the center of gravity of the fuselage and wing assemblies. This is shown in Figure 9.3. For each group, we define a reference frame. The fuselage as-

sembly's reference frame is denoted with capital X and Z , and $X = 0$ is at the nose of the airplane. The wing's reference frame is denoted with lowercase x and z and is attached to the leading edge of the mean aerodynamic chord (LEMAC). We have divided the operating empty mass into seven group masses. Each group mass can be normalized with respect to the maximum take-off mass (m_{MTO}) to define its *mass fraction*. Mass fractions are indicated with the "hat" symbol, i.e. \hat{m} . We define the following mass fractions:

1. propulsion group mass fraction, $\hat{m}_{eng} = m_{eng}/m_{MTO}$
2. fixed equipment mass fraction, $\hat{m}_{fe} = m_{fe}/m_{MTO}$
3. wing group mass fraction, $\hat{m}_w = m_w/m_{MTO}$
4. tail group mass fraction, $\hat{m}_t = m_t/m_{MTO}$
5. fuselage group mass fraction, $\hat{m}_{fus} = m_{fus}/m_{MTO}$
6. nacelle group mass fraction, $\hat{m}_n = m_n/m_{MTO}$
7. landing gear group mass fraction, $\hat{m}_{lg} = m_{lg}/m_{MTO}$

Empirical data exists on the mass fraction of each of these group masses. For example, Roskam has gathered data on various airplane categories and tabulated their group mass fractions in Ref. [14]. Using statistical averages, we can use this empirical data to estimate the mass of each group. Imagine that we have K reference airplanes for which we can find the group mass fractions normalized to their own maximum take-off mass. Then, for every group mass component, i , we can estimate the average mass fraction normalized to the maximum take-off mass of our own airplane as follows:

$$\hat{m}_{i, \text{av}} = \frac{\hat{m}_{OE}}{K} \sum_{k=1}^K \left(\frac{\hat{m}_{i, k}}{\hat{m}_{OE, k}} \right)_{\text{ref}} \quad (9.1)$$

You can repeat this process for all group mass fractions to reach an average value. The sum of all mass group fractions should equal the OEM mass fraction. However, we typically have an unaccounted mass fraction that can be computed as follows:

$$\hat{m}_{unacc} = \hat{m}_{OE} - \sum \hat{m}_{i, \text{av}} \quad (9.2)$$

The mass fractions for each mass group can then be estimated as follows:

$$\hat{m}_i = \hat{m}_{i, \text{av}} \left(\frac{1}{1 - \frac{\hat{m}_{unacc}}{\hat{m}_{OE}}} \right) \quad (9.3)$$

As a sanity check, you can then show that:

$$\sum \hat{m}_i \equiv \hat{m}_{OE} \quad (9.4)$$

The following example shows how an estimate of the mass fraction for each of the mass groups can be made.

Example 9.1

For the jet transport for which we showed the payload-range diagram in Example 5.12, estimate the mass fraction for each mass group.

The payload-range diagram in Example 5.12 is for a jet transport of medium range. We look for data in Ref. [14] and find tables with group mass data for Jet Transports.

From these tables, we select three reference airplanes that also fly a medium range: the McDonnel Douglas DC-9-30, the McDonnel Douglas MD-80, and the Boeing 737-200. We copy the values for each mass group into the table below the header of each aircraft. We also copy the operating empty mass fraction from these tables and compute the unaccounted mass fraction for each reference airplane. Note that the Boeing 737-200 has 5% of its operating empty mass unaccounted for in its group masses.

Subsequently, we employ (9.1) to compute the average mass fraction for each mass group, normalized to the maximum take-off mass of the airplane of Example 5.12. By adding all the group mass fractions, we find an unaccounted mass fraction of 0.029, which we proportionally distribute over the group mass fractions using (9.3). The resulting values are placed in the last column under “estimate.” Note that there is no unaccounted mass fraction in the last column, and therefore (9.4) is satisfied.

mass fraction	symbol	DC9-30	MD-80	B737-200	normalized average	estimate
propulsion group	\hat{m}_{eng}	0.076	0.079	0.071	0.075	0.080
fixed equip. group	\hat{m}_{fe}	0.175	0.182	0.129	0.162	0.171
wing group	\hat{m}_{wing}	0.106	0.111	0.092	0.103	0.109
tail group	\hat{m}_{t}	0.026	0.024	0.024	0.025	0.026
fuselage group	\hat{m}_{fus}	0.103	0.115	0.105	0.108	0.114
nacelle group	\hat{m}_{nac}	0.013	0.015	0.012	0.013	0.014
land. gear group	\hat{m}_{lg}	0.039	0.038	0.038	0.038	0.04
oper. empty mass	\hat{m}_{OEM}	0.538	0.564	0.521	0.553	0.553
unaccounted	\hat{m}_{unacc}	0	0	0.05	0.029	0

ASSIGNMENT 9.1

In this assignment, you will estimate the group mass fractions for your airplane based on three reference airplanes.

- Find a source that lists group mass fractions for reference airplanes that bear similarity to your airplane.
- Choose at least two, but preferably three or more reference airplanes from this source. The reference airplanes can be identical to the ones that you selected in Assignment 3.9 but they may also be different.
- For each reference airplane, list the group mass fractions for groups 1 through N in a table similar to the one below.
- List the operating empty mass fraction for each reference airplane in the table below.^a
- If applicable, compute the unaccounted mass fraction for each of your reference airplanes and list them in the table below.
- Compute the average group mass of your reference airplanes, normalized to the maximum take-off mass of your own airplane, which you computed in Assignment 5.7. List these values in the table below under “average.”
- Compute the unaccounted mass fraction from the averaged group mass

fractions.

- h. Make an estimate of the group mass fractions for your airplane by redistributing the unaccounted mass fraction proportionally over the N groups.
- i. Confirm that Equation 9.4 is satisfied for your estimated group mass fractions.

mass fraction	symbol	Ref1	Ref2	Ref3	normalized estimate	average
group 1	\hat{m}_1
\vdots	\vdots	\vdots	\vdots	\vdots	\vdots	\vdots
group N	\hat{m}_N
oper. empty mass	\hat{m}_{OE}
unaccounted	\hat{m}_{unacc}

^aIf you have computed the empty mass fraction in Assignment ??, also use the empty mass in this assignment

In addition to the group mass fractions, we use empirical data to estimate the location of the center of gravity of each group in their own reference frame. For example, the center of gravity of the fuselage group is assumed to lie at 40% of the fuselage length measured from the tip of the nose. We assume that the fixed equipment, mostly distributed within the fuselage, has its center of gravity at the same location (see Figure 9.3). The wing group's center of gravity is assumed to lie $0.4\bar{c}$ behind the LEMAC. For a jet engine, the center of gravity is assumed to be 40% of the nacelle length behind the highlight. The nacelle's center of gravity is assumed to coincide with that of the jet engine. For propeller-powered airplanes, the center of gravity of the engine (or motor) plus propeller is assumed to be located $0.4l_{ee}$ behind the front plane of the engine envelope (see Section 8.2.2).

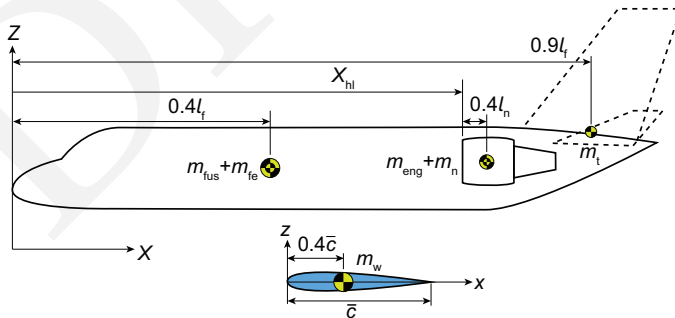


Figure 9.3: Location of the center of gravity for each component mass in the fuselage and wing reference frames.

In the present analysis, we neglect the contribution of the main and nose landing gear to the airplane's center of gravity. There are two reasons for this: 1) the landing gear has a relatively small mass fraction ($\hat{m}_{lg} \approx 0.04$) and 2) the nose landing gear and

main landing gear almost balance each other around the center of gravity of the airplane. Finally, we must choose the location of the tail's center of gravity. As we have not yet located the tail, we must assume a location. In Figure 9.3, we presume the tail's center of gravity is located at 90% of the fuselage length.

With the statistically determined group mass fractions (\hat{m}_i) and the estimated locations of their associated center of gravity locations (X_i or x_j), we can now estimate the location of the fuselage and wing assemblies. The mass fraction of the fuselage assembly is the summation of the mass fractions comprising the fuselage assembly:

$$\hat{m}_{\text{FA}} = \sum \hat{m}_i \quad (9.5)$$

where i is a counter for all mass groups in the fuselage assembly. The fuselage assembly's center of gravity (FACG) in the reference frame of the fuselage can be computed as follows:

$$X_{\text{FACG}} = \frac{\sum X_i m_i}{\sum m_i} = \frac{\sum X_i \hat{m}_i}{\hat{m}_{\text{FA}}} \quad (9.6)$$

The mass fraction of the wing assembly can be computed as follows:

$$\hat{m}_{\text{WA}} = \sum \hat{m}_j \quad (9.7)$$

where j is a counter for all mass groups belonging to the wing assembly. The wing assembly's center of gravity (WACG) is computed in the reference frame of the wing:

$$x_{\text{WACG}} = \frac{\sum x_j m_j}{\sum m_j} = \frac{\sum x_j \hat{m}_i}{\hat{m}_{\text{WA}}} \quad (9.8)$$

In Figure 9.4 you can see the wing and the fuselage joined together with the locations of the fuselage assembly and wing assembly centers of gravity indicated. Added together, the mass of these assemblies produces the operating empty mass (OEM). Its center of gravity is also shown as x_{OEMCG} . The OEM center of gravity is expressed in the reference frame of the wing because this intuitively refers to the airplane's stability. It is known from aerodynamics that an airfoil is neutrally stable around its quarter-chord point, i.e. $x = 0.25c$. This is called the aerodynamic center. An airplane also has an aerodynamic center known as the neutral point. The aerodynamic centers of the wing and tail surfaces mostly determine its location. To ensure a longitudinally stable airplane, the center of gravity must be ahead of the neutral point. You have to *choose* the location of the OEM center of gravity in the reference frame of the MAC. Typical values for the OEM center of gravity range between 15% and 30% of the mean aerodynamic chord. With a chosen x_{OEMCG} , the location of the LEMAC in the reference frame of the fuselage can be computed using the following formula:

$$X_{\text{LEMAC}} = X_{\text{FACG}} + \bar{c} \left[\left(\frac{x}{\bar{c}} \right)_{\text{WACG}} \frac{\hat{m}_{\text{WA}}}{\hat{m}_{\text{FA}}} - \left(\frac{x}{\bar{c}} \right)_{\text{OEMCG}} \left(1 + \frac{\hat{m}_{\text{WA}}}{\hat{m}_{\text{FA}}} \right) \right] \quad (9.9)$$

This equation ensures that the fuselage is located with respect to the wing in such a way that the center of gravity of the OEM is precisely located at the chosen position. If we convert it to the fuselage's reference frame, its location is computed as follows:

$$X_{\text{OEMCG}} = X_{\text{LEMAC}} + \bar{c} \left(\frac{x}{\bar{c}} \right)_{\text{OEMCG}} \quad (9.10)$$

In the following example, we will show how to perform these steps and locate the wing on the fuselage.

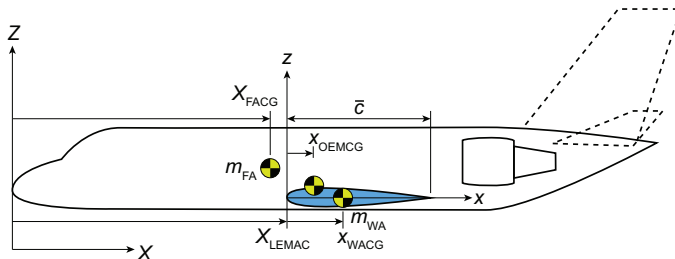


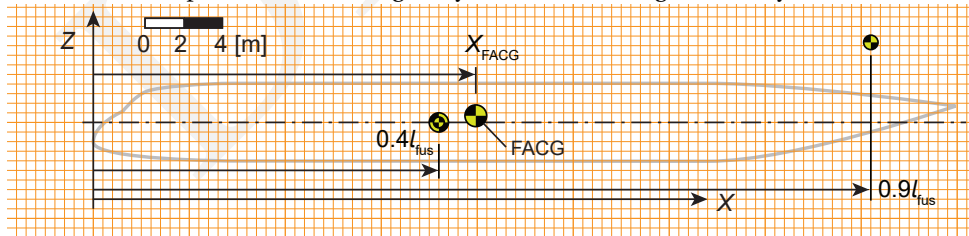
Figure 9.4: Wing positioning on the fuselage based on a chosen location of the operating-empty-mass center of gravity in the reference frame of the wing.

Example 9.2

The mass fractions that were estimated in Example 9.1 belong to the fuselage of Example 6.8 and the wing and propulsion system of Example 8.15. In this example, we determine the location of the wing in the reference frame of the fuselage, i.e. X_{LEMAC} .

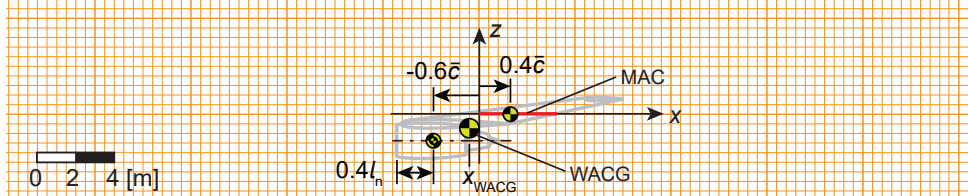
Before estimating the wing location, we first need to estimate the wing mass fractions of the fuselage and wing assemblies and determine their respective center of gravity locations. As seen in Example 8.15, the engine is attached below the wing and, therefore, belongs to the wing assembly.

We start with the fuselage assembly. Employing (9.5) and using the group mass estimates from Example 9.1, we compute the mass fraction of the fuselage to be $\hat{m}_{\text{FA}} = 0.31$. Using the guidelines presented above, we assume the location of the fuselage and fixed equipment mass to be at 40% of the fuselage length and the tail at 90% of the fuselage length. With (9.6) and $l_{\text{fus}} = 44.7 \text{ m}$ from Example 6.6, we compute the center of gravity of the fuselage assembly to be at $X_{\text{FACG}} = 19.8 \text{ m}$. In the figure below, we show the locations of the components' center of gravity and of the fuselage assembly.



For the wing assembly, we assume the wing center of gravity to be at 40% of the mean aerodynamic chord and the propulsion system and nacelle centers of gravity to be at 40% of the nacelle length. Using (9.7) and the data from Example 9.1, we compute the mass fraction of the wing assembly to be $\hat{m}_{\text{WA}} = 0.20$. Subsequently, we measure the location of the propulsion system center of gravity from our sideview drawing. In the reference frame of the wing, it is located at $x = -0.6\bar{c}$. We employ (9.8) with $\bar{c} = 4.1 \text{ m}$ from Example 8.2 to find the center of gravity of the wing assembly to be $x_{\text{WAGC}} = -0.25 \text{ m}$. In the figure

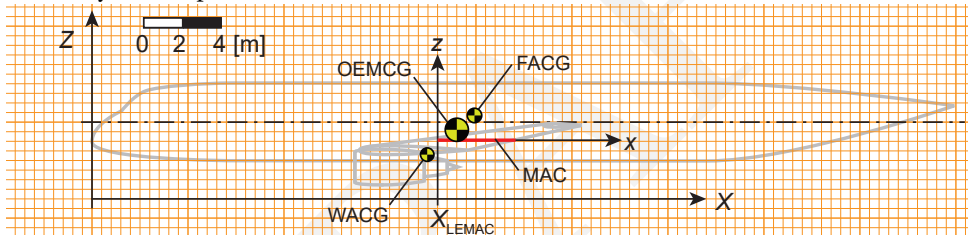
below, you can see the centers of gravity for the three group masses and the center of gravity of the wing assembly in the reference frame of the wing.



We choose the OEM center of gravity at the quarter chord point of the mean aerodynamic chord, i.e. $x_{\text{OEMCG}} \equiv 0.25\bar{c} = 1.0$ (m). We then employ (9.9) to compute the location of the leading edge of the mean aerodynamic chord in the reference frame of the fuselage:

$$X_{\text{LEMAC}} = 17.9 \text{ [m]} \approx 0.45l_{\text{fus}}$$

We subsequently combine the drawings of the fuselage and wing and locate the wing so that the LEMAC is at the calculated longitudinal position. You can see below that the center of gravity of the OEM is located between those of the wing assembly and fuselage assembly, as is expected.



When selecting the vertical location of the wing, we choose a position for the root airfoil between the passenger floor and the bottom of the fuselage. Finally, we compute the OEM center of gravity using (9.10):

$$X_{\text{OEMCG}} = 18.9 \text{ [m]}$$

The previous example showed how you can position the wing on the fuselage. Note that we did not explicitly explain how to compute the vertical location of the center of gravity. Theoretically, Equations 9.6 and 9.8 could be used but then with Z and z replacing X and x , respectively. Then, in the reference frame of the wing, the OEM center of gravity can be computed with:

$$z_{\text{OEMCG}} = \frac{\hat{m}_{\text{FA}} z_{\text{FACG}} + \hat{m}_{\text{WA}} z_{\text{WACG}}}{\hat{m}_{\text{FA}} + \hat{m}_{\text{WA}}} \quad (9.11)$$

A simpler approach is to assume the resulting OEM center of gravity to be on the fuselage's centerline, which is typically a good approximation, as can also be observed from Example 9.2.

ASSIGNMENT 9.2

In this assignment, you will determine the wing's location with respect to the fuselage.

- a. Using the estimated group mass fractions from Assignment 9.1, compute the fuselage and wing assembly mass fractions, \hat{m}_{FA} and \hat{m}_{WA} , respectively.
- b. Compute the location the fuselage and wing assemblies' center of gravity in their respective reference frames, i.e. X_{FACG} and x_{WACG} .
- c. Choose the center of gravity location of the operating empty mass in the frame of reference of the wing, i.e. x_{OEMCG} .
- d. Compute the location of the leading edge of the mean aerodynamic chord in the reference frame of the fuselage, i.e. X_{LEMAC} .
- e. Compute the location of the OEM center of gravity in the reference frame of the fuselage, i.e. X_{OEM} .
- f. Choose a vertical position of your wing with respect to your fuselage and add the wing to the side-view drawing of your fuselage.
- g. Plot the location of the OEM center of gravity in your side view drawing.

The OEM's chosen center of gravity location is the starting point for generating the loading diagram. The next step is to determine the location of the payload and fuel centers of gravity. For the payload, it is fair to assume that its center of gravity resides in the center of the cabin and vertically in the middle of the fuselage. If the fuel is located in a fuselage-based fuel tank like the LH₂ tank of Figure 6.2, the center of the tank should be taken. If the fuel is stored in the wing and the wing has no sweep, the fuel center of gravity can be chosen halfway between the front and rear spar on the MAC. However, it is more difficult to determine the location of a wing-based tank's center of gravity if that wing possesses a sweep angle and is tapered. In Chapter 12, we will generate a more elaborate loading diagram and properly estimate the fuel center of gravity. For now, we will leave it to your engineering judgment to estimate where the fuel CG is located. If the fuel tank center of gravity is estimated in the frame of reference of the wing and normalized by the MAC, it can be converted to the fuselage's reference frame as follows:

$$X_i = X_{LEMAC} + \bar{c} \left(\frac{x_i}{\bar{c}} \right) \quad (9.12)$$

where i refers to any mass component. For the fuel center of gravity $i = fCG$.

Once the centers of gravity of payload and fuel are determined, the center of gravity of each combination can be computed as follows:

$$X_i = \frac{\sum \hat{m}_i X_i}{\sum \hat{m}_i} \quad (9.13)$$

where i now represents the mass components OEM, maximum structural payload (pl max), and fuel (f). We have three combinations for which we need to evaluate the center of gravity: $i = OEM + pl\ max$, $i = OEM + f$, $i = OEM + pl\ max + f$. In the following example, a loading diagram is generated using this method.

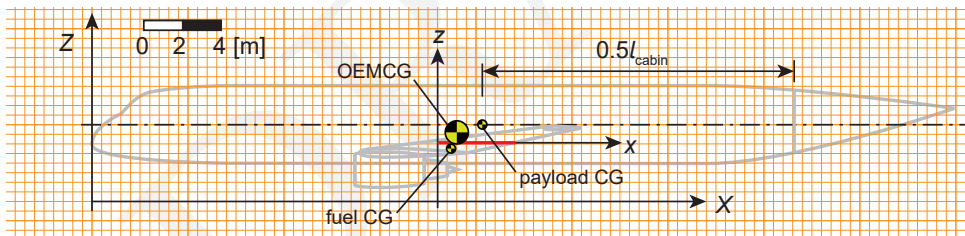
Example 9.3

In this example, we produce the loading diagram from the airplane of Example 9.2, with the mass data from Example 5.12.

From Example 5.12 we know the OEM, the maximum payload mass, and the fuel mass. We normalize each with the maximum take-off mass to find their respective mass fractions. The mass fraction and mass are listed in the first and second columns of the upper part of the table below.

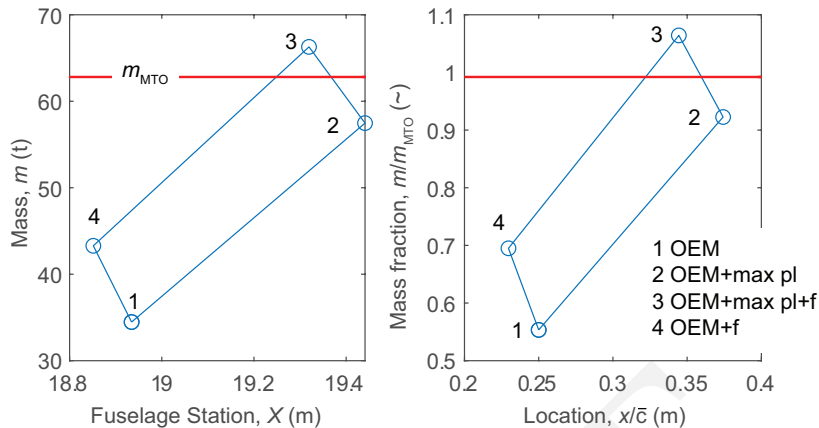
We subsequently measure the location of the payload center of gravity from our drawing, assuming it lies in the middle of the cabin and on the centerline (see the drawing below). We list the value in the third column of the table below. We assume the fuel to reside in wing tanks. Due to the sweep and taper of the wing, we presume the longitudinal position of the fuel CG to be at 15% of the MAC, i.e. $(x_{fCG}/\bar{c}) = 0.15$. The resulting location in the reference frame of the fuselage can be measured from the drawing and is listed in the third column in the table below.

i	$\hat{m}_i [~]$	$m_i [t]$	$X_i [m]$	$x_i/\bar{c} [~]$
OEM	0.55	34.5	18.9	0.25
max payload	0.37	23.0	20.2	0.56
fuel	0.14	8.8	18.5	0.15
OEM+max payload	0.92	57.5	19.4	0.37
OEM+max payload+fuel	1.06	66.3	19.3	0.34
OEM+fuel	0.69	43.3	18.9	0.23

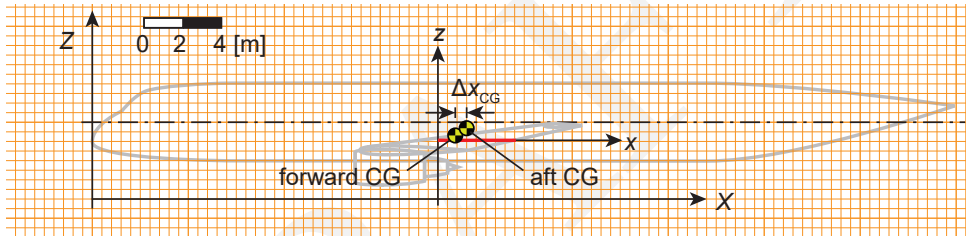


Next, we employ (9.13) to compute the mass fraction (\hat{m}_i) location of the center of gravity (X_i) for each combination of fuel and payload. We list them in the first and third row of the lower part of the table below. By multiplying the mass fraction by m_{MTO} , we also add the mass for each combination of fuel and payload. Finally, we use (9.12) to compute each mass fraction's location in the wing's reference frame and normalized to the MAC. Those values are listed in the fourth column of the table above.

With the data from the table above, we can draw a simplified loading diagram. In this example, we draw two instances of the loading diagram below. On the left-hand side, you can see the loading diagram expressed in dimensional form with the fuselage station on the horizontal axis and mass (m) on the vertical axis. On the right-hand side, we draw the same diagram but this time in non-dimensional form with the x/\bar{c} on the horizontal axis and the mass fraction $\hat{m} = m/m_{MTO}$ on the vertical axis.



The overall *center of gravity excursion* ranges between $0.23 < x/\bar{c} < 0.37$ and measures $\Delta x_{CG} = 0.14\bar{c} = 0.59$ m. We show the forward and aft centers of gravity in the side view of the airplane below:



In the previous example, the CG was located behind the CG of the operating empty mass. Therefore, when the payload was added, the center of gravity shifted to the back. The fuel tank was ahead of the CG of the operating empty mass, resulting in a forward shift of the CG when the fuel was added. The overall CG excursion was relatively small, and the forward and aft CG were located quite close. The vertical excursion of the CG is even smaller than the horizontal excursion. Therefore, it is justified to estimate the CG to reside on the fuselage's centerline or to base the vertical position on engineering judgment.

The process of estimating the center of gravity excursion is independent of the type of aircraft. However, if you have a battery-electric aircraft, there is no change in fuel mass over the mission. The simplified loading diagram then consists of only two points corresponding to the following masses: $m_{OE} + m_{bat}$ and $m_{OE} + m_{bat} + m_{pl\ max}$.

The process of finding the center of gravity excursion can be summarized in the following steps:

- Step 1* Group aircraft components in wing and fuselage assemblies
- Step 2* Make a statistical estimate of the component weight fractions
- Step 3* Compute the wing and fuselage assembly CG locations
- Step 4* Choose a desired CG location for the aircraft OEM in terms of MAC

Step 5 Compute the location of the LEMAC in the fuselage reference frame

Step 6 Determine the location of the fuel CG and payload CG

Step 7 Construct the simplified loading diagram

Step 8 Estimate the vertical location of the aircraft CG

In the following assignment, you will produce the loading diagram for your airplane.

ASSIGNMENT 9.3

In this assignment, you will produce the loading diagram of your airplane.

- a. Compute the mass fraction of the maximum payload and fuel with respect to the maximum take-off mass of your airplane.
- b. Compute the mass fraction for the following cases:
 1. OEM + max payload
 2. OEM + max payload + fuel
 3. OEM + fuel
- c. Estimate the location of the fuel and payload centers of gravity in the side view of your drawing of Assignment 9.2
- d. Compute the location of the center of gravity in the reference frame of the fuselage for the three cases.
- e. For each of the cases, compute the longitudinal location of the CG in the reference frame of the wing, normalized to the mean aerodynamic chord, i.e. x_i/\bar{c} .
- f. Construct the loading diagram for your airplane by plotting the three cases and the OEM condition. For the horizontal axis, use the normalized longitudinal position in the reference frame of the wing, x/\bar{c} , and on the vertical axis, use the mass fraction, \hat{m} .
- g. Draw the most forward and aft centers of gravity in the sideview of your drawing and erase the OEM center of gravity.
- h. State the longitudinal values of the forward and aft centers of gravity, i.e. $(x/\bar{c})_{\text{fwd CG}}$ and $(x/\bar{c})_{\text{aft CG}}$ as well as the CG excursion, $(\Delta x/\bar{c})_{\text{CG}}$.

The resulting forward and aft centers of gravity are needed to size the landing gear and the tail. We emphasize that the predicted excursion of the center of gravity can be improved by making a more refined loading diagram. This is covered in Chapter 12 and typically results in a somewhat larger value of Δx_{CG} compared to the value predicted in this chapter.

9.2. LANDING GEAR DESIGN AND INTEGRATION

The landing gear provides balance, stability, and control when the airplane is on the ground. More specifically, we distinguish the following functions of the landing gear:

1. Absorb landing and taxiing shocks
2. Provide the ability for ground maneuvering
3. Provide braking capability



Figure 9.5: Hard surface, small contact area, high pressure and small tires (left). Soft surface, large contact area, low pressure, and large tires (right). Photos by Charles Regina © and Greg Bishop ©, respectively.

4. Allow for airplane towing
5. Protect the ground surface

In this textbook, we limit our discussion to landing gear with wheels. The landing gear should be designed to prevent structural damage to the airplane, the tires, and the ground surface. In this section, we select the tires and position the landing gear in the three-view of our airplane.

The tires form the contact point between the airplane and the ground surface. The type of tire that is suitable for an airplane depends on the ground surface that is specified. In this respect, we talk about the *floatation* of the tires on the ground. Simply stated, the tire dimensions and the tire pressure need to be selected to stay “afloat” when the maximal vertical load is applied. The contact area between the surface and the tire is determined by the tire dimensions and its pressure. A small tire with high pressure has a relatively small contact surface. On a hard ground surface, it could stay afloat, but on a soft surface, such as grass, it might pierce into the mud. A soft ground surface, therefore, requires larger and softer tires. The two airplanes in Figure 9.5 show how the tire dimension is driven by the ground surface hardness.

9.2.1. DETERMINING THE NUMBER OF WHEELS AND STRUTS

For all CS-VLA and CS-23 airplanes, the main landing gear (mlg) has two wheels. Each wheel (w) is mounted to a single strut (s). A single nose wheel is part of the nose landing gear (nlg) or a tail wheel is fitted to the tail landing gear (tlg). In summary, we have:

$$N_w, \text{mlg} = 2 \quad (9.14)$$

$$N_s, \text{mlg} = 2 \quad (9.15)$$

$$N_w, \text{nlg} = 1 \text{ or } N_w, \text{tlg} = 1 \quad (9.16)$$

For CS-25 airplanes, determining the number of wheels and struts is more elaborate. The vertical load on a single tire depends on the weight of the airplane and the number of tires over which the weight is distributed. We use the maximum aircraft classification rating (ACR) that we derived in Assignment 3.3. The ACR expresses the relative

effect of an aircraft on a pavement for a specified standard subgrade strength. The ACR is expressed in hundreds of kilograms. The ACR is typically specified for the maximum take-off weight. The maximum take-off weight is related to the maximum take-off mass by $W_{MTO} = m_{MTO} \cdot g$. To determine the number of wheels, we take the following steps:

Step 1 From the required ACR, compute the derived single wheel load, DSWL in Newtons:

$$DSWL = \frac{G_1 \cdot 100 \cdot g}{2} \quad (9.17)$$

with G_1 being the first number in the ACR and g being the gravitational acceleration.

Step 2 Assume the maximum fraction of the weight that needs to be supported by the main landing gear, f_{mlg} . Also, assume the maximum weight fraction that needs to be supported by the nose landing gear f_{nlg} . To ensure steering, at least 8% of the airplane weight needs to be supported by the nose landing gear. Typically, no more than 15% of the weight is supported by the nose landing gear in the most forward center-of-gravity position.

Step 3 Based on your reference airplanes, assume the number of main landing gear struts, the number of main landing gear wheels, and the wheel assembly per strut. Do the same for the nose landing gear. Use the nomenclature from Table 9.1.

Step 4 Based on the previous step, make an assumption on the landing gear distribution factor, DF, based on the wheel assemblies of Table 9.1. Do this for the main landing gear and the nose landing gear.

Step 5 Compute the number of wheels according to the following formula:

$$N_{w, mlg} \approx \frac{f_{mlg} W_{MTO} \cdot DF_{mlg}}{DSWL} \quad (9.18)$$

$$N_{w, nlg} \approx \frac{f_{nlg} W_{MTO} \cdot DF_{nlg}}{DSWL} \quad (9.19)$$

Step 6 Round these numbers to make sure we have an even number of wheels and that you can produce the landing gear layouts of Table 9.1. You can use the following logic:

- If $N_{w, mlg} \leq 2$ then $N_{w, mlg} = 2$
- If $N_{w, mlg} > 2$ then round $N_{w, mlg}$ up to the nearest multiple of 4
- If $N_{w, nlg} \leq 1$ then $N_{w, nlg} = 1$ or $N_{w, nlg} = 2$
- If $N_{w, nlg} > 1$ then $N_{w, nlg} = 2$

You can decide to use two nose wheels rather than one if you wish to ensure an additional layer of redundancy in case of tire failure or to allow for smaller tires.

Step 7 Compare the number of wheels to the assumed number of wheels at *Step 3* of this process. If they are the same, continue to the next step. If they are different, choose one of the following options:

1. Repeat the process starting at *Step 4* with a different assumption for the distribution factor, DF.
2. Repeat this process starting at *Step 3* with the new number of wheels.

Step 8 Choose the number of struts for the main landing gear. Based on empirical data, we propose the following:

$$\text{For } N_w, \text{mlg} \leq 12, N_s, \text{mlg} = 2 \quad (9.20)$$

$$\text{For } N_w, \text{mlg} > 12, N_s, \text{mlg} = 3 \text{ or } N_s, \text{mlg} = 4 \quad (9.21)$$

Table 9.1: Landing gear wheel assembly configurations and associated distribution factor (DF). The minimum in DF is found when the wheels are positioned far apart. The maximum is found when the wheels are spaced very close together.

Name:	single	dual/ twin	single tandem	dual tandem/ twin tandem	triple twin tandem
Configuration:					
DF [min, max]	1.0	[1.0, 1.6]	[1.0, 1.2]	[1.0, 1.8]	[1.0, 2.0]

As you can see, the process of estimating the number of wheels could be iterative if the number of wheels at *Step 3* differs from *Step 6*. If this is the case, it means that the specified pavement requires a different landing gear layout for your airplane compared to your reference airplanes. In the following example, we will determine the number of wheels for a CS-25 airplane.

Example 9.4

In this example, the number of wheels and struts is determined for the CS-25 airplane of Example 5.12 with the ACR from Example 3.5. We follow the same steps as presented above.

Step 1 At maximum take-off weight, the following requirement should be satisfied: $\text{ACR} \leq 850/\text{F/C/W/T}$. Using (9.17), the derived single wheel load is:

$$\text{DSWL} = 420 \text{ [kN]}$$

Step 2 We assume that $f_{\text{mlg}} = 0.92$ and $f_{\text{nlg}} = 0.15$.

Step 3 We use the reference airplanes from Example 9.1, which apply to the airplane from Example 5.12. The following table shows the results in the first three columns and the assumptions for “my airplane” in the last column:

	DC9-30	MD-80	B737-200	my airplane
$N_{w, \text{mlg}}$	4	4	4	4
$N_{s, \text{mlg}}$	2	2	2	2
MLG wheel assembly	twin	twin	twin	twin
$N_{w, \text{nlg}}$	2	2	2	2
NLG wheel assembly	twin	twin	twin	twin

Step 4 Based on the range given in Table 9.1, we assume $DF_{\text{mlg}} = DF_{\text{nlg}} = 1.6$ to enable a compact layout of the landing gear wheels.

Step 5 Using (9.18) and (9.19), we compute $N_{w, \text{mlg}} \approx 2.2$ and $N_{w, \text{nlg}} \approx 0.3$.

Step 6 Applying rounding results in $N_{w, \text{mlg}} = 2$ and $N_{w, \text{nlg}} = 1$. However, we decide to have $N_{w, \text{nlg}} = 2$ in line with our reference aircraft to ensure that in case of tire failure, there is still a tire left to provide stability and control during a take-off or landing maneuver.

Step 7 We skip this step because the number of tires is identical to those on the reference aircraft

Step 8 Based on the number of wheels, we have two main landing gear struts, i.e., $N_{s, \text{mlg}} = 2$.

ASSIGNMENT 9.4

In this assignment, you will determine the number of wheels for your airplane.^a

- Compute the derived single wheel load of your airplane, based on the ACR requirement you computed in Assignment 3.3.
- Make an assumption for the maximum main landing gear load fraction, f_{mlg} , and the maximum nose landing gear load fraction, f_{nlg} .
- Based on your reference airplanes, assume the number of wheels for your main landing gear and for your nose landing gear.
- Choose a wheel layout per strut and assume a distribution factor (DF) for the main landing gear and nose landing gear.
- Compute the number of wheels that are required for the main landing gear and for the nose landing gear. Based on your calculations, decide on the number of wheels for your nose landing gear and main landing gear.
- How many struts do you need for your main landing gear?

^aThis assignment is only required if the certification basis is CS-25

9.2.2. DETERMINING THE TIRE PRESSURE AND SIZE

In this section, we determine the tire pressure and the size of the tires. The tire pressure and the tire dimensions determine the contact area for a given wheel load. As stated above, unpaved runways need a larger contact area to provide flotation than paved runways. For paved runways, the pavement classification rating (PCR) provides an upper bound for the tire pressure through the third entry, G_4 . Table 9.2 provides information

on the maximum allowable tire pressure for various runway surfaces. You can use this table to determine the tire pressure for your airplane.

Table 9.2: Proposed tire pressures for various runway surfaces based on empirical data. N.A. stands for “not applicable.”

Description of Surface	PCR G_4	Maximum allowable tire pressure, p_t (MPa)		
		lowest value	typical value	highest value
Soft, loose desert sand	N.A.	0.17	0.21	0.24
Wet, boggy grass	N.A.	0.21	0.28	0.31
Hard desert sand	N.A.	0.28	0.41	0.41
Hard grass	N.A.	0.31	0.41	0.48
pavement	Z	N.A.	N.A.	0.50
pavement	Y	0.50	0.93	1.25
pavement	X	1.25	1.38	1.75
pavement	W	1.75	N.A.	N.A.

It can be seen from Table 9.2 that for paved runways where G_4 is Z or W, there are no values listed. This is because, in practice, virtually all airplanes that land on paved surfaces have a tire pressure between 0.50 and 1.75 MPa. Therefore, the resulting G_4 of the aircraft classification rating (ACR) will either be X or Y, complying with Equation 3.3.

ASSIGNMENT 9.5

In this assignment you will determine the tire pressure for your landing gear wheels.

- Using Table 9.2, the type of runway surface, and the value of G_4 of the ACR,^a select the tire pressure for your landing gear wheels.
- Based on the selected tire pressure, do you need to update your ACR? If so, what is the updated ACR of your airplane at maximum take-off weight?

^aFor paved runways only

Tire sizing is done through the selection of tires from a database. To minimize the mass of the landing gear, you would typically select the smallest tires that can support the load that is exerted on the tire. The load that the tire can support is referred to as the *rated tire load*, F_t . In order to determine the tire dimensions, we first need to compute the load rating per tire and then use a lookup table to select the smallest tire that can bear that load at the tire pressure.

For the tires on the main landing gear, the maximum load is seen during the take-off maneuver. Despite the additional loads that are exerted during take-off rotation, we can consider the static loading conditions to be sizing the tires. The rated load per tire is computed by evenly distributing the maximum take-off weight over the number of wheels of the main landing gear, considering the load fraction corresponding to the most aft center-of-gravity position:

$$F_{t, \text{mlg}} = \frac{f_{\text{mlg}} W_{\text{MTO}}}{N_{w, \text{mlg}}} \quad (9.22)$$

For the nose landing gear, the highest load is found during a braking scenario where the center of gravity is located most forward. For a twin layout of the nose landing gear, an additional safety factor, f_{dif} , is applied to account for differences in tire wear and inflation pressure. Therefore, the maximum rated tire load is:

$$F_{t, \text{nlg}} = \frac{f_{\text{nlg}} f_{\text{dif}} W_{\text{MTO}}}{N_{w, \text{nlg}}} \quad (9.23)$$

with $f_{\text{dif}} = 1.07$.

With the tire pressure, p_t , and the tire load F_t , known, we can now select a tire from an available tire database. Ref. [17] includes tables stemming from the publications of the Rim and Tire Association (RTA) that have data for several tire types. You can consult these tables to select an appropriate tire. In lieu of these tables, we have included the data on for so-called *three part bias* tires in Figure 9.6. Each marker in this figure indicates an existing tire from the table of Ref. [17] corresponding to this tire type. Tires of equal dimension are connected by a colored line and have a label listing the tire diameter (D_t), the tire width (w_t), and the rim diameter (D_r). These tires differ in the number of plies that are used in the tire, which affects their rated tire load. Similar figures can be constructed for other tire types, but that is beyond the scope of this book.

To find the smallest tire for your airplane, you first find the intersection of tire pressure and tire load in the graph of Figure 9.6. Then, you find the line that is closest to this intersection but still above it. The tire dimensions belonging to this line are the tire dimensions for your landing gear. You can perform this exercise twice. Once for the tires of the main landing gear and once for the tires on the nose (tail) landing gear. In summary, the tire selection process comprises the following steps:

- Step 1* Select the tire pressure based on the runway surface type and/or the PCR. If necessary, update the ACR.
- Step 2* Determine the tire load for the main landing gear and nose (tail) landing gear tires.
- Step 3* Select the smallest tire with a rated load that is higher than the one computed in the previous step.

The following example demonstrates this process.

Example 9.5

In this example, we select the tires for the landing gear of Example 9.4. We follow the steps listed above.

- Step 1* The PCR that is listed for this airplane has $G_4 = W$. This means that there is no maximum tire pressure. However, we have seen that in practice, the tire pressure is always below 1.75 MPa. Based on Table 9.2, we select $p_t = 1.40$ MPa. We update the ACR at maximum take-off mass accordingly: $\text{ACR} = 850/\text{F/C/X/T}$.

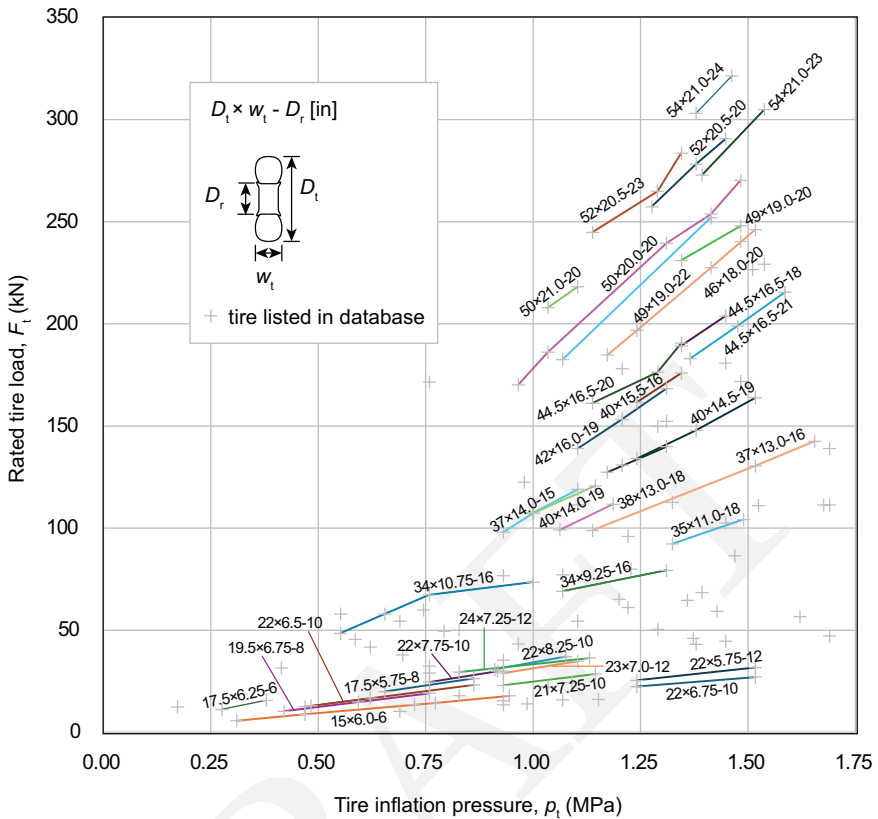


Figure 9.6: Dimensions of three-part bias tires related to the rated load and inflation pressure at static conditions. Data from Ref. [17].

Step 2 Using (9.22) and (9.23), we compute the main-landing-gear tire load and nose-landing-gear tire load, respectively:

$$F_{t, \text{mlg}} = 140 \text{ [kN]}$$

$$F_{t, \text{nlg}} = 65 \text{ [kN]}$$

Step 3 First, we find the intersection of $(p_t, F_t) = (1.40 \text{ [MPa]}, 140 \text{ [kN]})$ and select a main-landing-gear tire from Figure 9.6 with the dimensions: $40 \times 14.5 - 19$. Converting this to the metric system yields:

$$D_{t, \text{mlg}} = 1.0 \text{ [m]}$$

$$w_{t, \text{mlg}} = 0.36 \text{ [m]}$$

$$D_{r, \text{mlg}} = 0.48 \text{ [m]}$$

Secondly, we find the intersection of $(p_t, F_t) = (1.40 \text{ [MPa]}, 65 \text{ [kN]})$ and select a nose-landing-gear tire from Figure 9.6 with the dimensions: $35 \times 11 - 18$. Con-

verting this to the metric system yields:

$$D_{t, \text{nlg}} = 0.89 \text{ [m]}$$

$$w_{t, \text{nlg}} = 0.28 \text{ [m]}$$

$$D_{r, \text{nlg}} = 0.46 \text{ [m]}$$

In the previous example, we have used Figure 9.6. However, you can choose to use the tables from Ref. [17] directly to find an appropriate tire for your airplane. Alternatively, you can use a database from a tire manufacturer and select an appropriate tire from there. When there are multiple tires that could be used for the application, you use the following considerations in tire selection:

1. Drag during deployment. Larger tires cause more drag, which affects the take-off and landing performance.
2. Volume required for stowage. The smaller the tires, the less volume is needed for stowage.
3. Margin between rated tire load and maximum tire load. A margin allows for the mass of the airplane to increase during the design process without having to select a larger tire. It also allows for larger versions of the airplane to use the same tires.

In the following assignment, you will select the tire pressure and dimensions for your airplane tires.

ASSIGNMENT 9.6

In this assignment, you will size the rims and tires of your landing gear.

- a. Select the tire pressure for your tires and, if applicable, update the aircraft classification rating (ACR).
- b. Compute the maximum rated tire load for the main landing gear and the nose landing gear, respectively.
- c. Select the tires for your main landing gear and nose landing gear and report the dimensions of the tire diameter, tire width, and rim diameter.

9.2.3. INTEGRATING THE LANDING GEAR

When integrating the landing gear, we need to consider a number of implicit and explicit requirements. The first requirement is that the airplane should not tip on its tail during the take-off and landing maneuvers or during loading on the ground. Secondly, the landing gear should provide enough clearance to the ground surface during the landing and take-off maneuver. When turning, the aircraft should not tip over to its side. Finally, the nose wheel should be used to steer the airplane on the ground. We will use all of these requirements in the positioning of the landing gear. As a general objective, the landing gear should be as small as possible, which minimizes the mass as well as the volume. The latter is particularly important for retractable landing gear.

We will start the integration process with the longitudinal position of the main landing gear. Three requirements determine the longitudinal location of the landing gear: tip-over angle, the scrape angle and the ground clearance. In Figure 9.7, we show the

side view of an airplane with a nose landing gear and one with a conventional landing gear. In both cases, we assume that the ground plane is not aligned with the fuselage. In other words, the fuselage has a pitch attitude with respect to the ground plane, θ_{fus} . For the airplane with nose landing gear, the scrape angle and tip-over angles are drawn. For the airplane with a conventional landing gear, the tip-over angle and the clearance between the ground plane and the propeller are drawn. We will now discuss each of these constraints.

Consider Figure 9.7. For the airplane with the nose landing gear, the *tip-over angle* determines how much the airplane can rotate about the wheel axle before the CG gets behind the wheel axle. The value of the tip-over angle is derived from two requirements. The first requirement is that when the airplane brakes during a push-back maneuver, it does not tip on its tail as a result of its inertia. The second requirement is that when the airplane lands, the tip-over angle ensures that when the wheels of the main landing gear touch the ground, they produce a nose-down pitching moment with respect to the center of gravity. A typical value for the longitudinal tip-over angle is $\theta_{\text{tip-over}} \approx 15^\circ$. Conversely, for airplanes with conventional landing gear, the tip-over requirement ensures that the airplane does not tip on its nose when the brakes are applied during a landing maneuver or when the airplane lands on its main landing gear. For conventional landing gear, the most forward center-of-gravity position is critical for tip-over.

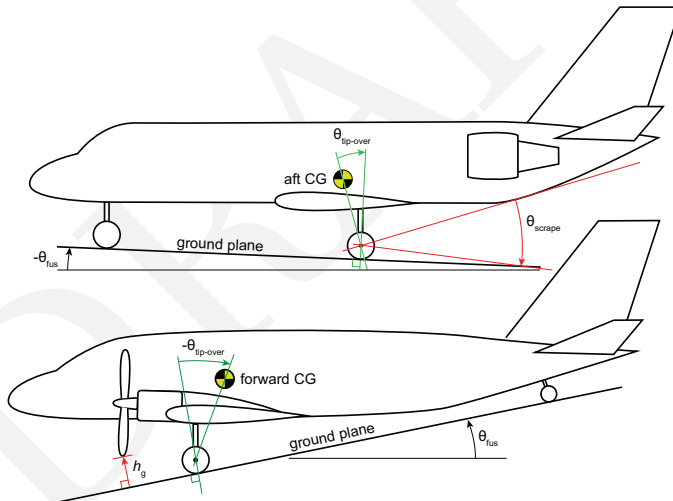


Figure 9.7: Definition of the scrape and tip-over angles for airplanes with nose landing gear (top) and conventional landing gear (bottom).

The *scrape angle* limits the pitch attitude the airplane can achieve while being on the ground. For airplanes with a nose landing gear, it is typically the aft fuselage that would touch the runway when the scrape angle is exceeded. Therefore, we have introduced an upsweep angle in the fuselage (see Chapter 6). For conventional landing gear, it is the front fuselage, engines, or propellers that are typically limiting the nose-down attitude while on the ground.

Ground clearance between the propeller or jet engine is a third requirement that must

be taken into account when integrating the landing gear. In Example 3.17, we showed that certification specifications demand a propeller ground clearance, h_g , of at least 18 cm in a nose-gear configuration and $h_g > 23$ cm for a conventional landing gear. Ground clearance is measured perpendicular to the ground plane as shown in lower part of Figure 9.7. For jet engines, ground clearance is required to prevent engines from sucking in dirt or debris from the runway and damaging the turbomachinery of the engine. This is referred to as *foreign-object damage* (FOD). To prevent FOD, engines should have a ground clearance of $h_g > 45$ cm.

When designing the main landing gear in the side view, a complication arises stemming from the shock absorbers and tires. You can imagine a scenario where the tires are completely deflated, and the shock absorber is fully compressed, resulting in the shortest landing gear length. Alternatively, when the shock absorber is fully deployed, and the tires are undeformed, the length of the gear is maximal. During dynamic ground maneuvers such as take-off and landing, the length of the gear depends on the instantaneous load, which, in turn, is governed by the weight and acceleration of the airplane. Even in static conditions, the deflection of the shock absorber is dependent on the weight of the airplane, which is affected by payload and fuel, as well as the spring stiffness of the shock absorber itself. Typical shock absorber strokes range between 30 and 50 centimeters, independent of the airplane's size. To keep the design process simple, we propose to assume that the tip-angle and scrape angle requirements can be applied to the static situation where we assume that two-thirds of the shock absorber is compressed and that the tire is perfectly circular.

If the main landing gear has a tandem, dual tandem, or triple tandem configuration, the wheels are connected to a so-called *bogie*. The landing gear strut is connected to the bogie by means of a pivot. When the airplane rotates with the wheels on the ground (for example, during the take-off maneuver), this rotation happens with respect to the bogie's pivot point. So, for landing gear bogies, the tip-over angle and the scrape angle are measured with respect to the pivot point instead of the wheel axle.

The position of the nose or tail landing gear is governed by two requirements that relate to the vertical load on the nose landing gear. In Figure 9.8 we show the weight force acting at the center of gravity and the resulting reaction loads at the nose and main landing gear, P_{nlg} and P_{mlg} , respectively. The distance measured along the ground plane between the center of gravity and nose and main landing gear is l_{nlg} and l_{mlg} , respectively. If we consider static equilibrium, we can relate the length l_{nlg} to the other quantities as follows:

$$l_{nlg} = \left(\frac{W}{P_{nlg}} - 1 \right) l_{mlg} = \left(\frac{1}{f_{nlg}} - 1 \right) l_{mlg} \quad (9.24)$$

The first requirement is the steering capability. In order to steer the airplane with the nose wheel, there needs to be a minimal load acting on the nose wheel. When the center of gravity is located most aft, the nosewheel experiences the lowest nosewheel load. A minimal load of 6% of the weight is required to enable steering, i.e. $f_{nlg} \geq 0.06$. The second requirement is the maximum load on the nose wheel strut, which should be evaluated at the most forward center of gravity position. The maximal load fraction of the nose landing gear is a design decision but is typically between 15% and 20%.

The process above describes the constraints of the landing gear design. Within these

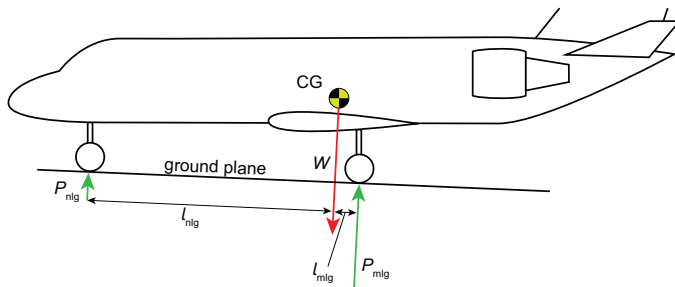


Figure 9.8: Ground forces exerted on the main landing gear to support the weight.

constraints, you must decide where to position the landing gear. For the main landing, the intersection between the two constraint curves for the scrape and tip-over angle is the most logical location. It ensures the shortest landing gear and the most forward position. the latter is important for minimizing the rotation speed of the airplane, i.e. the minimum speed that is required to rotate the airplane about its main landing gear during the take-off maneuver. For the nose landing gear, a range of positions between a minimal and maximal location may exist. The shortest gear with the lightest loading is typically preferred because it results in the lowest landing gear mass. Hence, the most forward position is preferred. However, if the landing gear needs to be retractable, it could be preferred to locate the nose gear further aft such that gravity and drag could help the deployment of the gear in case of a malfunction in the deployment system. If the nose gear swings forward or backward. The envisioned retraction path is part of the design of the landing gear.

In summary, the following design sequence is proposed to design the landing gear in the side view:

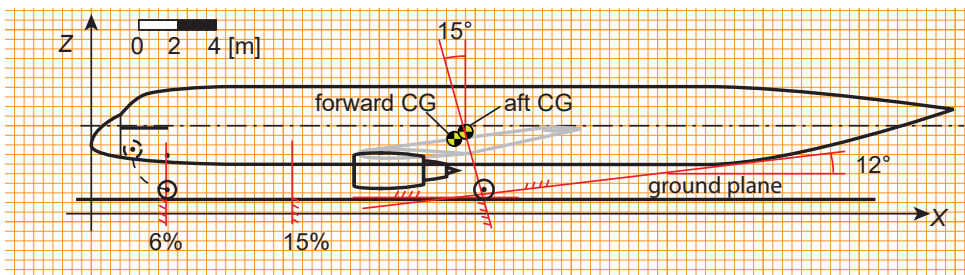
- Step 1* Determine the requirements for the tip-over angle, $\theta_{\text{tip-over}}$ and the scrape angle, θ_{scrape} .
- Step 2* Determine the minimal nose gear load fraction, $f_{\text{nlg, min}}$, to enable steering and choose the maximal nose gear load fraction, $f_{\text{nlg, max}}$, that should be structurally supported.
- Step 3* Choose the fuselage pitch angle on the ground, θ_{fus} .
- Step 4* In the side view, draw the constraint lines stemming from the tip-over angle, the scrape angle, and/or ground clearance, and choose the location of the main landing gear.
- Step 5* In the side view, draw the ground plane.
- Step 6* In the side view, draw the constraint lines stemming from the steering and nose-gear load requirement and choose the location of the nose landing gear.
- Step 7* If applicable, draw the retraction path of the main landing gear and/or nose landing gear in the side view.

In the following example, we show how this procedure can be used.

Example 9.6

In this example, we integrate the tires of Example 9.5 in the side view of Example 8.16. This airplane has a landing gear comprising two main gear struts and one nose gear strut. Each strut has two wheels. In order to locate the wheels in the side view, we follow the steps outlined above.

- Step 1** To ensure the airplane is not tipping over during take-off or pushback, we impose a tip-over angle of $\theta_{\text{tip-over}} = 15^\circ$. Based on a rudimentary assessment of our reference airplanes, we specify a scrape angle of $\theta_{\text{scrape}} = 12^\circ$ when the airplane is at 1-g conditions and at maximum take-off mass.
- Step 2** Following experience, we impose a minimal nose-gear load fraction of $f_{\text{nlg, min}} = 0.06$ to enable steering at the most aft CG position and a maximal nose-gear load fraction of $f_{\text{nlg, max}} = 0.15$ at the most forward CG position.
- Step 3** Because this airplane has under-the-wing engines, we choose to align the fuselage with the ground plane to ensure sufficient clearance between the engine and the ground. Therefore, we choose $\theta_{\text{fus}} = 0^\circ$.
- Step 4** We draw the tip-over angle constraint in our drawing below, where the hash marks indicate the unfeasible position for the wheel axle. Because the fuselage pitch angle is zero, we can measure the tip-over angle with respect to a vertical line perpendicular to the ground plane. Secondly, we draw a constraint line that is angled 12 degrees with respect to the ground plane and let it touch the lowest part of the fuselage. Finally we draw a constraint line parallel to the ground plane with a 50 cm clearance from the engine. The lowest part of the tire needs to be below this constraint line. We draw the wheel with its axle behind the tip-over constraint and the lowest part of the tire below the clearance constraint. We observe that the scrape angle constraint is not active in positioning the main landing gear tire.
- Step 5** Below the tire, we draw the ground plane. Because $\theta_{\text{fus}} = 0^\circ$, the ground plane is horizontal in our drawing.
- Step 6** We estimate l_{nlg} for the steering requirement at aft most center-of-gravity location by employing (9.24) with $l_{\text{mlg}} \approx 1.0$ and $f_{\text{nlg, min}} = 0.06$ to find $l_{\text{nlg}} = 16$ m. The maximum load is found when the center of gravity is most forward. Using the assumed load fraction and measuring $l_{\text{mlg}} \approx 1.5$, we find $l_{\text{nlg}} = 8.5$. Both constraints are drawn in the side view with the hashmarks indicating the unfeasible region. To minimize the load on the nose landing gear, the wheel is positioned as far forward as possible.
- Step 7** A simple retraction path for the nosewheel is shown where the nosewheel rotates forward into the fuselage below the flight deck floor and behind the front pressure bulkhead. This way of stowing the wheel has the advantage that both drag and weight could deploy the landing gear in case of a failure in the hydraulic (or electric) system.



In the previous example, you could see that we approximated the scrape angle of Figure 9.7 by drawing a constraint line with respect to the lowest side of the tire. This is a practical approach to positioning the wheel. Once the wheel is positioned, you can check whether the scrape angle is satisfied by measuring it in your drawing. Regarding the positioning of the nose landing gear, the previous example showed the most forward position. However, any position between the two constraints would be acceptable. The most forward position ensures the smallest load on the nose landing gear and, therefore, the lightest structure. However, the more forward the nose gear is positioned, the larger the turn radius on the ground. Also, note that we purposely positioned the X -axis of the axis system below the ground plane. This ensures that all Z -coordinates of the airplane geometry have a positive value. Even when the landing gear would become taller in later iterations of the design, its position would still be measured by a positive Z coordinate.

ASSIGNMENT 9.7

In this assignment you will integrate the landing gear of your airplane in the side view drawing.

- What constraints on the tip-over angle, $\theta_{\text{tip-over}}$, and scrape angle, θ_{scrape} , do you impose?
- What is the minimal nose gear load to enable steering, and what is the maximal nose gear load?
- What fuselage angle, θ_{fus} , do you choose?
- Draw the constraint lines for the main landing gear wheel and position it in the side view of your drawing
- Draw the ground plane.
- Draw the constraint lines for the nose landing gear and position the nose landing gear.
- If applicable, draw the retraction path for the main landing gear and/or nose landing gear.

The next step is to integrate the landing gear in the front view of the drawing. Traditionally, the nose landing gear is positioned on the centerline of the airplane, although there have been airplanes that deviated from this rule. The lateral position of the main landing gear is more elaborate and primarily influenced by the following constraints:

- Prevent lateral turnover during a turn maneuver on the ground.

2. Ensure there is sufficient clearance between the airplane and the ground even when the airplane has a bank angle
3. Ensure ground clearance in case the suspension on one of the main landing gear legs is fully compressed and the attached tires are deflated.

Each one of these requirements may be sizing the minimum required *track width*, i.e. the lateral distance between the outermost main landing gear wheels. We shortly discuss each requirement before proceeding with a step-by-step method to determine the lateral position of the main landing gear.

When an airplane with a tricycle landing gear makes a tight turn on the ground, there is the risk of lateral turnover. Due to inertial forces, the center of gravity then passes an imaginary line between the nose wheel and the outermost main landing gear wheel. The wider the gear track, the lower the chance that lateral turnover occurs. A typical way to translate the requirement to prevent lateral turnover is to specify a maximal lateral turnover angle, ψ , which is defined in Figure 9.9. Note that ψ increases with the height of the center of gravity above the ground, h_{CG} , as well as with the more forward location of the center of gravity. Therefore, the most forward position of the center of gravity needs to be considered. In order to protect an airplane from lateral turnover $\psi \leq 55^\circ$, although examples exist where ψ is higher due to the limited track width of the landing gear. However, you must keep in mind when ψ is specified too high, this limits the lateral stability of the airplane on the ground. To satisfy the requirement of a maximal lateral turnover angle, ψ , the lateral position of the main landing gear should be:

$$Y_{mlg} \geq \frac{l_{mlg} + l_{nlg}}{\sqrt{\frac{l_{nlg}^2 \tan^2 \psi}{h_{CG}^2} - 1}} \quad (9.25)$$

with l_{mlg} and l_{nlg} defined as in Figure 9.9. Note that the same analysis is applicable to conventional landing gear, although in that case, the most aft center of gravity should be considered.

In Figure 9.10, the ground clearance angle between the main landing gear and the tip and engine is shown in red. When an airplane comes in for a landing, some margin in bank angle (ϕ) is required to steer the airplane. Therefore, you would like to make sure that the landing gear is positioned in such a way that it is the wheels that touch the ground first. A typical minimal bank angle is $\phi \geq 8^\circ$. For jet airplanes with a nose landing gear, the nacelle height above the ground plane (h_{nac}) results in the following requirement on the lateral position of the main landing gear:

$$Y_{mlg} \geq Y_e - \frac{h_{nac}}{\tan \phi} \quad (9.26)$$

For a propeller airplane, h_{nac} should be replaced with the propeller height, h_{prop} .

When a conventional landing gear is selected combined with wing-mounted tractor propellers, the nose-high attitude of the airplane results in a relatively large clearance between propellers and the ground plane. To mimic a realistic landing scenario, the ground clearance constraint constraint must, therefore, be evaluated at an attitude of

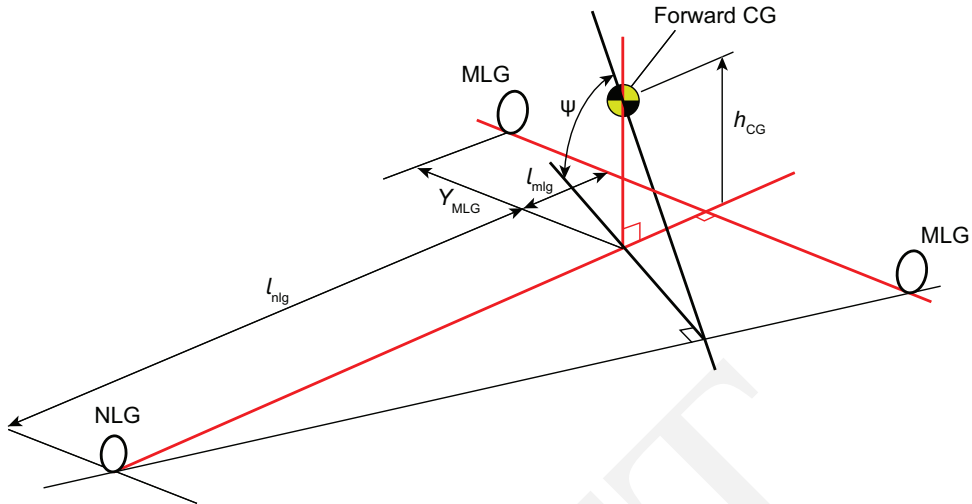


Figure 9.9: The lateral turnover requirement limits the turnover angle, ψ .

zero degrees. For this particular case, Equation 9.26 should be replaced by:

$$Y_{\text{mlg}} \geq Y_{\text{prop}} - \frac{\Delta Z_{\text{prop}}}{\tan \phi} \quad (9.27)$$

where Y_{prop} is the lateral position of the (outermost) wing-mounted propeller and ΔZ_{prop} is the distance between the lowest part of that propeller and the ground plane when the fuselage is aligned with the ground plane. The latter is computed as follows:

$$\Delta Z_{\text{prop}} = \frac{h_{\text{prop}} + (X_{\text{prop}} - X_{\text{mlg}}) \sin \theta_{\text{fus}}}{\cos \theta_{\text{fus}}} \quad (9.28)$$

where X_{prop} is the location of the propeller in the fuselage reference frame, and h_{prop} is the height of the propeller above the ground plane when the airplane is on all three wheels on the ground. The propeller height can best be measured in your side-view drawing.

Now, let us consider the tip clearance. If the tip of the wing is behind the center of gravity of the airplane, it rotates down when the airplane has a nose-high attitude. To ensure that the tip does not scrape the ground when the airplane is at its scrape angle, the lateral position of the main landing gear should be:

$$Y_{\text{mlg}} \geq \frac{b_w}{2} - \frac{h_{\text{tip}} + (X_{\text{mlg}} - X_{\text{tip}}) \sin \theta_{\text{scrape}}}{\tan \phi} \quad (9.29)$$

where X_{tip} is the trailing edge of the wing tip. The longitudinal distance between the main landing gear and the tip, as well as the tip height (h_{tip}), can be measured from your side-view drawing.

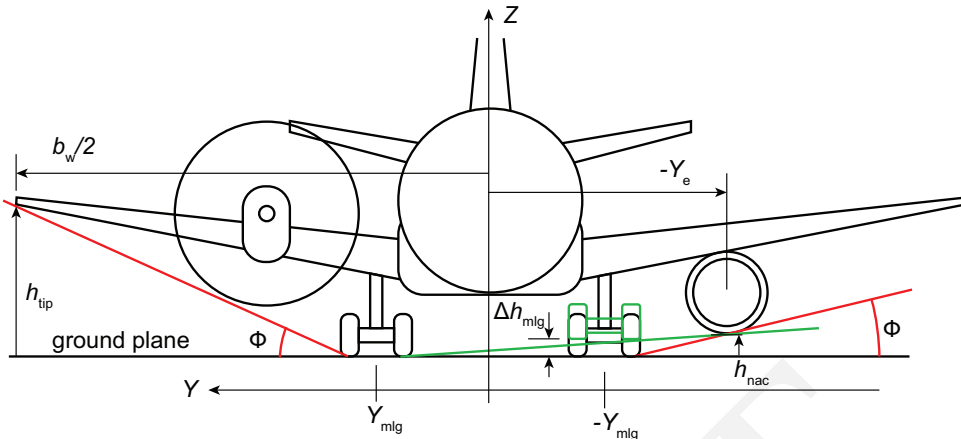


Figure 9.10: Various ground clearance angles, ϕ

In Figure 9.10, the green lines show the bank angle that results when one of the two main landing gear struts is fully compressed and the tire is deflated. The minimum lateral position to ensure ground clearance when the outermost landing gear is in this state can be computed as follows:

$$Y_{\text{mlg}} \geq \frac{\Delta h_{\text{mlg}}}{2h_{\text{nac}} - \Delta h_{\text{mlg}}} Y_e \quad (9.30)$$

where Δh_{mlg} is the change in height above the ground plane when the suspension is fully compressed and the tire is fully deflated, h_{nac} is the nacelle height above the ground, and Y_e is the lateral engine position. The change in main-landing gear height can be computed as follows:

$$\Delta h_{\text{mlg}} = as + \frac{D_t - D_r}{2} \quad (9.31)$$

where s is the total stroke of the suspension system, a is the fraction of the total stroke between 1-g compression and full compression, D_t is the tire diameter, and D_r is the rim diameter as defined in Figure 9.6. For wing-mounted tractor propeller aircraft with conventional landing gear, we have to correct for the fuselage attitude on the ground. In that case, Equation 9.30 should be replaced by:

$$Y_{\text{mlg}} \geq \frac{\Delta h_{\text{mlg}}}{2\Delta Z_{\text{prop}} - \Delta h_{\text{mlg}}} Y_{\text{prop}} \quad (9.32)$$

where ΔZ_{prop} is computed by (9.28) and Y_{prop} is the lateral position of the (outermost) wing-mounted propeller.

The previous requirements specified a minimal lateral position of the landing gear. But what would be the most optimal position? That question does not have a straightforward answer, and there are a few aspects to consider. First of all, there is the aspect of integration with the primary structure of the aircraft. The landing gear strut should be

positioned as close as possible to the primary structure, such as a wing spar or a fuselage frame. For wing-mounted propeller aircraft, the landing gear might be integrated into the same fairing as the engine. This would result in reduced wetted area. For jet engines, the strut must not be positioned in the exhaust of the engine. Finally, a wider landing gear track increases the turn radius on the ground, making the minimal track width optimal to allow tight maneuvering on the ground. For retractable landing gear, the retraction path must also be considered feasible, and there should be sufficient volume to store the landing gear.

In summary, we propose the following design sequence to integrate the landing gear in the front view of your airplane drawing:

- Step 1* Determine the requirements for the lateral turnover angle, ψ , and the maximum bank angle, ϕ
- Step 2* Select a landing-gear stroke, s , and the fraction between full compression and 1-g compression, a .
- Step 3* Compute the minimal lateral position of the main landing gear to satisfy the lateral turnover requirement.
- Step 4* Compute the minimal lateral position of the main landing gear to satisfy the nacelle or propeller clearance requirement in case of a banked landing.²
- Step 5* Compute the minimal lateral position of the main landing gear to satisfy the wing tip clearance requirement.
- Step 6* Compute the minimal lateral position of the main landing gear to satisfy the nacelle or propeller clearance requirement in case of one fully compressed main landing gear strut and (a) deflated tire(s).³
- Step 7* Determine the position of the main landing gear strut(s) in the front view of your airplane drawing. For retractable landing gear, draw the retraction path and the stowed landing gear, and draw additional structural elements and/or fairings when required.
- Step 8* Determine the position of the main landing gear strut(s) in the top view. For retractable landing gear, draw the stowed landing gear and draw additional structural elements and/or fairings when required.

In the following example, we shall demonstrate how the landing gear can be integrated into the front view of the airplane.

Example 9.7

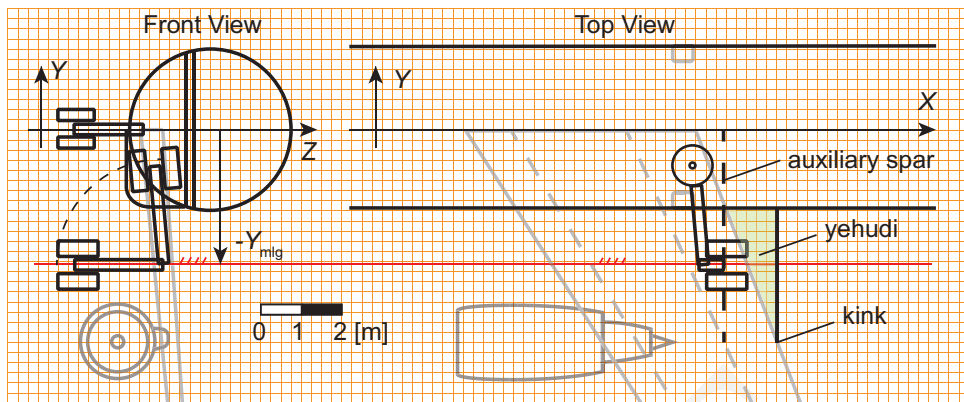
In this example, we will determine the lateral position of the main landing gear for the airplane of Example 9.6.

- Step 1* Following Roskam, we require a maximal lateral turnover angle of $\psi \leq 55^\circ$. Based on common design practice for commercial transport aircraft, we require a minimal bank angle during landing of $\phi \geq 8^\circ$.

²Only applicable for wing-mounted engines

³Only applicable for wing-mounted engines

- Step 2** We choose a 40-cm stroke ($s = 0.4$ m) for the main landing gear suspension system. In addition, we assume that 2/3 of the stroke is compressed under 1-g conditions, i.e. $a = 1/3$.
- Step 3** To determine the gear track to satisfy the lateral turnover requirement, we first measure the lengths and height from the side-view drawing considering the most forward CG position. We have: $l_{\text{mlg}} = 1.4$ m, $l_{\text{nlg}} = 14$ m, and $h_{\text{CG}} = 3.5$ m. With these values, we compute with (9.25): $Y_{\text{mlg}} \geq 2.7$ m.
- Step 4** Since our airplane configuration has engines mounted below the wing, we need to consider the minimum engine clearance between the engine and the ground. We have $h_{\text{nac}} = 0.50$ m and $Y_e = 5.2$ m from the side-view drawing and top-view drawing, respectively. Employing (9.26), we can compute that $Y_{\text{mlg}} \geq 1.7$ m.
- Step 5** To ensure tip clearance under a banked landing, we first measure the position of the main landing gear and the tip in our side view drawing: $X_{\text{mlg}} = 20$ m, $X_{\text{tip}} = 25$ m, $h_{\text{tip}} = 3.5$ m. Using (9.29) with a scrape angle of $\theta_{\text{scrape}} = 12^\circ$, we compute $Y_{\text{mlg}} \geq -2.6$ m.
- Step 6** To ensure nacelle clearance in case of a fully compressed landing gear strut and deflated tires, we employ (9.31) with $D_t = 1.0$ m and $D_r = 0.48$ m to get $\Delta h_{\text{mlg}} = 0.39$ m. Based on that, we use (9.30) to compute $Y_{\text{mlg}} \geq 3.4$ m.
- Step 7** Based on the previous analyses, we conclude that the final engine clearance requirement is the active requirement for the minimal lateral position of the main landing gear strut, i.e. $Y_{\text{mlg}} \geq 3.4$ m. In the front view below, we draw this constraint as a line parallel to the Z -axis. We decide to position the main landing gear strut at the location of the constraint. The hinge point for the main strut is assumed to be located in the wing. When we draw the retraction path and include the extension of the gear by 2/3rd of the stroke, we can see that the landing gear can mostly be stowed below the cabin floor. However, the lower wheel protrudes outside of the fuselage perimeter. Therefore, we add a fairing around the landing gear to ensure it is not exposed to the flow in the stowed configuration. Finally, we add the nose landing gear on the symmetry plane of the airplane.
- Step 8** In the top view, we first position the wheels at the desired location in the deployed configuration and in the stowed configuration. We decide to have an angled hinge line to allow the gear to swing forward as well as upward. We position the pivot point itself close to the aft face of the rear spar to shorten the load path. To provide sufficient volume for the strut in the wing and to allow the integration of a trailing-edge flap, we add a triangular wing surface so the wing, colloquially known as a *yehudi*. This results in a kink in the wing surface and allows the positioning of the *auxiliary spar*, which increases the structural strength of the wing and provides structural attachment points for flap systems and/or spoiler panels. The *yehudi* introduces a *kink* in the trailing edge of the wing and increases its planform area.



In the previous example, you could see that positioning a retractable main landing gear requires a careful balance between multiple considerations. In the end, we drew a landing gear that looked plausible, which took inspiration from our reference airplanes. One of the implicit decisions that we made was the spacing between the two wheels on each strut. This was done quite intuitively based on the landing gear of the reference airplanes. However, it is good to know that the spacing between the wheels affects the distribution factor (DF) and, therefore, the ACR, as we discussed in Section 9.2.1. Here, you can see that the spacing also affects the required volume for stowing the landing gear. Spacing between the wheels is also required to provide braking systems.

In deciding the position of the landing gear hinge point, we assumed that we could connect the main landing gear (close to) the rear spar. The load path from the landing gear to the main spar would be relatively short, and the landing gear loads would be transferred to the fuselage through the wing box. Therefore, we do not require additional fuselage frames to be reinforced. However, we did add an additional spar as well as additional wing area. This means that the actual wing area is larger than the reference area and that we have lowered the wing loading. In subsequent iterations of the design, we must take this into account.

If the landing gear is mounted to the fuselage, the fuselage frames must be strengthened to introduce the landing gear loads to the fuselage. To cater for the required lateral position of the main landing gear, additional structure is often required to enable this (see also our discussion in Section 4.3). If the landing gear is retractable, an aerodynamic fairing is added to cover the stowed landing gear as well as the auxiliary structure that protrudes outside the fuselage to support the landing gear. This fairing is often referred to as a *sponson*.

In the subsequent assignment, you will integrate a landing gear with your airplane.

ASSIGNMENT 9.8

In this assignment, you will determine the lateral position of the main landing gear in the front view of your drawing.

- List the requirements for the maximum lateral turnover angle, ψ , and the

- minimum bank angle, ϕ .
- b. Choose a stroke for your main landing gear suspension system, along with a fraction of the stroke that is compressed in 1-g conditions.
 - c. Compute the minimum lateral position of the main landing gear strut in order to satisfy the lateral turnover requirement.
 - d. Compute the minimum lateral position of the main landing gear strut in order to satisfy the nacelle/propeller clearance requirement.^a
 - e. Compute the minimum lateral position of the main landing gear strut in order to satisfy the tip clearance requirement
 - f. Compute the minimum lateral position of the main landing gear strut in order to satisfy the engine clearance requirement in case of a fully compressed suspension system and a deflated tire.^b
 - g. Position the main landing gear and nose landing gear in the front view of your drawing. If applicable, draw the retraction path of the landing gear, draw additional structural elements, and/or draw the changed outer mold line.
 - h. Position the main landing gear and nose landing gear in the top view of your drawing. If applicable, draw the retraction path of the landing gear, draw additional structural elements, and/or draw the changed outer mold line.

^aOnly applicable for wing-mounted propulsion systems

^bOnly applicable for wing-mounted propulsion systems

9.3. TAIL SURFACE SIZING

The tail of the airplane comprises a horizontal tailplane and a vertical tailplane. Each of these has three functions: to stabilize, to control, and to balance the airplane. These functions are performed in the air but also during the high-speed portions of the take-off ground roll and landing ground roll. In this section, we will present a method to dimension these tail surfaces and show how they can be integrated with the airplane. A more refined method for tail sizing will be presented in Chapter 12.

9.3.1. VERTICAL TAILPLANE DESIGN AND INTEGRATION

The function of the vertical tail is to provide directional stability to the airplane, enable yaw control through the rudder, and provide a balancing force in case of asymmetric thrust. Sufficient directional stability is required to damp out the *Dutch roll* motion of the airplane. The Dutch roll is a motion in which the airplane periodically rolls and yaws. Directional control is required, particularly at low speeds, to enable a landing and take-off in cross-wind conditions. Directional control is achieved by deflecting a trailing-edge control surface known as the *rudder*. Providing equilibrium is particularly important in a one-engine inoperative condition of multi-engine airplanes.

We propose to use the so-called *tail volume* method to determine the dimension of the vertical tailplane. The tail volume, V_v is defined as the product of the tail arm and the

surface area of the tail, i.e.:

$$V_v = S_v l_v \quad (9.33)$$

where S_v is the planform surface area of the vertical tailplane and l_v is the longitudinal distance between the aerodynamic center of the vertical tailplane and the aft center of gravity of the airplane (see Figure 9.11). Note that we define part of the tailplane area as being in the fuselage, similar to the definition of the wing planform area. The vertical location is determined by positioning the midpoint of the root chord on the upper curve of the tail cone.

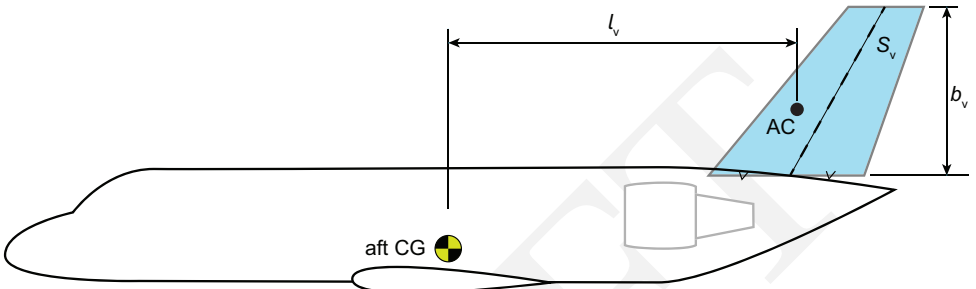


Figure 9.11: Definition of the vertical tailplane area and tail arm.

To enable the use of statistical data from other airplanes to size the tailplane of our airplane, we compute the tail volume coefficient:

$$\bar{V}_v = \frac{S_v l_v}{S_w b_w} \quad (9.34)$$

where S_w and b_w are the wing area and span, respectively. Tail volume coefficients for various airplane classes are published in Ref. [14]. We propose you use the data from this reference to make a first estimate of the tail volume coefficient for your airplane's vertical tailplane. Minima and maxima for each airplane category as defined in Ref. [14] are presented here:

$$\begin{aligned} \text{Single Engine Propeller Driven Airplanes: } & 0.024 \leq \bar{V}_v \leq 0.047 \\ \text{Twin Engine Propeller Driven Airplanes: } & 0.041 \leq \bar{V}_v \leq 0.097 \\ \text{Agricultural Airplanes: } & 0.021 \leq \bar{V}_v \leq 0.054 \\ \text{Business Jets: } & 0.059 \leq \bar{V}_v \leq 0.093 \\ \text{Regional Turboprop Airplanes: } & 0.065 \leq \bar{V}_v \leq 0.121 \\ \text{Jet Transport Airplanes: } & 0.038 \leq \bar{V}_v \leq 0.120 \end{aligned} \quad (9.35)$$

As you can see from the list above, there is quite a large spread in tail volume coefficients within one category as well as between categories. This indicates that sizing of the vertical tailplane is not straightforward and presents quite some uncertainty at this stage of the design. Nonetheless, a tail volume coefficient must be chosen in order to

proceed with the design and integration of the vertical tailplane. More detailed aerodynamic analysis is subsequently required to demonstrate compliance with requirements for balance, stability, and control.

The planform shape of the vertical tailplane is typically trapezoidal, similar to a straight tapered wing. Therefore, three planform parameters need to be selected: the aspect ratio, the taper ratio, and the (leading-edge) sweep angle. How do you select these planform parameters? To answer that question, we first give you a qualitative feeling for the effect of the change of each parameter on a variety of tailplane characteristics. These characteristics apply to both vertical *and* horizontal tailplanes.

Let us start with the aspect ratio. The larger the aspect ratio, the larger the effectiveness of the tailplane. In other words, for a given change in inflow angle, the resulting side/lift force increases with increasing aspect ratio. This is favorable for stability. Similarly, an increased aspect ratio increases the effectiveness of the control surface and reduces the moment that is required to deflect it. On the other hand, the inflow angle at which stall occurs is also lowered when the aspect ratio increases, which is unfavorable for the ability to balance the airplane over a wide variety of inflow angles. Finally, an increasing aspect ratio also increases the mass of the tailplane due to the larger span combined with a lower thickness.

If we decrease the taper ratio of the tailplane, the tip chord decreases, and the root chord increases. This results in a reduction in the mass of the tailplane. However, the small tip chord could decrease the stall inflow angle due to flow separation at the tip. The effectiveness of the tail surface as a stabilizer or control surface is not directly affected by the taper ratio.

The sweep angle of the tailplane allows for a longer moment arm, assuming the tail is attached to the same location. While the sweep angle reduces the effectiveness of the vertical tailplane, the effect is quite small due to the relatively small aspect ratio of the vertical tailplane. Increasing the sweep angle typically increases the stall inflow angle, which is beneficial. The leading edge sweep angle and the taper ratio affect the local sweep angle of the hinge line of the rudder. Rudder effectiveness is reduced whenever the hinge line is swept. Finally, sweeping the vertical tail increases its structural span, which increases its weight.

Reference [8] provides empirical data for these planform parameters for turboprop and turbofan airplanes. Based on this data, we observe that these parameters have the following bandwidth:

$$1 \leq R_v \leq 2 \quad (9.36)$$

$$0.3 \leq \lambda_v \leq 0.7 \quad (9.37)$$

$$\left. \begin{array}{l} \text{prop: } 0 \\ \text{jet: } \Lambda_{w, LE} \end{array} \right\} \leq \Lambda_{v, LE} \leq 50^\circ \quad (9.38)$$

For T-tailed airplanes, the aspect ratio is typically lower than for conventional tails, and the taper ratio is closer to 1. This is to enable a strong enough support structure for the horizontal tailplane. Therefore, for T-tailed airplanes, we advise choosing an aspect ratio closer to the lower bound of (9.41) and a taper ratio towards the upper bound of (9.42).

We propose the following design sequence to design the vertical tailplane:

- Step 1* Choose the longitudinal location of the vertical tail aerodynamic center
- Step 2* Determine the moment arm from the vertical tailplane's aerodynamic center to the most aft center of gravity position
- Step 3* Compute the vertical tail area using a chosen volume coefficient
- Step 4* Determine the sweep angle, aspect ratio, and taper ratio of the vertical tailplane
- Step 5* Determine span, root chord, tip chord, and MAC
- Step 6* Position the vertical tailplane in the side view of your drawing

The following example demonstrates the application of this process.

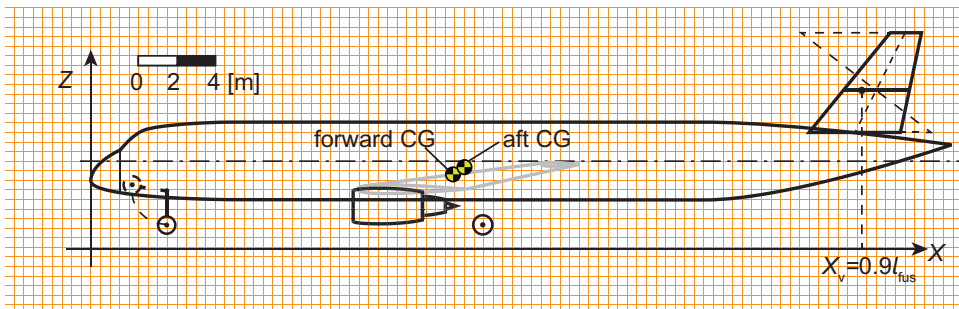
Example 9.8

In this example, we size the vertical tailplane for the airplane of Example 9.7. We follow the step-by-step process outlined above:

- Step 1* We choose the location of the vertical tailplane aerodynamic center to be at 90% of the fuselage length, i.e. $X_{ac,v} = 40$ m.
- Step 2* With the most aft CG at $X_{cg,aft} = 19.4$ m (See Example 9.3), we have a moment arm of $l_v = 21$ m.
- Step 3* We choose a volume coefficient of $\bar{V}_v = 0.105$ based on data from reference airplanes having wing-mounted jet engines. Using (9.34), we compute the vertical tail area to be: $S_v = 17 \text{ m}^2$.
- Step 4* For the planform parameters, we make the following decisions: $R_v = 1.6$, $\lambda_v = 0.35$, and $\Lambda_{v,LE} = 40^\circ$
- Step 5* We employ the equations from Section 8.1.3 that were presented for the wing to compute the dimensions of the vertical tailplane, i.e. (8.4), (8.5), and (8.6). In addition, we use the graphical approach from Example 8.2 to estimate the mean aerodynamic chord of the vertical tailplane. This results in the following parameters:

$$b_v = 5.1 \text{ [m]} \quad c_{r,v} = 4.8 \text{ [m]} \quad c_{t,v} = 1.7 \text{ [m]} \quad \bar{c}_v = 3.5 \text{ [m]}$$

- Step 6* We integrate the vertical tailplane with the fuselage in our side view drawing, ensuring that the aerodynamic center is located at the chosen longitudinal position (see below). Note that the vertical location is determined by letting the midpoint of the root chord intersect the upper curve of the tail cone.
- Step 7* The integration of the vertical tailplane in our top view and front view drawing will be performed in Example 9.10.



The process above helps you to size the vertical tailplane and position it in the side view drawing. If you choose a thickness-to-chord ratio, you can also compute the thickness of the root and tip airfoil. For now, it is enough to assume a symmetric profile for the vertical tailplane. As a guideline, you can use a thickness-to-chord ratio close to the one you have chosen for the wing. In the aerodynamic design of the vertical tailplane, a more detailed assessment will be performed to determine the best airfoil geometry for this surface. In the subsequent assignment, you will practice designing a vertical tailplane.

ASSIGNMENT 9.9

In this assignment, you will design the vertical tailplane and integrate it with your side view drawing.

- Choose a longitudinal location for the aerodynamic center of the vertical tailplane in the reference frame of the fuselage.
- What is the moment arm, l_v , between the aft center of gravity and the aerodynamic center of the vertical tailplane?
- Choose a volume coefficient and compute the vertical tailplane area, S_v .
- Choose values for the aspect ratio (\mathcal{A}_v), taper ratio (λ_v) and leading-edge sweep angle, $\Lambda_{v, LE}$.
- Calculate the span, root chord, and tip-chord of the vertical tailplane, and graphically determine the length of the mean aerodynamic chord (\bar{c}_v).
- Position the vertical tail plane on the fuselage in the side view drawing.
- Add the vertical tailplane in the front view and top view of your drawing.

The vertical tailplane that we have designed provides us with directional stability, control, and equilibrium. In the next section, we will find out how the horizontal tailplane is designed to perform the same functions in the longitudinal direction.

9.3.2. HORIZONTAL TAIL PLANE DESIGN AND INTEGRATION

Similar to the vertical tailplane, the horizontal tailplane has three functions. First of all, it provides longitudinal stability to the airplane. In other words, if the airplane encounters a wind gust that pitches the nose up, the horizontal tailplane ensures that a nose-down pitching moment is generated to bring the nose back to the equilibrium position. In this equilibrium state, the pitching moment generated by the aircraft-less-tail about the

center of gravity is balanced by a force on the horizontal tailplane. Here, the horizontal tailplane differs from the vertical tailplane in the sense that the vertical tailplane does not generate any net forces in steady, symmetric flight. The horizontal tailplane *does* provide a net force in order to balance the airplane. Depending on the pitching moment that is generated by the aircraft-less-tail, this net force can be upward (lift) or downward (downforce). The final function of the vertical tailplane is to provide a means of longitudinal control. This can be done through the deflection of a trailing-edge control surface known as the *elevator* or by means of rotating the horizontal tailplane as a whole. In the latter case, we call this an *all-flying tail* or *stabilator*.

The size of the horizontal tailplane can be determined by one or more requirements. The horizontal tailplane needs to be large enough to provide sufficient longitudinal stability at the most aft center of gravity, to balance the aircraft up to the stall angle of attack with full flaps and forward center of gravity, and to rotate the airplane about the main landing gear wheel at the forward center of gravity. In Chapter 12, we will show how each of these requirements can be evaluated and how the tail size and wing position can be chosen to minimize the size of the tail. In this section, we use a simplified method that relies on an empirically determined tail-volume coefficient, \bar{V}_h .

Similar to the vertical tail-volume coefficient, we define the horizontal tail-volume coefficient as follows:

$$\bar{V}_h = \frac{S_h l_h}{S_w \bar{c}_w} \quad (9.39)$$

where l_h is the horizontal tail arm, i.e. the length between the aerodynamic center of the horizontal tailplane and the aft center of gravity, S_h is the horizontal tailplane area, S_w is the wing area, and \bar{c}_w is the mean aerodynamic chord of the wing. The horizontal tailplane and corresponding arm are defined in Figure 9.12. While the vertical tail volume coefficient is normalized with the span of the wing, the horizontal tail volume coefficient is normalized with the mean aerodynamic chord. We use the data from [14] to provide typical lower and upper bounds for the tail volume coefficients for various classes of airplanes:

$$\begin{aligned} &\text{Single Engine Propeller Driven Airplanes: } 0.49 \leq \bar{V}_h \leq 0.83 \\ &\text{Twin Engine Propeller Driven Airplanes: } 0.46 \leq \bar{V}_h \leq 1.07 \\ &\text{Agricultural Airplanes: } 0.31 \leq \bar{V}_h \leq 0.79 \\ &\text{Business Jets: } 0.51 \leq \bar{V}_h \leq 0.99 \\ &\text{Regional Turboprop Airplanes: } 0.83 \leq \bar{V}_h \leq 1.47 \\ &\text{Jet Transport Airplanes: } 0.54 \leq \bar{V}_h \leq 1.48 \end{aligned} \quad (9.40)$$

Note that for all categories, there is a relatively large difference between minimum and maximum values. This implies that when you choose a tail volume coefficient, you have to be aware that this choice directly affects the size of the vertical tailplane. A larger tailplane is more likely to satisfy the requirements on stability, balance, and control, while it contributes to a larger wetted area and thereby increases the zero-lift drag coefficient. Determining the tail volume coefficients of your reference airplanes can help you in choosing an appropriate value.

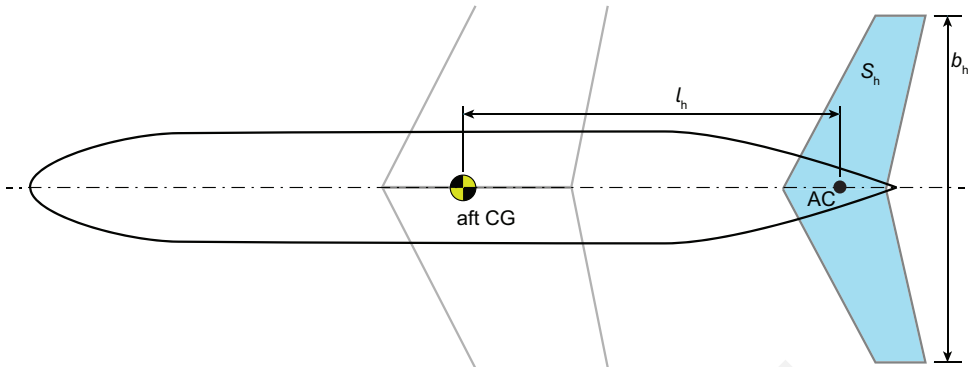


Figure 9.12: Definition of the horizontal tail plane area and tail arm.

The aspect ratio, taper ratio, and sweep angle of the horizontal tailplane must also be determined. An increase in aspect ratio increases the effectiveness of the tailplane as a stabilizing surface, increases the effectiveness of the elevator, and decreases the moment required to deflect the control surface. However, it also reduces the stall angle of attack and increases the (structural) mass of the horizontal tailplane. Lowering the taper ratio decreases the mass of the tailplane but could decrease the stall angle of attack due to an early onset of tip stall. The effectiveness as a control surface or stabilizing surface is hardly influenced by the taper ratio. Increasing the sweep angle, on the other hand, does reduce the effectiveness of the horizontal tailplane. However, it also increases the stall angle of attack, creates a gradual stall behavior, and postpones adverse compressibility effects to higher Mach numbers.

Obviously, the chosen value for each planform parameter is a trade-off between the positive and negative attributes discussed above. Following Obert [8], we suggest the following guidelines for choosing the planform parameters:

$$3 \leq AR_h \leq 5 \quad (9.41)$$

$$0.3 \leq \lambda_h \leq 1 \quad (9.42)$$

$$\left. \begin{array}{ll} \text{prop:} & \Lambda_{h, 3\bar{c}/4} = 0 \\ \text{jet:} & \Lambda_{w, \bar{c}/4} \leq \Lambda_{h, \bar{c}/4} \leq 40^\circ \end{array} \right\} \quad (9.43)$$

If a horizontal tailplane is part of a T-tail configuration, the taper ratio is typically chosen towards the upper bound, i.e. $0.6 \leq \lambda_h \leq 1$. This is to ensure that the root chord of the horizontal tailplane is not larger than the tip chord of the vertical tailplane. When choosing the aspect ratio, the same consideration should be taken into account.

To design the horizontal tailplane and to integrate it with the airplane, the following sequence is proposed:

Step 1 Choose the longitudinal location of the horizontal tailplane quarter-chord point in the reference frame of the fuselage.

Step 2 Determine the moment arm to the most aft center-of-gravity position.

- Step 3* Choose a tail volume coefficient and compute the tail area.
- Step 4* Determine the sweep angle, aspect ratio, and taper ratio.
- Step 5* Determine span, root chord, tip chord, and mean aerodynamic chord.
- Step 6* Position the horizontal tailplane in the top view of your drawing.
- Step 7* Position the horizontal tailplane in the front view and side views of your drawing.

In the following example, we demonstrate how this process can be applied.

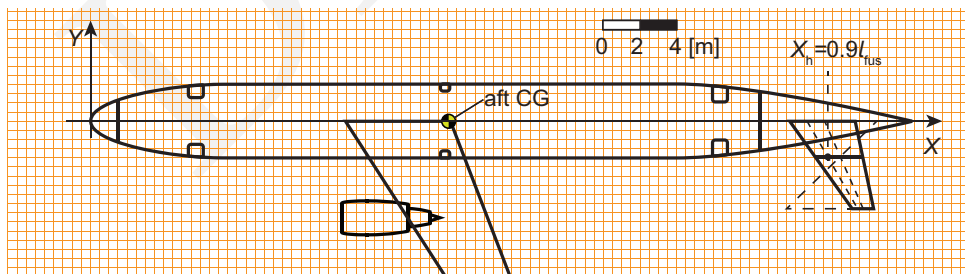
Example 9.9

In this example, we design a horizontal tailplane for the airplane of Example 9.8. We follow the steps outlined above.

- Step 1* We choose the location of the aerodynamic center of the horizontal tailplane to be at 90% of the fuselage length, i.e. $X_{ac,h} = 40$ m.
- Step 2* The tail arm is $l_h = 19.4$ m, see Example 9.8.
- Step 3* We choose a volume coefficient of $\bar{V}_h = 1.0$ and employ (9.39) to find $S_h = 22 \text{ m}^2$.
- Step 4* We choose the following planform parameters: $\mathcal{A}_h = 4.0$, $\lambda_h = 0.40$, and $\Lambda_h, \tilde{\sigma}/4 = 30^\circ$.
- Step 5* We use equations (8.4), (8.5), and (8.6) to compute the span, root chord, and tip chord. Subsequently, we graphically construct the horizontal tailplane and measure the mean aerodynamic chord (see below). This results in the following values:

$$b_h = 9.3 \text{ [m]} \quad c_{r,h} = 3.5 \text{ [m]} \quad c_{t,h} = 1.2 \text{ [m]} \quad \bar{c}_h = 2.5 \text{ [m]}$$

- Step 6* We integrate the tail in the top view below.
- Step 7* We will position the tail in the front view and the side view of our drawing in Example 9.10



The previous example showed how the horizontal tailplane can be designed and integrated with the fuselage. From a practical viewpoint, it is easiest to first draw the horizontal tailplane by itself. Subsequently, you copy the corner points from this drawing to the top view drawing of the airplane. This makes it easier to position the tailplane. In the

subsequent assignment, you will design and integrate the horizontal tailplane with your airplane.

ASSIGNMENT 9.10

In this assignment, you will design the horizontal tailplane and integrate it with your three-view drawing.

- a. Choose a longitudinal location for the aerodynamic center of your horizontal tailplane in the reference frame of the fuselage.
- b. Measure the tail arm, l_h .
- c. Choose a suitable volume coefficient, V_h , and calculate the horizontal tailplane area, S_h .
- d. Choose the following planform parameters: \mathcal{A}_h , λ_h , and $\Lambda_h, \bar{c}/4$.
- e. Compute the horizontal tail span, root chord, tip chord, and mean aerodynamic chord lengths.
- f. Integrate the horizontal tail plane in the top view, front view, and side view of your drawing, respectively.

9.4. TUNING THE THREE-VIEW DRAWING

With the landing gear and tailplanes added, we can now proceed to fine-tune our three-view drawing. The following guidelines can help you clean up your drawing and ensure that key elements are clearly visible. Make sure that an axis system is included in all three views.

In the top view of your drawing, you can remove the lines that show the edges of the wing inside the fuselage. Only the part of the wing that is outside the fuselage remains. The location of the spars and the landing gear wheels should be included. If the landing gear is retractable, also show the retracted landing gear wheels. The mean aerodynamic chord of the wing should be indicated on the center line along with the forward and aft center of gravity locations. It is instructive to show the bounds of the (reference) wing area, S_w , and tailplane area, S_h . For pressurized cabins, show the front and aft pressure bulkheads. Finally, show the locations of the emergency exits if they are visible in this view.

In the front view of your drawing, add the vertical and horizontal tailplane. If you have a low-tail configuration, you can choose to add a small dihedral angle to your horizontal tailplane. This ensures that when the airplane rolls during rotation, the tip of the tail does not scrape the ground. If a yehudi has been added to your wing, the thickness of the inboard wing should be increased, assuming that the thickness-to-chord ratio is constant. Therefore a subtle kink in the wing geometry is introduced in the front view. Naturally, the front view shows the (deployed) landing gear. If the landing gear gear is retractable, also show its stowed position. Finally, add the passenger floor, including its thickness.

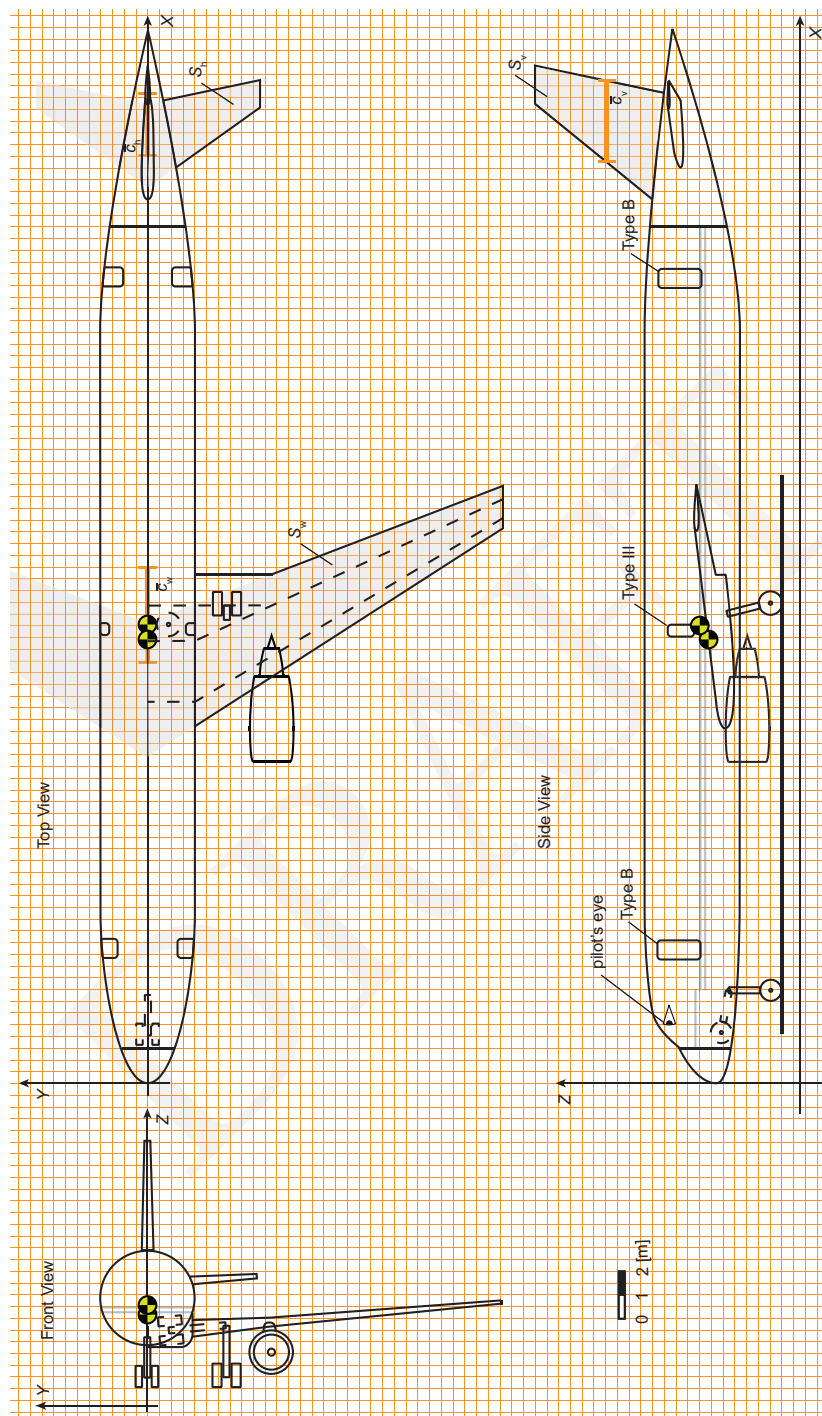
In the side view of your drawing, ensure that the wing is properly drawn. If a yehudi has been added, the wing gets a larger root profile. Also, make sure to only draw the part of the wing that is outside of the fuselage. This also applies to the horizontal tailplane. Also, add the mean aerodynamic chord of the vertical tailplane and indicate the vertical

tail area, S_v . Show the emergency exits and annotate each of them with the type that you have chosen. Show the landing gear, and, if applicable, also show the stowed position of the landing gear. In the fuselage, add the pressure bulkheads (if applicable), the passenger floor, and the pilot's eye.

Example 9.10

In this example, we fine-tune the three-view drawing of the passenger airplane that we have presented throughout the chapter.

The figure below shows the final three-view drawing. We have used the recommendations described in this paragraph to clean up the drawing and make sure that all the relevant information is included.



The reference area that we have used in the example above excludes the additional area that has been added by the yehudi. This definition of the reference area was used by airplane manufacturers such as McDonnel Douglas and Fokker. Other manufacturers, such as Airbus and Boeing, use slightly different definitions of the reference area. In the following assignment, you will fine-tune your three-view drawing.

ASSIGNMENT 9.11

In this assignment, you will fine-tune your drawing.

1. Clean up your drawing by following the guidelines presented above.
2. Using shading or light hash marks to indicate the (reference) area of your wing, horizontal tailplane, and vertical tailplane.
3. Clearly draw the mean aerodynamic chord of the wing, horizontal tailplane, and vertical tailplane.
4. If applicable, show the stowed position of the landing gear in the three-view drawing.
5. Make sure that your drawing has a scale, that each view has an axis system, and that a ground plane is added to the side view.

While the airplane of Example 9.10 already looks complete, there are still important items that have been omitted. Primary control surfaces, i.e., ailerons, elevators, and rudders, have not yet been designed. Also, high-lift devices such as flaps or slats have not been added. Some airplanes also have spoilers on the wing to dump lift, provide roll control, and/or provide air braking. These also need to be added. These aspects will be treated in Chapters 11 and 12.

The fact that we now have a complete airplane geometry gives us the opportunity to analyze this geometry and replace many of the assumptions that we have made with improved estimations. Therefore, Chapter 10 will show how we can perform our first design loop and further refine our design.

10

AIRCRAFT ANALYSIS AND DESIGN ITERATION I

- 10.1.** ESTIMATION OF THE DRAG POLAR
- 10.2.** ESTIMATION OF PROPULSION SYSTEM CHARACTERISTICS
- 10.3.** RESULT OF DESIGN ITERATION ON DESIGN OBJECTIVE
- 10.4.** EFFECT OF DESIGN PARAMETERS ON DESIGN OBJECTIVE
[Add section about tank volume analysis + modification of PR diagram.]

11

WING DESIGN REVISITED AND DESIGN ITERATION II

- 11.1. DESIGN OF ROLL CONTROL SURFACES**
- 11.2. DESIGN OF HIGH-LIFT SYSTEM**
- 11.3. ESTIMATION OF MAXIMUM LIFT COEFFICIENT**
- 11.4. RESULT OF DESIGN ITERATION ON DESIGN OBJECTIVE**
- 11.5. EFFECT OF WING DESIGN PARAMETERS ON DESIGN OBJECTIVE**

12

EMPENNAGE DESIGN REVISITED AND DESIGN ITERATION III

- 12.1. STABILITY AND CONTROL REQUIREMENTS**
- 12.2. COMPONENT WEIGHT ESTIMATION**
- 12.3. GENERATION OF LOADING DIAGRAM**
- 12.4. SIZING FOR LONGITUDINAL STABILITY, EQUILIBRIUM AND
CONTROL**
- 12.5. LONGITUDINAL WING POSITIONING REVISITED**
- 12.6. SIZING FOR DIRECTIONAL STABILITY, EQUILIBRIUM, AND
CONTROL**

13

AUTOMATION OF THE AIRPLANE DESIGN PROCESS

- 13.1. FORMALIZING THE CONSTRAINED DESIGN OPTIMIZATION PROBLEM**
- 13.2. SETTING UP THE MULTIDISCIPLINARY DESIGN AND ANALYSIS WORKFLOW**
- 13.3. PERFORMING AUTOMATED DESIGN ITERATIONS**

BIBLIOGRAPHY

- [1] Airbus. *A320 Aircraft Characteristics Airport and Maintenance Planning*. Tech. rep. Blagnac, France, Dec. 2020.
- [2] Valentin Batteiger et al. *Accelerating the path towards carbon-free aviation*. en. Ed. by Jens Friedrichs et al. Braunschweig, 2023. DOI: 10 . 24355 / dbbs . 084 - 202207041441-0. URL:<https://doi.org/10.24355/dbbs.084-202207041441-0>.
- [3] T. C. Corke. *Design of Aircraft*. Prentice Hall, 2003. ISBN: 9780130892348.
- [4] EASA. *Acceptable Means of Compliance (AMC) and Guidance Material (GM) to Annex VIII Specialised Operations [PART-SPO]*. Tech. rep. 31 October 2016.
- [5] D.S. Lee et al. “The contribution of global aviation to anthropogenic climate forcing for 2000 to 2018”. In: *Atmospheric Environment* 244 (2021), p. 117834. ISSN: 1352-2310. DOI: <https://doi.org/10.1016/j.atmosenv.2020.117834>. URL: <https://www.sciencedirect.com/science/article/pii/S1352231020305689>.
- [6] J. D. Mattingly et al. *Aircraft Engine Design*. Reston, VA: American Institute of Aeronautics and Astronautics, 2018.
- [7] M. C. Y. Niu. *Airframe Structural Design: Practical Design Information and Data on Aircraft Structures*. 2nd ed. Adaso Adastra Engineering Center, 1999.
- [8] E. Obert. *Aerodynamic Design of Transport Aircraft*. Delft: IOS Press, 2009.
- [9] International Civil Aviation Organization. *Aerodrome Design Manual - Part 3 - Pavements (Doc 9157 - Part 3)*. Tech. rep. International Civil Aviation Organization, 2022.
- [10] Pieter Jan Proesmans. “Aircraft Design for Minimal Climate Impact (working title)”. PhD thesis. Delft University of Technology, 2024.
- [11] Pieter-Jan Proesmans and Roelof Vos. “Airplane Design Optimization for Minimal Global Warming Impact”. In: *Journal of Aircraft* 59.5 (2022), pp. 1363–1381. DOI: 10.2514/1.C036529.
- [12] D. P. Raymer. *Aircraft Design: A Conceptual Approach*. Washington, DC: AIAA, 1989.
- [13] J. Roskam. *Airplane Design Part I: Preliminary Sizing of Airplanes*. Lawrence, KS, USA: DARcorporation, 1989.
- [14] J. Roskam. *Airplane Design Part II, Preliminary Configuration Design and Integration of the Propulsion System*. Design, Analysis and Research Corporation (DARcorporation), 2017.
- [15] J. Roskam. *Airplane Design, Part VI: Preliminary Calculation of Aerodynamic, Thrust and Power Characteristics*. Lawrence, KS: DARcorp, 1990.

- [16] G. J. J. Ruijgrok. *Elements of Airplane Performance*. Delft, The Netherlands: Delft University Press, 1989.
- [17] Kristian Schmidt and Roelof Vos. "A Semi-Analytical Weight Estimation Method for Oval Fuselages in Conventional and Novel Aircraft". In: *AIAA SciTech*. January. National Harbor: AIAA, 2014, pp. 1–18.
- [18] E. Torenbeek. "Elements of Aerodynamic Wing Design". In: *Advanced Aircraft Design*. Chichester, West Sussex, UK: John Wiley and Sons, Ltd., 2013. Chap. 10.
- [19] E. Torenbeek. *Essentials of Supersonic Commercial Aircraft Conceptual Design*. Chichester, Uk: John Wiley & Sons Ltd., 2020.
- [20] E. Torenbeek. *Synthesis of subsonic airplane design*. Delft, The Netherlands: Delft University Press, 1976.
- [21] E. Torenbeek. *The initial calculation of range and mission fuel during conceptual design*. en. Tech. rep. LR-525. Delft University of Technology, Faculty of Aerospace Engineering, 1987.
- [22] E. Torenbeek and G. H. Berenschot. *De berekening van het omspoeld gondeloppervlak van enkel- en dubbelstroom straalmotoren voor civiele vliegtuigen*. Tech. rep. Memorandum M-445. Technische Hogeschool Delft, afdeling Luchtvaart- en Ruimtevaarttechniek, 1983.
- [23] E. Van Hinte and M. Van Tooren. *First Read This*. nai010 publishers, 2013. ISBN: 9064506434.
- [24] Roelof Vos and Saeed Farokhi. *Introduction to Transonic Aerodynamics*. Vol. 110. Fluid Mechanics and Its Applications. Dordrecht: Springer Netherlands, 2015. ISBN: 978-94-017-9746-7. DOI: 10.1007/978-94-017-9747-4. URL: <http://link.springer.com/10.1007/978-94-017-9747-4>.
- [25] R. de Vries, M. Hoogreef, and R. Vos. "Range Equation for Hybrid-Electric Aircraft with Constant Power Split". In: *Journal of Aircraft* 57 (3 2020).
- [26] Reynard de Vries, Malcom Brown, and Roelof Vos. "Preliminary Sizing Method for Hybrid-Electric Distributed-Propulsion Aircraft". In: *Journal of Aircraft* 56.6 (2019), pp. 2172–2188. DOI: 10.2514/1.C035388. URL: <https://doi.org/10.2514/1.C035388>.
- [27] R. Whitford. "Chapter 3: Fuselage Design". In: *Design for Air Combat*. London, UK: Jane's, 1987, pp. 148–160.

INDEX

- adiabatic, 157
- advisory circular, 39
- aft pressure bulkhead, 114
- aircraft classification rating, 23, 243,
 - 246
- airliner
 - regional, 43
- airplane
 - configuration, 47
 - reference, 43
- airport, 22
- airworthiness requirements, 27
- altitude
 - critical ~, 155
- AMC, 31
- analysis
 - fidelity, 3
- anhedral, 201
- APU, 39, 105, 114
- aspect ratio, 80
- aspirated engine, 155
- atmosphere, 150
- auxiliary power units, 39
- avgas, 50
- avionics, 105
- bank angle, 64
- basic empty mass, 78
- bending moment relief, 55
- biofuel, 51
- budget, 197
- bulkhead
 - aft pressure~, 114
 - front pressure~, 114
- bypass
 - flow, 216
 - ratio, 216, 217
- bypass ratio, 90
- center of gravity, 10, 230
 - excursion, 240
- CFR, 28
- chord
 - mean aerodynamic, 190, 192
- clearance, 111
 - ground ~, 201, 250, 255
- climb
 - gradient, 33, 165
 - rate of ~, 160
- cockpit
 - window, 110
- conceptual design, 8
- conventional tail, 71
- convergence, 10
- core
 - flow, 216
- critical altitude, 155
- CS, 28
- design
 - conceptual, 8
 - criteria, 3
 - detailed, 9
 - engineering, 1
 - freeze, 9
 - objective, 3, 15
 - option, 47
 - options, 2
 - payload, 22
 - point, 179
 - preliminary, 8
 - problem, 2
 - process, 1
 - structure matrix, 10
 - variables, 2
- dihedral, 199

- effect, 199
- dihedral angle, 66
- distributed propulsion, 57
- diversion, 19
- drag
 - form ~, 196
 - polar, 80
- drag coefficient
 - zero-lift, 80
- drag count, 168
- Dutch roll, 261
- EASA, 28
- ECS, 105
- efficiency
 - propulsive, 88
 - volumetric ~, 53
- elevator, 266
- elevon, 75
- emergency evacuation, 107, 134
- emergency exits, 36
- empty mass, 78
- energy
 - reserve , 91
- engine
 - envelope, 205
 - opposed piston ~, 205
 - reciprocating, 205
- equation of state, 150
- evacuation, 107
- FAA, 28
- FAR, 28
- field of view, 110
- fineness ratio, 109, 208
- flat-rated engine, 155
- flight deck, 135
- floatation, 242
- foreign object damage, 63, 251
- frames, 112
- friction coefficient
 - equivalent, 82
- front pressure bulkhead, 114
- fuel
 - sustainable aviation ~, 49
- fuselage, 105
- double-bubble, 113
- gas generator, 216
- general aviation, 42
- grazing angle, 111
- ground clearance, 111, 134
- ground handling, 114
- highlight, 218
- horizontal tailplane, 71
- hot and high, 150
- hydrogen, 51
- hydrogen-electric, 51
- ICAO, 41
- IFR, 42
- International Standard Atmosphere, 150
- inverter, 208
- ISA, 142
- isentropic process, 157
- knocking, 50
- landing field length, 148
- landing gear
 - conventional, 112
- lateral stability, 63, 199
- lateral turnover, 255
- LH₂, 51
- lift
 - distribution, 188
- lift coefficient
 - maximum, 142, 145
- lift equation, 13
- lift-to-drag ratio, 80
- liquefied natural gas, 52
- LNG, 52
- longerons, 112
- mass
 - empty, 78
 - fraction, 232
 - maximum take-off ~, 230
 - operating empty, 78
 - operating empty ~, 230
- mass-specific energy, 79

- mission
 diversion, 19
 nominal, 19
 profile, 18
- need, 16
- nitrogen oxide, 50
- NOx, 50
- operating empty mass, 78
- Oswald factor, 80, 85
- over-nose angle, 111, 210
- overall pressure ratio, 216
- parasite drag area, 83
- pavement
 classification number, 23, 243
 classification rating, 22, 245
- payload
 design ~, 17, 22, 98
- payload-range diagram, 98
- performance, 2
- pitching moment, 58
- planform, 186
- plug, 219
- power
 lapse, 155
 loading, 141
- power loading, 141
- preliminary
 design, 8
 sizing, 77
- pressure
 total, 157
- pressure drag, 109
- problem statement, 2
- propfan, 57
- propulsion
 distributed, 57
- propulsive efficiency, 88
- PSFC, 87
- pusher configuration, 55
- pylon, 57, 223
- range
 auxiliary, 100
- design ~, 22, 98
equivalent, 91
equivalent ~, 79
ferry, 100
nominal, 19
- rated tire load, 246
- reference airplane, 43, 77
- requirement, 2
 top-level aircraft, 8
- requirements
 top-level aircraft, 17
- rolling moment, 63
- rolling moment due to sideslip, 199
- rudder, 261
- ruddervator, 74
- scrape angle, 250
- seed, 16
- shock absorber, 251
- sideslip, 63
- sizing, 3, 12, 182
 preliminary, 77
- span efficiency factor, 85
- spar
 auxiliary ~, 259
 front ~, 194
 rear ~, 194
- specific energy, 79
- speed
 cruise, 153
 minimum, 144
 stall, 28
- sponson, 63, 260
- stabilator, 266
- stability
 lateral ~, 63, 199
- stall
 deep ~, 72
- stall speed, 28
- structure
 fuselage ~, 112
- sustainable aviation fuel, 49
- sweep angle, 186
- tail
 all-flying ~, 266

- volume, 261
- tailplane
 - horizontal, 265
 - vertical, 261
- take-off
 - field length, 173
- take-off configuration, 173
- taper ratio, 72, 186, 188
- technology
 - maturity, 7
- temperature
 - total, 157
- temperature lapse rate, 150
- thickness-to-chord ratio, 195
- thin-walled structure, 112
- thrust, 142
 - lapse, 156
- thrust-to-weight ratio, 141, 142
- time
 - turnaround, 49
- tip-over angle, 250
- top-level aircraft requirements, 17
- total pressure, 157
- total temperature, 157
- track width, 255
- tractor configuration, 55
- TSFC, 87
- turbine inlet temperature, 217
- turbofan, 28, 48, 89
- turboprop, 28, 48
- turnaround time, 49
- ULD, 117
- unit load device, 114
- unity equation, 79
- upsweep, 111
- vertical tailplane, 71
- VFR, 42
- view angle
 - downward, 110
 - upward, 110
- visibility, 110, 134
- wetted area, 82
- wing
 - box, 65
 - loading, 141
 - planform, 186
 - straight-tapered, 190
- yawing moment, 56
- yehudi, 259